UNIVERSIDADE ESTADUAL DE CAMPINAS
Faculdade de Engenharia Mecânica

ENRICO OLIVEIRA ROCHETI

# Evaluation of Weigh-in-Motion Techniques Through Simulation and Experimental Data

# Análise de Técnicas de Pesagem em Movimento por Meio de Simulação e Dados Experimentais

Campinas

2024

**ENRICO OLIVEIRA ROCHETI**

# Evaluation of Weigh-in-Motion Techniques Through Simulation and Experimental Data

# Análise de Técnicas de Pesagem em Movimento por Meio de Simulação e Dados Experimentais

Dissertation presented to the School of Mechanical Engineering of the University of Campinas in partial fulfillment of the requirements for the degree of Master in Mechanical Engineering, in the area of Mechatronics.

Dissertação apresentada à Faculdade de Engenharia Mecânica da Universidade Estadual de Campinas como parte dos requisitos exigidos para a obtenção do título de Mestre em Engenharia Mecânica, na área de Mecatrônica.

Orientador: Prof. Dr. Rodrigo Moreira Bacurau

ESTE TRABALHO CORRESPONDE À VERSÃO FINAL DA DISSERTAÇÃO DEFENDIDA PELO ALUNO ENRICO OLIVEIRA ROCHETI, E ORIENTADA PELO PROF. DR. RODRIGO MOREIRA BACURAU.

Campinas

2024

Ficha catalográfica
Universidade Estadual de Campinas (UNICAMP)
Biblioteca da Área de Engenharia e Arquitetura
Rose Meire da Silva - CRB 8/5974

R586e

Rocheti, Enrico Oliveira, 1995-
Evaluation of weigh-in-motion techniques through simulation and experimental data / Enrico Oliveira Rocheti. – Campinas, SP : [s.n.], 2024.

Orientador: Rodrigo Moreira Bacurau.
Dissertação (mestrado) – Universidade Estadual de Campinas (UNICAMP), Faculdade de Engenharia Mecânica.

1. Pesagem em movimento. 2. Transporte rodoviário - Tarifas. 3. Transporte - Regulamentação. 4. Engenharia de transportes. I. Bacurau, Rodrigo Moreira, 1988-. II. Universidade Estadual de Campinas (UNICAMP). Faculdade de Engenharia Mecânica. III. Título.

Informações Complementares

**Título em outro idioma:** Análise de técnicas de pesagem em movimento por meio de simulação e dados experimentais
**Palavras-chave em inglês:**
Weigh-in-motion
Road transport - Tariffs
Transport - Regulation
Transport engineering
**Área de concentração:** Mecatrônica
**Titulação:** Mestre em Engenharia Mecânica
**Banca examinadora:**
Rodrigo Moreira Bacurau [Orientador]
Pablo Siqueira Meirelles
Anderson Wedderhoff Spengler
**Data de defesa:** 10-10-2024
**Programa de Pós-Graduação:** Engenharia Mecânica

**Identificação e informações acadêmicas do(a) aluno(a)**
- ORCID do autor: https://orcid.org/0000-0001-6678-9137
- Currículo Lattes do autor: http://lattes.cnpq.br/4002142721423969

**UNIVERSIDADE ESTADUAL DE CAMPINAS**
**FACULDADE DE ENGENHARIA MECÂNICA**

**DISSERTAÇÃO DE MESTRADO ACADÊMICO**

# Evaluation of Weigh-in-Motion Techniques Through Simulation and Experimental Data

# Análise de Técnicas de Pesagem em Movimento por Meio de Simulação e Dados Experimentais


Autor: Enrico Oliveira Rocheti

Orientador: Prof. Dr. Rodrigo Moreira Bacurau


A Banca Examinadora composta pelos membros abaixo aprovou esta Dissertação:

**Prof. Dr. Rodrigo Moreira Bacurau, Presidente**
**DMC/FEM/UNICAMP**

**Prof. Dr. Pablo Siqueira Meirelles**
**DMC/FEM/UNICAMP**

**Prof. Dr. Anderson Wedderhoff Spengler**
**DEM/CTJ/UFSC**

A Ata de Defesa com as respectivas assinaturas dos membros encontra-se no SIGA/Sistema de Fluxo de Dissertação/Tese e na Secretaria do Programa da Unidade.

Campinas, 10 de Outubro de 2024

*Don't settle for less, even the genius asks questions. Be grateful for blessings.*
*Don't ever change, keep your essence.*

Tupac Amaru Shakur, *Me Against The Word*

# ACKNOWLEDGEMENTS

After overcoming these great challenges, I am truly grateful to those who helped me to get this far.

To my parents, who have always supported me throughout my life. They have encouraged me, above all, to pursue my studies and seek knowledge.

To my girlfriend, who has been by my side for the past 10 years, showing me a kind of love and kindness I had never experienced before.

To Professor Rodrigo, who not only opened the door to this opportunity but also provided guidance and support, always helpful and understanding.

To all my friends with whom I had the pleasure of sharing this journey in a new city, from graduation to my Master's.

Thank you all very much.

This study was supported by the Instituto de Pesquisas Eldorado.

# RESUMO

O tráfego de caminhões com carga acima do permitido é uma das principais causas de danos ao pavimento das rodovias. Para identificar e multar caminhões sobrecarregados, balanças de pesagem estática são geralmente utilizadas, exigindo a parada dos veículos, o que resulta em atrasos e custos de transporte. Uma alternativa é a Pesagem em Movimento (WIM), capaz de pesar os caminhões na rodovia sem necessidade de paradas. No entanto, para aplicação em pesagem punitiva, os sistemas WIM devem fornecer medições confiáveis e precisas, o que é desafiador devido à dinâmica dos veículos em movimento. Ao longo dos anos, diversos métodos foram propostos para calcular o peso de veículos em movimento, visando melhorar a acurácia desses sistemas. Esses métodos são divididos em duas fases: a estimativa de cargas instantâneas dos eixos e a estimativa do peso bruto total (PBT) do veículo. Este estudo avalia a precisão e a acurácia de sistemas WIM, abordando os métodos e algoritmos de pesagem por meio de análises experimentais e simulações. As simulações avaliaram diferentes configurações de sistema, com resultados indicando que o uso de mais de oito sensores não apresenta uma redução de erro considerável. A distância entre sensores teve impacto mínimo em baixas velocidades e maior relevância em velocidades mais altas. Em relação aos estimadores avaliados nas simulações, o simples cálculo do valor médio mostrou-se uma escolha prática para sistemas WIM, com resultados robustos em diversos cenários. Nas análises experimentais, métodos de estimativa de carga instantânea do eixo foram testados com um caminhão de seis eixos, e o método de Área sob o Sinal apresentou erros na faixa de 5% para a maioria dos casos, sendo o método de maior acurácia.

**Palavras–chave**: *Weigh-in-motion*, Estimativa de Peso Dinâmico, Pesagem Punitiva.

# ABSTRACT

The traffic of trucks with loads above the permitted limit is one of the main causes of pavement and road damage. To identify and penalize overloaded trucks, static weighing scales are generally used, requiring vehicles to stop at highway weigh stations, resulting in delays and increased transportation costs. An alternative to avoid this inconvenience is through Weigh-in-Motion (WIM) systems, capable of weighing trucks on the highway without requiring them to stop. For WIM systems to be employed in direct enforcement, they must provide reliable and accurate measurements, which is challenging due to the dynamics of moving vehicles. Over the years, various methods for calculating the weight of moving vehicles have been proposed, as the accuracy of WIM systems heavily depends on the weight estimation methods employed. These estimation methods are typically divided into two phases: instantaneous axle load estimation and gross vehicle weight estimation. This study evaluates the accuracy and precision of WIM systems, focusing on these weight estimation methods through both simulations and experimental analyses. Simulations assessed different system layouts and estimation algorithms (estimators), with results indicating that using more than eight sensors provides diminishing returns in error reduction. Sensor spacing had a minimal impact on errors at lower speeds but became more significant at higher speeds. Regarding estimators, the simple mean value calculation proved to be a reliable choice for WIM systems, providing robust results across various scenarios. Experimentally, instantaneous axle load estimation methods were tested on a six-axle truck, with the Area Under the Signal method showing errors around the 5% margin in most cases, making it the most accurate method.

**Keywords**: Weigh-in-motion, Dynamic Weight Estimation, Direct Enforcement.

# LIST OF FIGURES

# LIST OF TABLES

# CONTENTS

# 1 INTRODUCTION

This chapter provides a brief introduction to Weigh-In-Motion (WIM) systems, highlighting their importance and challenges to identify overloaded trucks. The main goals of this work are presented, focusing on exploring methods to estimate vehicle weight in motion using both simulated and real-world data. Finally, the chapter provides an overview of the structure of this thesis.

## 1.1 Motivation

Road infrastructure plays a crucial role in economic and social development, facilitating interconnectivity between regions and contributing to overall progress. The proper maintenance of highways is a fundamental factor in ensuring efficiency, safety and reducing traffic congestion.

One of the factors that causes highway degradation is the traffic of overloaded trucks, which is a concern for infrastructure authorities and transportation departments worldwide. When trucks carry loads that exceed the recommended weight limits, they exert excessive pressure on the road surface, leading to various types of damage, such as pavement deformation, rutting, structural damage, bridge and culvert damage (Pais *et al.*, 2013). Furthermore, they pose safety risks to other vehicles.

Considering this, effective weight measurement of trucks and heavy vehicles is essential to enforce compliance with weight regulations, contributing to the preservation of road infrastructure and safety. Developing accurate and efficient systems for measuring vehicle weights is crucial to address these concerns (Sujon; Dai, 2021). Traditionally, truck weighing has relied on static or very low-speed scales (operating at speeds below 5 km/h), requiring vehicles to stop or nearly stop at designated weigh stations or weighing sites. While these methods provide considerable accuracy, they present various inconveniences and limitations, including traffic congestion, queues, and delays for drivers (Benekohal *et al.*, 2000). Both static scales and very low-speed scales can be financially inefficient and time-consuming, requiring significant resources from highway concessionaires and vehicle operators (Giacinto *et al.*, 2021).

To overcome these challenges, Weigh-In-Motion (WIM) systems have emerged as an efficient solution. WIM technology enables the measurement of vehicle weights while they are in motion on the road, eliminating the need for vehicles to stop or divert to designated weighing points. By integrating weight measurement into the normal flow of traffic, WIM systems provide real-time data without disrupting the efficiency of the transportation network.

Weigh-in-motion systems are generally categorized into two types: low-speed (LS-WIM) and high-speed (HS-WIM) systems. LS-WIM sites are typically located near toll booths or motorway entries, requiring vehicles to travel within a speed range of 10 to 20 km/h. HS-WIM systems are designed to dynamically weigh vehicles traveling at any speed within legal limits (up to 90 km/h in most countries), eliminating the need for specific infrastructure such as toll booths and dedicated low-speed points along highways (Benekohal *et al.*, 2000).

Legislation related to truck weighing varies across different countries and regions, but there are common elements. These elements include the need for identification of the vehicle's silhouette (number of axles and distance between them), measuring axle and the overall weight of the vehicle, establishing maximum allowable error margins, and specifying the range of vehicle speeds for precise weight measurement. In the European Union, the accuracy requirements for Weigh-In-Motion systems are determined by the R134 standard developed by the International Organization for Legal Metrology (OIML) (International Organization of Legal Metrology (OIML), 2006). The primary accepted WIM standard in the United States is the ASTM E1318-09 (ASTM International, 2010). These standards generally define different accuracy classes, specifically the maximum permissible error in relation to the true static weight of a vehicle or axle. The most accurate systems (Type I in ASTM E1318-09 Standard and Class 0.2 or A in OIML R134) are suitable for direct enforcement purposes, while other systems with lower accuracy classes are often used for data collection, and traffic and vehicle monitoring. In Brazil, recent legislation from INMETRO details the metrological requirements for automated Weigh-In-Motion (Instituto Nacional de Metrologia, Qualidade e Tecnologia (INMETRO), 2022). This legislation introduces Classes 1 (with a maximum permissible error of 5% in GVW estimation) and A (with an 8% maximum permissible error in static axle load) as the highest levels of precision. However, it is still under consideration whether these systems, especially HS-WIM systems, can be utilized for direct enforcement purposes in the Brazilian territory.

Weigh-In-Motion systems use load sensors to obtain the weight of moving vehicles as they pass over the WIM site. The collected sensor data is then processed and analyzed using algorithms to estimate the weights of individual axles and the overall weight of the vehicle, also known as Gross Vehicle Weight (GVW) (Burnos *et al.*, 2007; Cebon; Winkler, 1991). Systems equipped with more than one sensor are often labeled as multiple-sensor Weigh-In-Motion systems (MS-WIM). The continuous advancements in sensor technology, data processing techniques, and machine learning algorithms have significantly enhanced the accuracy and efficiency of WIM systems over time.

One of the challenges faced by WIM systems is their exposure to various weather conditions, as they are installed in open-air areas. This exposure can lead to decreased sensor accuracy (Lu; Tolliver, 2023). Calibration algorithms have been used to mitigate this issue, often requiring a pre-weighted vehicle in the calibration process (Gajda *et al.*, 2021; Huhtala *et al.*, 2000). Advanced auto-calibration methods have been studied in recent years (Burnos; Gajda, 2020; Burnos, 2008). However, they have not been widely adopted in WIM applications due to their requirement for complex and long-term datasets.

A crucial factor that influences the precision and accuracy of WIM systems is the impact of dynamic loads generated by the moving vehicles during measurement (Oubrich *et al.*, 2017; Saburdo; Topolev, 1964). The mechanical oscillations of a vehicle's suspensions and tires can lead to erroneous weight estimations for individual axles, as the instant measurements may coincide with the high or low point of these oscillations. While weather conditions such as wind force can impact these oscillations, they are primarily influenced by the mechanical properties of the vehicles, the quality of the road surface, and the speed at which the vehicles are traveling (Cebon; Winkler, 1991; Oubrich *et al.*, 2017).

These factors significantly impact the accuracy of WIM systems, which has very restrictive requirements for the direct enforcement of moving vehicles. Various techniques have been proposed to enhance the precision of these systems, this work categorizes them in two stages: the estimation of the instantaneous axle weights applying weighing algorithms and methods on the signals captured by WIM sensors; and the estimation of the Gross Vehicle Weight (GVW), by utilizing different methods, also known as estimators, to calculate the true axle load based on the instantaneous axle load measurements obtained from the sensors.

One of the major challenges in developing WIM systems is validating different techniques and setups. This process involves expensive experimental tests that require modifying system infrastructure (e.g., sensor distance), conducting tests with various trucks of different models, and performing system calibrations. Therefore, simulation is a crucial tool in WIM design, allowing for a preliminary assessment of the performance of various weighing techniques and approaches to system implementation. In this context, in this work we developed a simulator to evaluate GVW estimators under different system configurations. Additionally, experimental data were used to analyze different instantaneous axle load estimation algorithms.

## 1.2 Objectives

The present work proposes a performance evaluation of methods to estimate the instantaneous axle and gross vehicle weights of vehicles in motion using simulated and experimental data. To achieve this goal, the following objectives were defined:

1. Study and comprehend the advantages and limitations of the main weighing methods applied in Weigh-In-Motion systems;
2. Implement a simulator to evaluate methods to estimate the Gross Vehicle Weight;
3. Explore Weigh-In-Motion system layouts through simulations, varying parameters such as the number of sensors, sensor spacing, and vehicle parameters. This helps further understanding of the layout impact in dynamic weighing measurement;
4. Implement methods to estimate the instantaneous axle load using real data collected from an experimental site and evaluate their performances.

## 1.3 Structure

This work is structured as follows: In Chapter 2, an overview of WIM systems is provided, covering aspects such as weighing sensors, the influence of road surface and weather conditions on weight measurements, and techniques for system calibration. Chapter 3 introduces the effect of dynamic loads on WIM systems, focusing on a review of weight estimation techniques. These techniques are categorized into dynamic axle weight estimation and Gross Vehicle Weight (GVW) estimation. Chapter 4 details the implementation and design of the proposed methodologies, including both simulation and experimental analyses. In Chapter 5, we present the results of these analyses, including simulation and experimental data. Chapter 6 presents the main conclusions and suggestions for future work. Appendix A includes additional simulation results that complement the analysis presented in Chapter 5.

# 2 WEIGH-IN-MOTION OVERVIEW

This chapter provides an overview of Weigh-In-Motion (WIM) systems, presenting knowledge of their basic elements and concepts. Initially, WIM sensors are discussed, such as load cells, bending plates, piezoelectric and fiber optic sensors. Then, the effects of road surface quality and weather conditions on WIM systems are discussed. Lastly, this chapter examines different calibration methods, including the use of a pre-weighed vehicle and continuous calibration methods, also known as auto-calibration.

The content of this chapter was adapted from the paper (Rocheti; Bacurau, 2024), which was published as part of this research.

## 2.1 Sensors

The most fundamental hardware component of a WIM system is its sensors, which are used to measure the vehicle's load passing over the road. Although there are different types of weight sensors for different applications, WIM systems require sensors with robust mechanical characteristics (heavy vehicles axle's load can reach up to 20 tons) and high immunity from climate variations, as these sensors are installed directly into the road and exposed to all sorts of weather conditions. The main sensors used for permanent WIM sites as a weighing platform include load cells, bending plates, fiber optic sensors (FOS), and piezoelectric sensors (Janota *et al.*, 2016; Al-Qadi *et al.*, 2016). Each type of sensor has its advantages and disadvantages in the WIM applications, and these characteristics will be discussed below. Besides weighing sensors, inductive loops are installed in the pavement at the beginning and end of each system. These loops are used to initiate a weighing measurement and to detect its end. This work won't discuss inductive loops, as they are not a key part of WIM systems.

### 2.1.1 Load Cells

Load cells are devices that convert a mechanical force, such as the vehicle's weight, into an electrical quantity, such as voltage, current, or resistance. Typically, load cells use strain gauge-type sensors; the most common configuration uses a pair of strain gauges placed on opposite sides of a machined shear beam's web. Connected in a Wheatstone bridge circuit, the strain gauges convert resistance changes into voltage changes. These voltage changes are proportional to the strains experienced by the web, enabling the calculation of the applied load (Al-Qadi *et al.*, 2016; Zhang *et al.*, 2007; Agape *et al.*, 2019). The Wheatstone full-bridge and half-bridge configuration allow for temperature variation compensation, which is highly effective for WIM systems frequently exposed to various weather conditions (Tutak, 2014; Lee *et al.*, 1995).

Although not common, load cells can also use a hydraulic system to measure mechanical force. This type of load cell consists of a plate atop hydraulic cylinders changing its pressure based on the load applied to the cell (Al-Qadi *et al.*, 2016; Agape *et al.*, 2019).

Load cell-type sensors are generally installed in the pavement; they are known for being robust, reliable, and one of the most accurate sensors for weighing in motion applications (Al-Qadi *et al.*, 2016; Zhang *et al.*, 2007; Agape *et al.*, 2019). They are also very durable and resilient systems, with an average lifetime durability of 12 years. However, considering its installation and maintenance costs, load cells are one of the most expensive technologies for WIM sensors (Zhang *et al.*, 2007; Agape *et al.*, 2019; Ryguła *et al.*, 2021).

### 2.1.2 Bending Plates

Bending plate sensors consist of steel plates, called weigh pads, with strain gauges mounted on the underside. The sensors are embedded in asphalt, with the flexible plate on top and the strain gauges on the bottom (Al-Qadi *et al.*, 2016; Zhang *et al.*, 2007; Agape *et al.*, 2019).

These types of sensors have lower accuracy when compared to load cells (Agape *et al.*, 2019). They are not usually recommended for HS-WIM systems as they can be damaged easily by high-speed heavy vehicles passing over them, reducing their accuracy and longevity. Also, most bending plate sensors have wider weigh pads when compared to piezoelectric, fiber optic sensors, and load cell sensors, meaning their inertia to respond to a force applied from a high-speed vehicle will be greater (Agape *et al.*, 2019).

### 2.1.3 Piezoelectric Sensors

Piezoelectric sensors are constructed from materials such as ceramics, polymers, and quartz, which have an asymmetric crystal structure that generates an electric charge proportional to the mechanical force applied on them (Kwon, 2007). This phenomenon is referred to as the piezoelectric effect (Al-Qadi *et al.*, 2016).

Piezoceramic and piezopolymer sensors typically have small diameters and are revested with flat brass or metal channels reinforced with fiberglass, similar to conventional coaxial cables (Al-Qadi *et al.*, 2016; Wang *et al.*, 2009). However, these two types of piezoelectric sensors are susceptible to temperature changes, and compensation is required during weighing measurements (Gajda *et al.*, 2015). Additionally, they have a significant degree of heterogeneity sensitivity along their length, reducing their accuracy and making them primarily suitable for axle detection and vehicle classification.

On the other hand, piezoelectric quartz technology is composed of materials insensitive to temperature changes, resulting in higher accuracy in weight measurements (Kwon, 2007; Hallenbeck; Weinblatt, 2004). Although more expensive than other piezoelectric sensors, quartz-based piezo sensors are a good option for in-motion vehicle weighing due to their superior accuracy (Wang *et al.*, 2009; Kwon, 2007; Gajda *et al.*, 2015; Al-Qadi *et al.*, 2016; Hallenbeck; Weinblatt, 2004).

### 2.1.4 Fiber Optic Sensors

A fiber optic cable is a light conductor composed of a photoconductive material coated with a reflective layer. This technology is widely used in various systems, including medical devices, high-speed data transmission, and Weigh-In-Motion systems.

Fiber optic sensors (FOS) used on WIM systems typically operate using two main principles: Bragg grating and fiber's photo-elastic property (Batenko *et al.*, 2011a). Fiber Bragg grating sensors (FBG) are based on the principle of wavelength shifting, where a slight change in the load applied to the sensor results in a corresponding change in the light wavelength reflected from the sensor (Li *et al.*, 2009).

Other types of FOS use the principle of fiber's photo-elastic property. The variation of optical properties of the sensor under a certain type of strain, such as changes in light signal polarization, phase, or frequency, can be used to measure the load being applied to the sensor (Zhang *et al.*, 2015; Grakovski; Pilipovecs, 2017c). For example, the load applied to an FOS can be measured using the phase shift between the vertical and horizontal polarization modes of the fiber's optical signal.

Fiber optic sensors are immune to EMI (Electromagnetic Interference) and, therefore, are a suitable option for WIM systems in noisy environments. Due to the absence of metallic components, their long-term stability can provide a lifetime of 20-30 years of operation. Despite these advantages, they are mainly used today for vehicle detection and counting due to their dependence on temperature and the effect of the vehicle speed on its accuracy (Zhang *et al.*, 2015; Grakovski; Pilipovecs, 2017c; Batenko *et al.*, 2011a; Agape *et al.*, 2019). Temperature compensation techniques, especially for FBG sensors, have been explored to address this issue (Li *et al.*, 2019; Xiong *et al.*, 2019).

## 2.2 Road Surface

Road surface is another factor that significantly influences the accuracy of WIM systems. Pavement irregularities and texture can directly impact load distribution across the sensors, leading to inaccurate weight measurements. A smooth road surface, without the presence of cracks and potholes, is necessary for the efficient operation of the vehicle's suspension system, minimizing road noise and vibration (Huang, 1993). High-quality pavement plays a crucial role in providing more accurate weight results (Gajda *et al.*, 2015). Previous work has highlighted the importance of having a flat and horizontal road segment at least 30 meters long before the vehicle passes over the WIM sensors (Batenko *et al.*, 2011a).

Currently, the most used surface types for WIM systems are concrete and bituminous (Gajda *et al.*, 2015). In the aforementioned study, an evaluation of the road surface quality for the installation of a WIM system was made. Measurements were conducted to determine the suitability of the road surface, including road profiles obtained through a profilograph and geodetic measurements. The unevenness and quality of the road surface were assessed based on these measurements and compared to the standard defined by International Organization for Standardization (1995). The installation site chosen was a bituminous surface selected after the tests were carried out.

Additionally, the study by Ryguła *et al.* (2021) assessed the pavement quality of a WIM site in Poland, following the recommendations shown in COST 323 (Jacob *et al.*, 2002). This specification defines pavement characteristics, such as pavement deflection, rut depth, and longitudinal evenness to classify the WIM site into three categories: Excellent (I), Good (II), and Acceptable (III). The authors of Ryguła *et al.* (2021) employed a Falling Weight Deflectometer (FWD) to measure the pavement's dynamic and static deflections.

Road unevenness increases the impact of dynamic loads on WIM systems, as it's detailed in Section 3.1, thereby reducing overall system accuracy. Considering all these factors is crucial when selecting the appropriate installation location for WIM systems.

## 2.3 Weather Conditions

Weather conditions can significantly impact on the accuracy and reliability of WIM systems. Extreme temperatures, wind, rain, and snow can all cause errors in the measurement of vehicle weight (Lu; Tolliver, 2023; Administration, 2018).

Temperature influences on WIM systems are directly related to the type of sensors used. As noted in Section 2.1, some sensors are more sensitive to temperature variations than others. For instance, piezoceramic and piezopolymer sensors have relatively high sensitivity to temperature, while others, such as piezoelectric quartz, are less sensitive. Strain gauge-type and fiber optic sensors can exhibit reduced sensitivity to temperature variations, but only when subjected to appropriate compensation methods. Another factor to consider is the effect of road and pavement temperature on WIM accuracy. Higher temperatures can cause thermal expansion of the pavement and sensors, impacting the accuracy of WIM systems (Gajda *et al.*, 2013; Gajda; Burnos, 2016). Moreover, rain and snow can accumulate on sensors' surface, causing them to malfunction or providing inaccurate readings due to humidity exposure or low temperature.

To overcome these temperature-related effects, a compensation method was proposed to compensate for thermal effects on the sensors (Burnos, 2008). The proposed temperature compensation method was tested in a WIM system equipped with piezoelectric sensors. The results demonstrated a relative root-mean-square error of 0.0164 when comparing the temperature-corrected data to the actual load. Nevertheless, the temperature correction demands continuous monitoring of asphalt temperature, pre-calibration procedures, and long-term data recording (Burnos, 2008).

Besides the effect of high humidity and low temperatures, rain and snow can also affect the road surface condition. Wet or icy road conditions can cause the tires of the vehicles to lose traction and slide, which can result in errors in the weight measurements taken by WIM systems (Carlson; Vieira, 2021).

Wind forces can generate air currents that change the forces acting on the vehicle, causing it to sway, lift or lean, affecting WIM sensors' readings (Lu; Tolliver, 2023). High-sided vehicles, such as trucks with empty containers or trailers, are particularly susceptible to the influence of wind due to their larger surface area and higher vulnerability to crosswinds (Hucho; Ahmed, 1998). The aerodynamic interactions between the wind and the vehicle can lead to changes in the vertical load distribution and lateral stability (Balsom *et al.*, 2006). Consequently, these wind-induced effects can introduce measurement errors in the readings obtained by WIM systems, especially in regions or areas prone to high wind speeds or where wind conditions frequently fluctuate.

## 2.4 System Calibration

System calibration is the process of adjusting the output of a measuring system to match the known or expected input. Calibration is a critical step in ensuring the accuracy and reliability of measurement systems, as it establishes a reference relationship between the measured signal and the true value of the measurement. WIM sensors are installed outdoors, making them susceptible to various weather conditions. Fluctuations in WIM system parameters, including temperature changes and aging effects, generate inaccurate measurements that can result in significant errors in data analysis and decision making. Therefore, calibration is a important procedure for these systems.

Several calibration methods have been proposed for WIM systems employing static, dynamic, and continuous calibration methods (Cole; Cebon, 1989; Burnos, 2008; Burnos *et al.*, 2007; Burnos; Gajda, 2020; Pratt *et al.*, 2022; Gajda *et al.*, 2021; Huhtala *et al.*, 2000). Each of these methods has its advantages and disadvantages, and the most effective method depends on the specific requirements of the WIM system and the application.

One simple way to calibrate WIM systems is to apply a known mechanical force on the weighing sensors and compare it with the force measured by the system. For example, a static hydraulic calibrator can be used as demonstrated by Cole and Cebon (1989). While these static methods provide an initial calibration analysis of the system, they are generally used together with other dynamic calibration methods, providing a more accurate system adjustment.

The most common dynamic method used for WIM system calibration is using a pre-weighed vehicle. The vehicle, weighted on a high-precision static scale, is driven over the sensor for several runs, and the measurements of the dynamic weight are related to the static weight using a simple linear regression or other mathematical models (Gajda *et al.*, 2015; Burnos *et al.*, 2007; Cebon; Winkler, 1991). This process yields calibration coefficients that are used to determine the static weight from the dynamic measurements. The study by Gajda *et al.* (2021) evaluated four different estimators (algorithms) for estimating the static characteristic coefficients based on measurement results of the pre-weighed vehicle. The obtained results demonstrate the potential to enhance the accuracy of WIM systems through these algorithms, indicating the need for further research with these methods. On the other hand, methods based on a pre-weighed vehicle necessitate multiple trucks repeatedly traversing the measurement site, leading to significant logistical challenges and often requiring the closure of a road section for regular traffic (Burnos, 2008).

Ongoing calibration procedures, also known as auto-calibration or continuous calibration, have been extensively studied for Weigh-In-Motion systems (Burnos, 2008; Burnos; Gajda, 2020; Pratt *et al.*, 2022). These methods involve continuous estimation of the calibration coefficients, eliminating the need for repetitive passes of pre-weighed trucks. While some approaches may utilize pre-weighed vehicles initially for system calibration, ongoing calibration eliminates the requirement for periodic calibration using test trucks. In the research by Burnos (2008) and Burnos and Gajda (2020), the authors proposed an auto-calibration method for continuously estimating the calibration coefficient based on a known reference quantity. The axle load of specific vehicle classes can be used as the reference quantity. For example, precise static weighing of a large population revealed that the weight of the first axle of a two-axle tractor with a three-axle semi-trailer has a relative standard deviation of approximately 7.3% (Burnos, 2008). With these known references exhibiting small random variability, the loads exerted by these vehicles serve as reference values for estimating the calibration coefficient. Additionally, Pratt *et al.* (2022) presents a system that continuously calibrates WIM systems using static scale data from downstream truck inspection stations. The system utilizes an automated closed-loop algorithm to match vehicles at both locations and uses the static weight scale data as the calibration reference for WIM. The algorithm minimizes the error between WIM and static Gross Vehicle Weight measurements based on vehicle class and speed.

Another innovative approach to WIM system calibration was introduced by the WAVE Project (Huhtala *et al.*, 2000). They have used an instrumented three-axle single-unit truck equipped with strain gauges and accelerometers to measure bending and vertical acceleration, allowing for the estimation of dynamic axle loads. The instantaneous dynamic axle load is then compared to the WIM sensor reading. The challenge was identifying the relevant segment of the dynamic load measurements to synchronize them with the WIM sensor measurements.

These are just a few examples of the calibration methods for WIM systems. It is important to note that the effectiveness of each method depends on various factors, including the type of WIM system (LS-WIM or HS-WIM), the accuracy requirements, the employed sensors, and the operating conditions. Therefore, careful consideration should be given to selecting the most suitable calibration method for a particular system.

# 3 WEIGH-IN-MOTION METHODS REVIEW

In-motion weighing involves two stages: (i) capturing samples of the dynamic tire forces and estimating the instantaneous axle loads; and (ii) estimating the static gross weight using the instantaneous loads obtained in the first stage. This chapter provides a brief analysis of works related to both of these stages. It begins with an introduction to dynamic loads, offering a fundamental understanding of load signals generated by moving vehicles. Then, it delves into the first stage, which encompasses instantaneous axle weight estimation algorithms. Finally, it explores the second stage, focusing on the estimation of Gross Vehicle Weight. The discussion considers the impact of system layout and examines statistical and numerical methods to estimate the vehicle weight.

The content of this chapter was adapted from the paper (Rocheti; Bacurau, 2024), which was published as part of this research.

## 3.1 Dynamic Loads of Moving Vehicles

To accurately determine the static weight of a moving vehicle with maximum precision, the vehicle needs to exert all its vertical forces on perfectly round and dynamically balanced rolling wheels, maintaining a constant speed on a smooth, level surface within vacuum. Under these ideal conditions, none of the vehicle components would experience vertical acceleration (Lee; Ferguson, 1983; Mimbela *et al.*, 2003). Such ideal circumstances never exist in practical situations, which makes WIM challenging.

The overview presented in Chapter 2 has discussed several key factors that impact the dynamic load of a moving vehicle, such as:

1. Road surface factors: longitudinal and transverse profile, cross slope and curvature;
2. Weather conditions: wind speed and direction, road surface and ambient temperature, rain, ice and snow;
3. Vehicle factors: speed and acceleration, axle and vehicle body configuration, suspension system, center of gravity (distribution of load inside the trunk), air pressure inside the tires, and vehicle aerodynamic characteristics. These topics will be discussed in this chapter.

The closer the actual conditions align with the ideal conditions, the more accurately the vehicle's weight can be estimated by measuring the vertical forces applied to the road surface using load sensors.

Vehicle oscillation is classified into transverse and longitudinal oscillations (Figure 3.1). Transverse oscillations are usually compensated by measuring the entire axle weight, either by summing left and right sensor readings or using a single sensor for the whole axle. However, dealing with longitudinal oscillations requires a more thorough examination and consideration of multiple sensors measuring the dynamic weight (Grakovski *et al.*, 2013; Grakovski; Pilipovecs, 2017a).

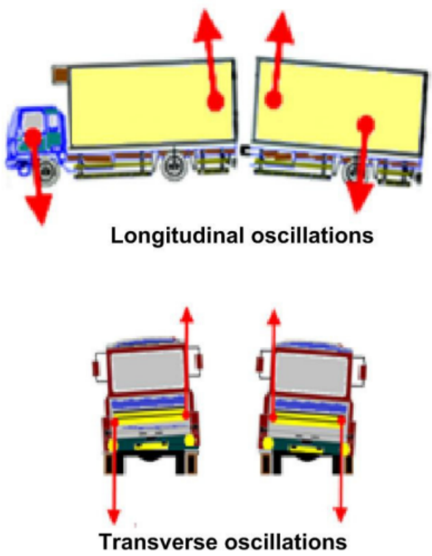


Figure 3.1 – Vehicle longitudinal and transverse oscillations (Grakovski; Pilipovecs, 2017a).

### 3.1.1 Simulated Load Signal

Some pioneering studies have introduced the Equation (3.1) as a starting point for representing the load signal of a vehicle traveling at a constant speed (Saburdo; Topolev, 1964; Cebon, 1990; Cebon; Winkler, 1991). This equation has served as a theoretical foundation in numerous studies conducted in recent years (Ono, 2003; Burnos *et al.*, 2007; Gajda *et al.*, 2015):

$$P(t) = P_0 + \sum_{k=1}^{M} P_k \cdot sin(2\pi f_k t + \phi_k). \tag{3.1}$$

In the equation above, $P_0$ represents the static load of the vehicle, $M$ denotes the number of dynamic harmonic components in the load signal, and $P_k$, $f_k$, and $\phi_k$ represent the parameters of these dynamic components (amplitude, frequency, and phase angle, respectively). The value of $M$ in Equation (3.1) depends on the vehicle suspension models under consideration. For the sake of simplicity, it is often set as $M = 1$ or $M = 2$, which correspond to the effects of vertical balancing and wheel hopping of the vehicle, respectively (Gajda *et al.*, 2015; Burnos *et al.*, 2007).

In order to gain a deeper understanding of the load signal described in Equation (3.1), various dynamic vehicle models based on the mass-spring-damper system, which represents the vehicle suspension system, have been proposed (Mangeas *et al.*, 2002; Cebon; Winkler, 1990; Oubrich *et al.*, 2017; Oubrich *et al.*, 2018). These models can be utilized to generate simulations by applying their equations of motion and setting the relevant vehicle parameters and constants. In addition to the vehicle equation of motion, simulations might also consider the road surface profile and the vehicle speed. As proposed by Mangeas *et al.* (2002), the simplest model is a one-degree-of-freedom (1DOF) spring-damper system that treats the suspension and tire as a single block (Figure 3.2).

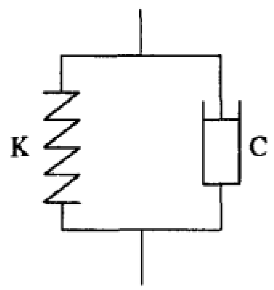


Figure 3.2 – Suspension/tire block model (Mangeas *et al.*, 2002).

The study conducted by Cebon and Winkler (1990) employed two other models to represent the vehicle dynamic system. The first model is the quarter-car model (Figure 3.3(a)), which is a 2DOF system. It accurately reproduces suspensions that generate a large low-frequency wheel force spectral peak due to the motion of the sprung mass. The second model is the walking-beam model (Figure 3.3(b)), which has 3DOF. It represents suspensions that generate large dynamic wheel loads due to the motion of the unsprung mass, particularly the lightly damped pitching of the walking-beam.

Furthermore, the longitudinal half-vehicle model of two axles was used by Oubrich *et al.* (2017) and Oubrich *et al.* (2018). This model is similar to the walking-beam model, but it has 4DOF. It considers body movements (rebound and pitch), axle (rebound), and the influence

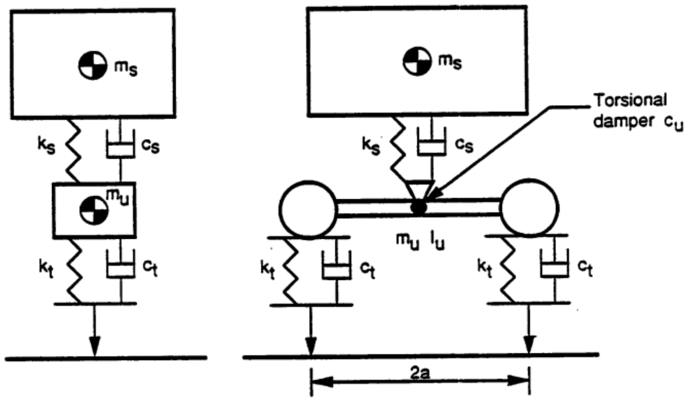


Figure 3.3 – Quarter-car model (a) and Walking-beam model (b) (Cebon; Winkler, 1990).

of gravitational forces (Figure 3.4).

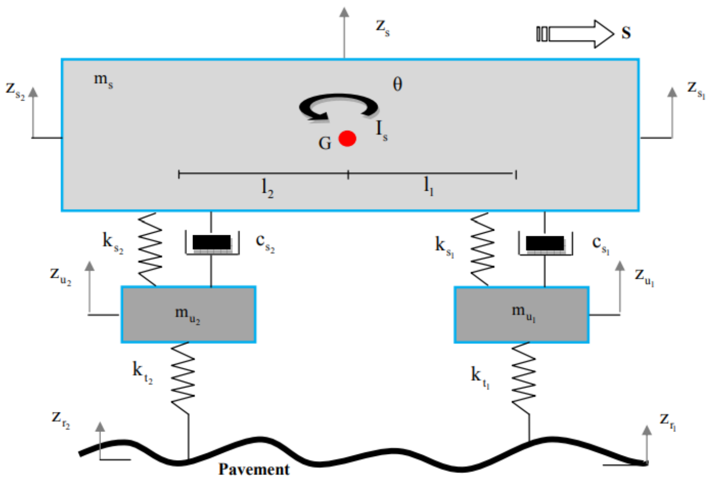


Figure 3.4 – Half longitudinal vehicle model (Oubrich *et al.*, 2017).

One of the most complete vehicle models was the non-linear two-dimensional vehicle model proposed by Cole and Cebon (1992). It represents a truck with four axles, two on the tractor and two on the trailer. This system includes non-linear leaf spring elements and has 11DOF. The sprung masses of the tractor and trailer were assumed to be rigid, and the influence of the trailer suspension radius arms was also included in the model.

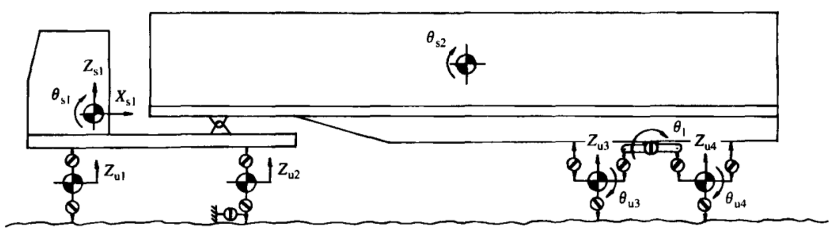

Figure 3.5 – Non-linear two-dimensional vehicle model with 11 degrees of freedom (Cole; Cebon, 1992).

It is important to note that the presented models are simplified and/or specific, and do not provide high-fidelity representations of the dynamics of all vehicle types in real-world scenarios (Cebon; Winkler, 1991). A significant challenge in these models lies in the vehicle parameters used, as they are typically not provided by vehicle manufacturers, and obtaining them experimentally is often impractical.

Several studies have conducted simulations using different vehicle models and surface road profiles (Oubrich *et al.*, 2017; Mangeas *et al.*, 2002; Cebon; Winkler, 1991; Cebon; Winkler, 1990; Oubrich *et al.*, 2018). These simulations allow the observation of dynamic mass variation across different road profiles (Figure 3.6). The waveforms observed in these studies exhibit a sum of sinusoidal signals, consistent with the theoretical signal proposed in Equation (3.1).

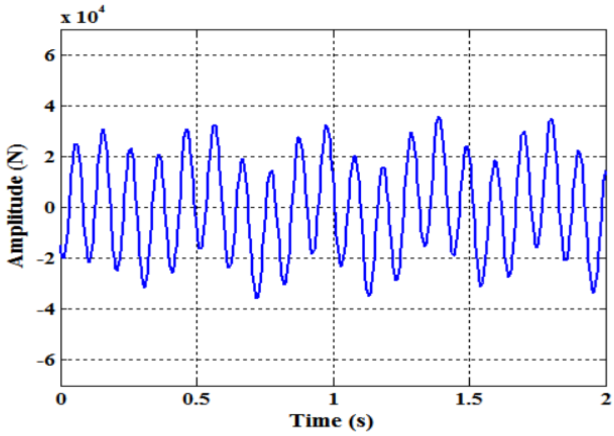


Figure 3.6 – Dynamic loads of the half longitudinal vehicle model traveling at 40 km/h (Oubrich *et al.*, 2017).

The study by Oubrich *et al.* (2017) employed the half-vehicle model of two axles to simulate dynamic load waveforms for two different road profiles and three different vehicle speeds per road profile. These simulations indicate that the dynamic loads experienced by the vehicle are significantly influenced by the vehicle speed, even when the road profile unevenness varies within the range of -1 cm to 1 cm. Based on this road profile, the conducted simulations reveal that a vehicle speed of 100 km/h exhibits oscillations twice as high as a speed of 70 km/h and six times higher than a speed of 40 km/h. In comparison to the static mass of the vehicle, the dynamic load variations range from 0% to 30% of the static load modulus (Oubrich *et al.*, 2017).

Another interesting analysis is to observe the frequency spectrum of this simulated signal. Research by Oubrich *et al.* (2017) and Cebon and Winkler (1991) has shown that the simulated signal exhibits two main frequency ranges: $f_1$ and $f_2$ (Figure 3.7). The frequency range $f_1$, typically around 1 to 5 Hz, corresponds to the dominant modes of the vehicle's sprung mass, including bounce and pitch movements. This frequency range is influenced by factors such as the vehicle's total mass, mass distribution, and suspension system characteristics. The frequency range $f_2$, approximately 8 to 15 Hz, is associated with the vehicle's unsprung mass parameters, primarily the tires and suspension components.

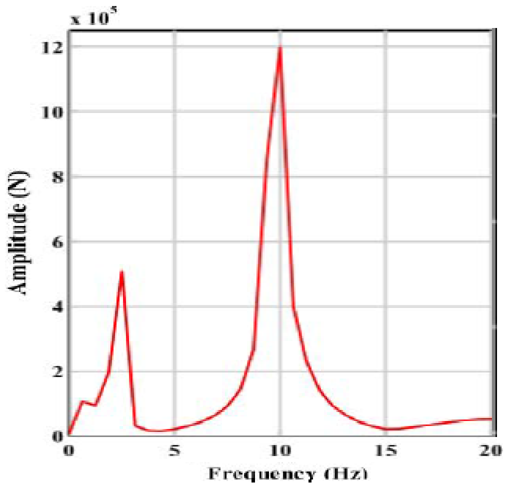


Figure 3.7 – Spectral density for the half longitudinal vehicle model traveling at 70 km/h, adapted from (Oubrich *et al.*, 2017).

Vehicle models are valuable tools for conducting preliminary studies at lower costs, eliminating the need for field measurements. However, since models offer only approximations of real-world systems, implementing high-precision WIM systems requires experimental measurements to ensure reliability and practical application.

### 3.1.2 Experimental Load Signal

To enhance the analysis of the dynamic load of a vehicle, field tests are conducted, with a primary focus on understanding the dynamic force signals in real-world conditions (Gajda *et al.*, 2015; Huhtala *et al.*, 2000; Cebon; Winkler, 1991; Ryguła *et al.*, 2021). Measuring the load signal of a moving vehicle is not a trivial task. The width of WIM sensors is generally smaller than half a meter, which is insufficient to capture the load signal for a significant duration, such as capturing the natural frequencies observed in simulation results (Oubrich *et al.*, 2017; Cebon; Winkler, 1991). Some studies have employed accelerometers to instrument the moving vehicle's wheels as it traverses the road. The sensor readings are then used to reconstruct the load signal of the vehicle (Gajda *et al.*, 2015; Huhtala *et al.*, 2000). Figure 3.8 displays the load signal of the driving axle across three vehicle passes in a single WIM system.

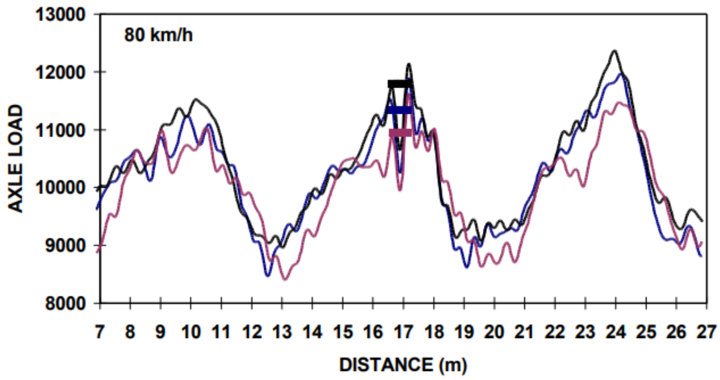


Figure 3.8 – Dynamic load of the driving axle over one WIM system, three vehicle passes (Huhtala *et al.*, 2000).

The frequency spectrum of the reconstructed signal obtained by Gajda *et al.* (2015) is presented in Figure 3.9. The spectrum observed from the real load signal is similar to the one observed in vehicle model simulations (Figure 3.7), exhibiting low-frequency components in the range of 1 to 4 Hz ($f_1$) and another peak at approximately 8 Hz ($f_2$). Although the tests conducted by Gajda *et al.* (2015) and Jacob (2001) focused on a specific type of heavy vehicle, various studies suggest that these two main frequencies, $f_1$ and $f_2$, typically fall within the ranges of 1 to 5 Hz and 8 to 15 Hz, respectively (Burnos *et al.*, 2007; Wang *et al.*, 2009; Jacob, 2001; Grakovski; Pilipovecs, 2018; Cole; Cebon, 1992).

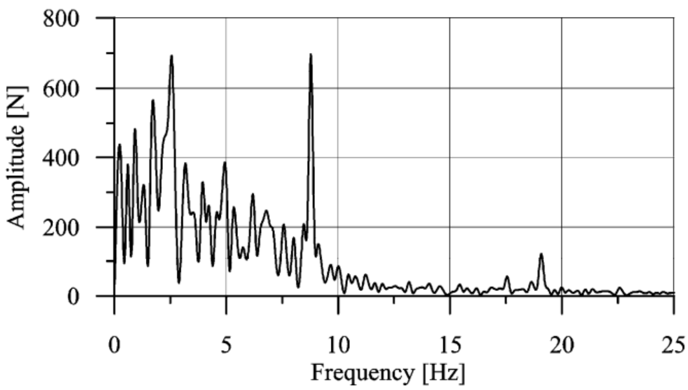


Figure 3.9 – Frequency spectrum of the dynamic load signal from the instrumented vehicle (Gajda *et al.*, 2015).

The analysis of vehicle load signals obtained at different speeds demonstrates that dynamic oscillations vary in amplitude as a function of the vehicle's speed. As indicated by the simulation results presented in Section 3.1.1, vehicle speed is expected to have a significant impact on load oscillation, and this impact has been demonstrated experimentally in the research by Jacob (2001) and Gajda *et al.* (2015). Figures 3.10 and 3.11 illustrate this effect, with variations in amplitude of up to 40% when compared to the static load (Jacob, 2001; Gajda *et al.*, 2015), exceeding those observed in simulations using vehicle models.

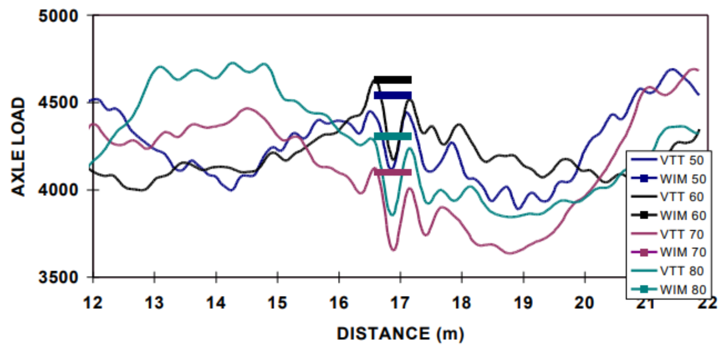


Figure 3.10 – Dynamic axle load of the steering axle at four speeds (Huhtala *et al.*, 2000).

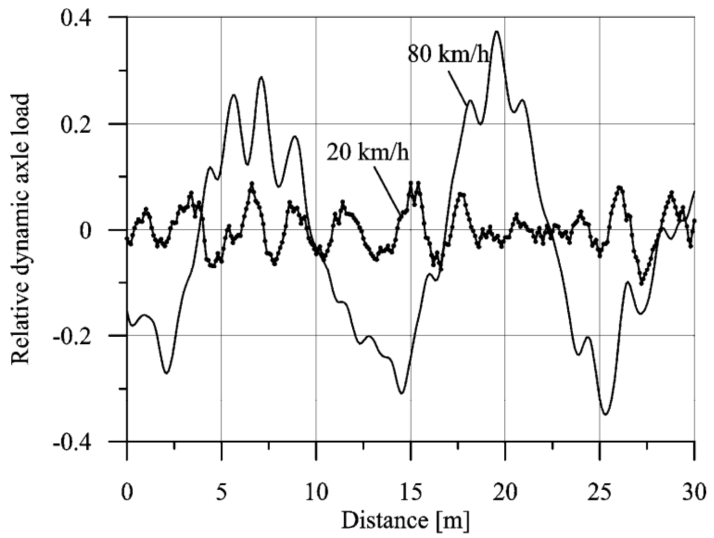


Figure 3.11 – Relative changes in the dynamic load of a single axle of the instrumented vehicle at two speeds as a function of the distance traveled (Gajda *et al.*, 2015).

It is important to note that WIM systems are typically installed on straight and level roads to minimize the influence of dynamic load generated by unevenness and curved road surfaces. However, the effect of vehicle speed on the dynamic load is beyond the control of WIM system designers. When installing these systems on regular highways, which generally have speed limits of at least 60 or 80 km/h for heavy vehicles, the accuracy of static weight estimation is inevitably impacted by the vehicle speed.

## 3.2 Axle Weight Estimation

Estimating the Gross Vehicle Weight (GVW) begins with the measurement of the individual axle weights. However, direct vehicle instrumentation using accelerometers or load cells is impractical for real-world applications where many vehicles must be weighed daily. Thus, weighing sensors are utilized to sample the force exerted by the vehicle as it passes over them.

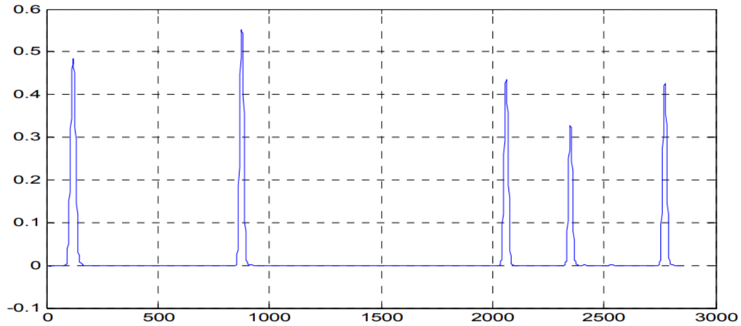


Figure 3.12 – Sensors' output when an empty truck passes it at 90 km/h (Grakovski *et al.*, 2013).

The WIM sensors convert the applied load into an electrical signal proportional to the force. This electrical signal is digitized and can be processed by a computer or other digital device, usually involving analog-to-digital converters (ADCs) and analog and digital signal processing techniques.

The digitized signal is then used to estimate a vehicle's instantaneous axle weight using algorithms. In the case of static scales, the read values are converted into static weight using a formula provided by the sensor's manufacturer, typically based on a linear curve. However, in Weigh-In-Motion (WIM) applications, the weight cannot be assumed as a constant value throughout the sensor reading due to the dynamic components of moving vehicles (Cebon; Winkler, 1991) and bandwidth of the sensors, as discussed in Sections 2.1 and 3.1, and to the fact that the vehicle tire footprint is generally larger than the sensor width. Consequently, the measured signal requires processing by an algorithm to estimate the instantaneous load of the axle accurately.

It is important to mention two vehicle parameters that directly influence the WIM signal: the vehicle speed and the tire footprint of the vehicle (Kwon, 2007). As discussed in Section 3.1, the vehicle speed affects the vehicle's oscillations and, from the sensor's perspective, determines the number of signal samples obtained by the sensor. Since the sensor width and the sampling rate of the analog-to-digital converter (ADC) component are typically constant, the number of samples obtained during a weighing operation is inversely proportional to the vehicle speed. Lower speeds result in wider curves, while higher speeds produce narrower curves (Kwon, 2007; Wang *et al.*, 2009).

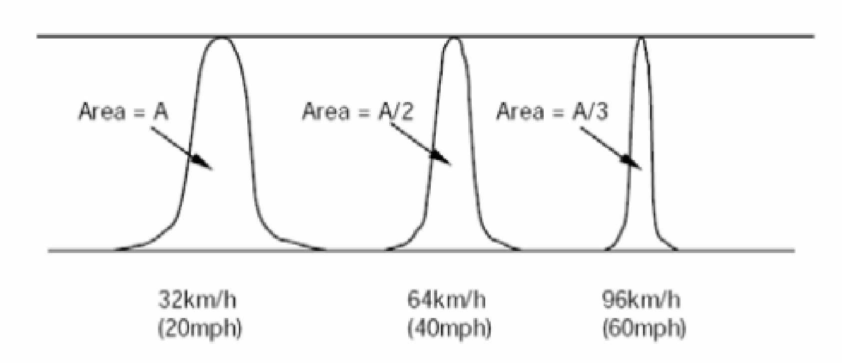


Figure 3.13 – WIM signal at different speeds (Kistler, 2004).

The vehicle tire footprint is another external factor that impacts the sensor's reading. The area of the tire footprint is determined by the tire width and the air pressure inside the tire. The sensor width is generally smaller than the tire footprint, especially for heavy vehicles with larger tires, which is the main focus of weight tracking on roads. Therefore, the peak of the WIM signal does not represent the entire wheel load but rather only a portion of the total load corresponding to the tire footprint in contact with the sensor (Figure 3.14). It is possible to see in Figure 3.15 the signal measured from a wheel with 4,500 N and different tire pressures (Kwon, 2007). It is worth noting that as the air pressure inside the tire decreases, the area of the footprint increases while the peak of the signal decreases, as can be seen in Figure 3.15. One crucial relationship between the measured signal and the tire footprint is that, although signal peak varies, the area under it remains constant across different tire pressures for the same vehicle (Kistler, 2004).

These effects must be considered by the weighing algorithms. While obtaining the air pressure inside the tire is challenging in WIM systems, determining the vehicle speed is relatively simple, especially in a multiple-sensor Weigh-In-Motion system (MS-WIM). By measuring the time difference between the same axle passing over two different sensors and knowing the distance between them, it is possible to calculate the approximate vehicle speed.

The challenge in evaluating these methods lies in determining the ground truth of the instantaneous axle load. The impact of the dynamic load at the moment the sensors take their measurements is unknown unless the vehicle is instrumented. This uncertainty reinforces one of the reasons why most Weigh-In-Motion systems employ several load sensors and incor-

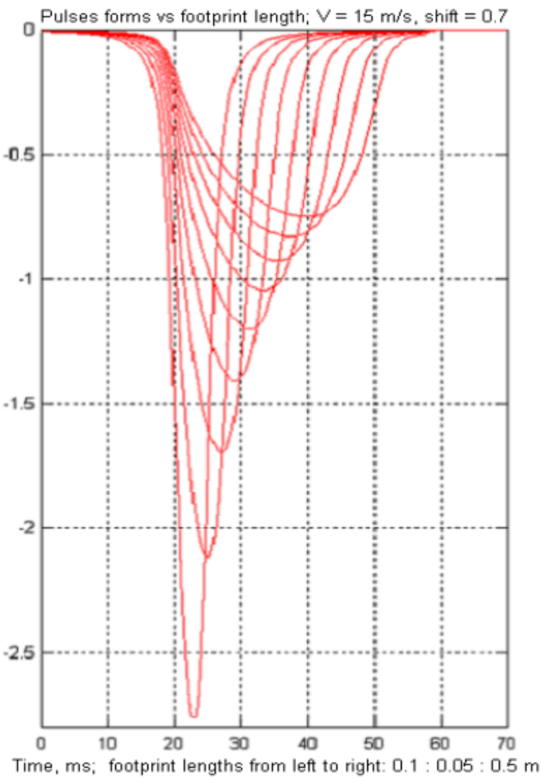


Figure 3.14 – Waveform of WIM signal vs footprint lengths (Grakovski *et al.*, 2013).

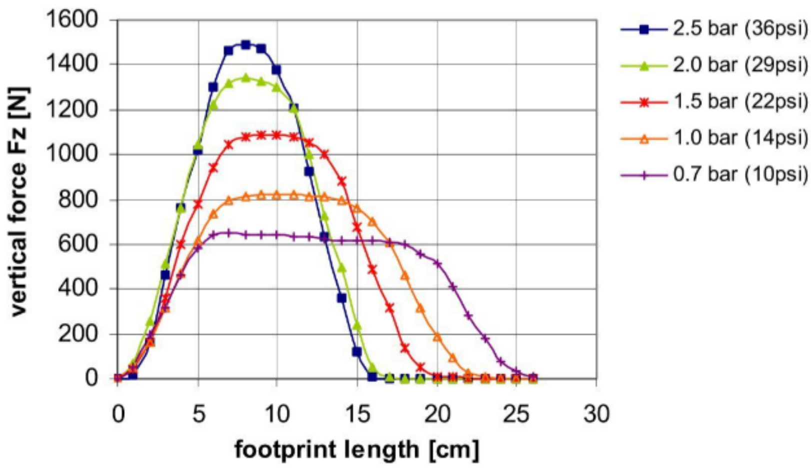


Figure 3.15 – Footprint lengths with different tire inflation pressure (Kistler, 2004).

porate some form of calibration procedure, typically involving the use of various vehicle types traveling at different speeds.

The correct estimation of the axle static weight impacts calculating the Gross Vehicle Weight (GVW); thus, this step is crucial for achieving an accurate and reliable WIM system. Below, an exploration of various methods documented in the literature for estimating axle weight based on the WIM signal is presented.

### 3.2.1 Basic Method

The Basic Method for calculating the weight of an axle over a sensor involves multiplying the wheel's contact area (tire footprint) on the sensor by the air pressure inside the tire (Grakovski *et al.*, 2014). In Equation (3.2), $W$ represents the weight of an axle or half-axle (depending on the system layout), $A_{\text{tire}}$ is the area of the wheel's footprint, and $P_{\text{tire}}$ is the air pressure inside the tire, which is proportional to the axle weight according to Newton's 3rd law:

$$W = A_{\text{tire}} \cdot P_{\text{tire}}. \tag{3.2}$$

The values required in Equation (3.2) are typically not directly measured in WIM systems. However, if the vehicle speed can be measured, as commonly implemented in MS-WIM systems, it becomes possible to estimate the tire footprint area using the length of the sensor output (usually, a voltage signal) and the vehicle speed. The tire width can be assumed as a fixed value based on the vehicle type. The air pressure inside the tire can be considered proportional to the peak amplitude of the WIM pulse (Figure 3.15) or even obtained from the manufacturer's recommendations for a given vehicle type (Batenko *et al.*, 2011b). While more sophisticated methods for estimating the parameters in Equation (3.2) are discussed in subsequent sections of this chapter, it is important to note that this fundamental method serves as the foundation for other methods employed in practical systems.

### 3.2.2 Peak Voltage

The Peak Voltage Method involves extracting the maximum value from the WIM signal. This peak value is then multiplied by a calibration coefficient ($\alpha$), which is determined through experimental measurements using a vehicle with a known weight. The resulting product provides an estimation of the axle or half-axle weight (Kwon, 2007; Kistler, 2004):

$$W = \alpha \cdot V_{max}. \tag{3.3}$$

Although the Peak Voltage Method is relatively insensitive to the vehicle's speed (Figure 3.13), it is important to note that the signal peak may not directly correspond to the actual wheel load. This discrepancy arises because the load sensor is typically only partially covered by the tire footprint, which is also unknown. Moreover, the peak voltage value is influenced by the air pressure inside the vehicle's tire, as different pressure values can significantly

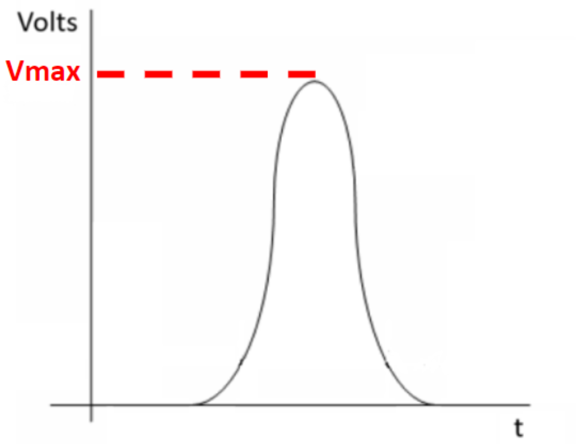


Figure 3.16 – Output signal of a single axle highlighting the signal peak, adapted from (Kwon, 2007).

impact the amplitude of the WIM pulse (Figure 3.15). Accurately measuring the air pressure inside the tire is often impractical in real WIM systems. Consequently, the precision of the Peak Voltage Method may be compromised without precise measurement and compensation of this parameter.

### 3.2.3 Area Under The Signal

This method involves integrating the signal measured by the sensor over the duration of contact between the vehicle's wheel and the sensor (Cebon; Winkler, 1991; Kwon, 2007; Kistler, 2004). The resulting area is then adjusted using the vehicle speed ($S$) and the calibration coefficient ($\alpha$), obtained during the calibration process:

$$W = \alpha \cdot S \int V(t)dt. \tag{3.4}$$

Measuring the vehicle speed is crucial for the reliability of this method since the speed directly affects the area of the WIM signal. As the vehicle's speed increases, the signal obtained from the sensor becomes narrower (Figure 3.13). In the calibration process, several runs are conducted with a pre-weighed vehicle at different speeds to enhance the accuracy of this method.

From a computational standpoint, the Area Under The Signal Method can be processed in real-time execution since it basically involves summing the sensor samples. Therefore, this algorithm is a convenient way to calculate the weight of the vehicle's axle, and it is widely employed by sensor manufacturers for WIM applications (Kistler, 2004).

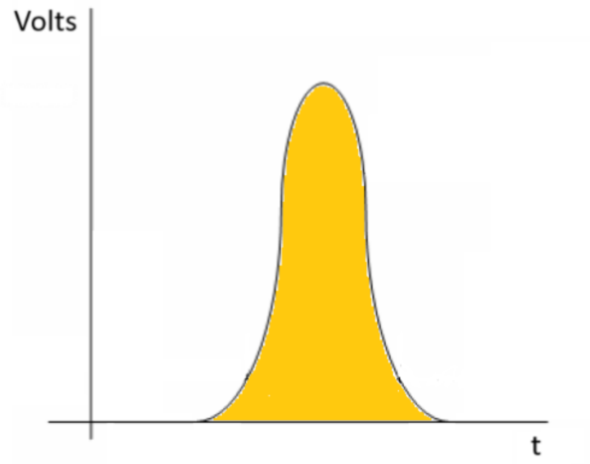


Figure 3.17 – Output signal of a single axle highlighting the signal area, adapted from (Kwon, 2007).

### 3.2.4 Re-sampling of Area

The Re-sampling of Area algorithm is proposed by Kwon (2007) as a method to enhance the accuracy of the Area Under The Signal technique. While the practical implementation of the Area Under The Signal method involves adding the digital samples of the load sensor and multiplying them by the sampling period, this approach can be fully accurate only if the sensor width is nearly zero, which is not the case in real-world applications. Consequently, the area under the signal curve does not accurately represent the wheel force applied to a single punctual region on the ground but rather a convolution of the wheel footprint load with respect to the sensor width.

To address the effect of the non-zero sensor width, Kwon (2007) proposes sampling the signal with a new period $T_L$, referred to as the re-sampling period, as shown in Equation (3.5):

$$T_L = L/S, \tag{3.5}$$

where $L$ represents the sensor width, and $S$ is the vehicle speed. It is worth noting that, although most measurement systems operate with fixed sampling rates, the re-sampling period calculated by Equation (3.5) can be achieved through downsampling techniques, such as discarding samples.

The algorithm suggests utilizing sensor samples with the period $T_L$ to prevent sample overlap. For instance, if a vehicle travels at 10 m/s and the load sensor has a width of 0.05 m, samples are obtained every 5 ms. This ensures that the area of the tire footprint over the sensor in one sample is outside in the next sample, effectively avoiding sample overlap.

Within the period $T_L$, sample points are determined, and the load is divided into $N$ slices, each with a width equal to the sensor width. The algorithm treats the weight of each slice independently and then combines them to calculate the total weight. The measurements for each slice ($V_j$) are summed and adjusted by the vehicle speed ($S$) and the calibration coefficient ($\alpha$), as shown in Equation (3.6):

$$W = \alpha \cdot S \sum_{j=1}^{N} V_j. \tag{3.6}$$

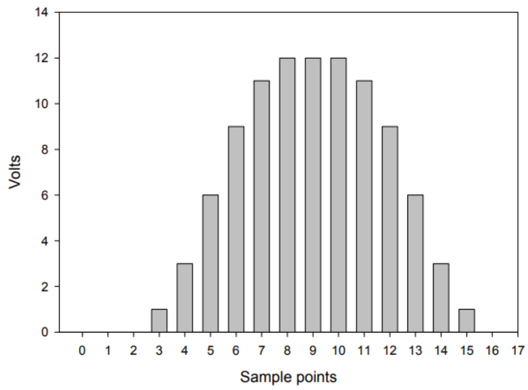


Figure 3.18 – Re-sampling of area signal example with $N = 13$ (Kwon, 2007).

The study by Kwon (2007) conducted numerical tests and simulations to evaluate the Re-sampling of Area Method. However, it should be noted that the study does not include the results of practical testing using real signals. Although the study indicates an improvement in accuracy compared to the area integral method, there is a need for further evaluation of this method.

### 3.2.5 Tire Footprint Reconstruction

The Tire Footprint Reconstruction Method is based on Equation (3.2). However, a new technique for estimating the area of the tire footprint is presented in the research Grakovski *et al.* (2014) and Grakovski *et al.* (2015). The authors employed fiber optic sensor (FOS) signals from a real WIM system to analyze the forces between the vehicle wheel and the road (or the sensor), decomposing the signal into its odd and even components.

This approach is based on the fact that the tire-road system can be modeled by considering the interaction between two forces: the friction forces and the vertical weight of the wheel (Figure 3.19). Thus, the waveform captured by weight sensors can be separated into its

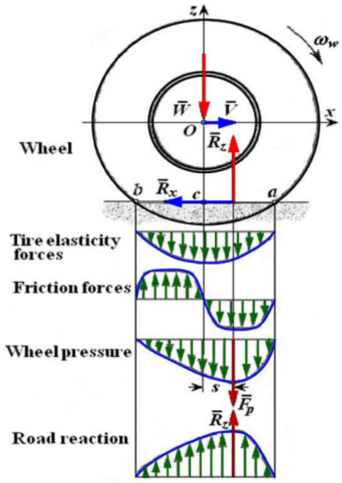


Figure 3.19 – Vertical and tangent components of forces in wheel's dynamics (Grakovski; Pilipovecs, 2017a).

vertical component, which corresponds to the weight of the static wheel (this component should be symmetrical according to the wheel geometry), and its tangential component, which represents the friction force and depends on factors such as pavement and wheel material properties, wheel speed, and weight (Grakovski; Pilipovecs, 2017a; Grakovski *et al.*, 2014) (Figure 3.20). The tangential component should have an asymmetric waveform.

The decomposition of the non-symmetric signal (Figure 3.20(a)) into its symmetric and asymmetric components can be achieved through polynomial approximation using the least squares method or by applying the standard even-odd decomposition of the signal with a finite window (Grakovski *et al.*, 2014).

The proposed technique for reconstructing the wheel footprint involves estimating the wheel's footprint using the footprint length, calculated by multiplying the pulse length by the wheel speed (i.e., vehicle speed) and an elliptical approximation based on the maximum and minimum points of the asymmetric component of the signal (Figure 3.21). This method assumes that the vehicle moves uniformly; thus, the friction force is as minimal as possible (rolling friction without sliding friction). The tire pressure used in Equation (3.2) is obtained using the Peak Voltage Method, and in combination with the footprint approximation, the axle or half-axle weight is calculated using the Basic Method (Grakovski *et al.*, 2014).

In Grakovski and Pilipovecs (2016), a different sensor layout was used to further enhance the estimation of the wheel footprint further, as illustrated in Figure 3.22(a). This layout involved installing a first group of sensors transversally on the road and a second group of sensors diagonally on the road. After appropriate calibration, this layout was capable of

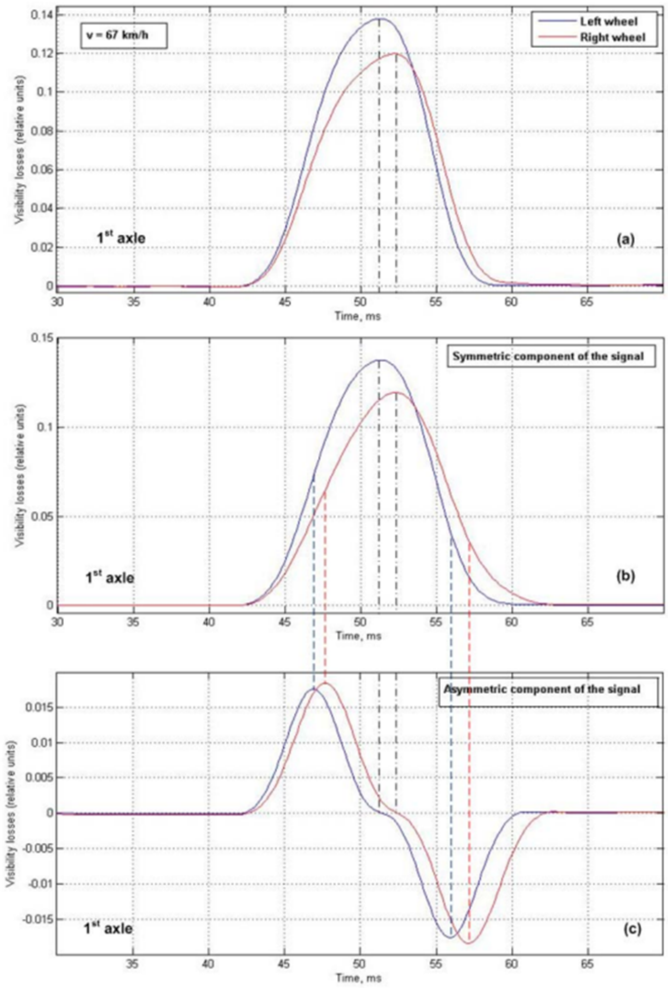


Figure 3.20 – (a) FOS output signal, (b) Approximated vertical weight component (symmetric), and (c) Approximated asymmetric component depending on horizontal velocity and friction (Grakovski *et al.*, 2014).

estimating the dynamic tire width of a vehicle by utilizing the difference in pulse width between transversal and diagonal sensors (Figure 3.22(c)).

The study presented by Grakovski and Pilipovecs (2017b) combined this layout with the footprint estimation technique described by Grakovski *et al.* (2014) and Grakovski *et al.* (2015) to calculate the half-axle weight of a vehicle using the dynamic area of the tire footprint and the tire pressure waveform, as presented in Equation (3.7). This weight calculation method is a hybrid approach incorporating elements of the Basic Method and the Area Under The Signal Method.

$$W = \int_{l_F}^{l_B} w(l)dl, \tag{3.7}$$

where $w(l) = A_{\text{tire}} \cdot P_{\text{tire}}$ is the weight distribution (Figure 3.23(b)) along the tire footprint length

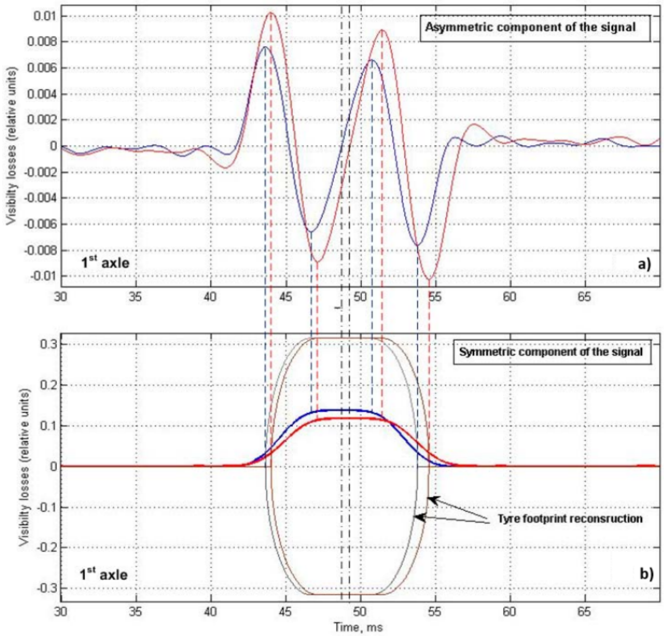


Figure 3.21 – (a) Approximated asymmetric component, and (b) approximated vertical weight component (symmetric) and tire footprint reconstruction in case of minimal friction condition (Grakovski *et al.*, 2014).

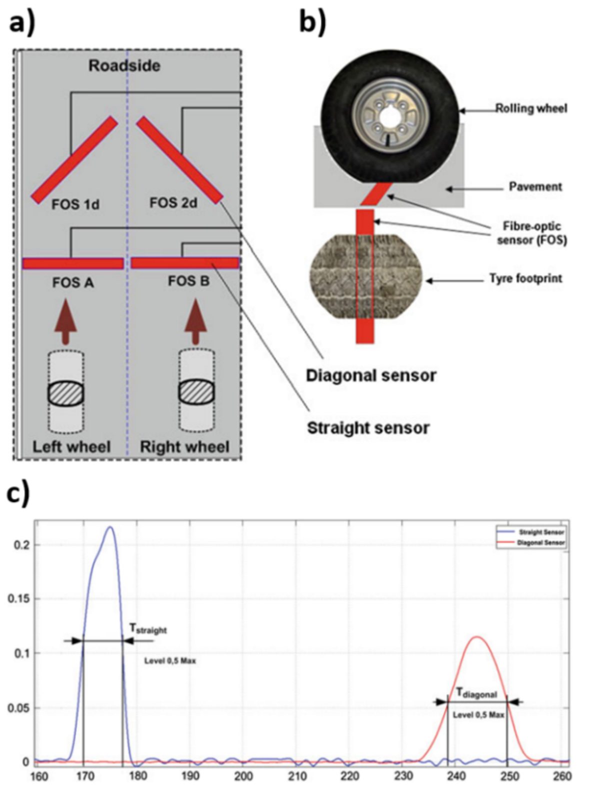


Figure 3.22 – (a) System layout, (b) Fibre optic sensors position against the vehicle wheel, and (c) Normalized and filtered signals of straight (FOS A) and diagonal (FOS 1d) sensors (Grakovski; Pilipovecs, 2016).

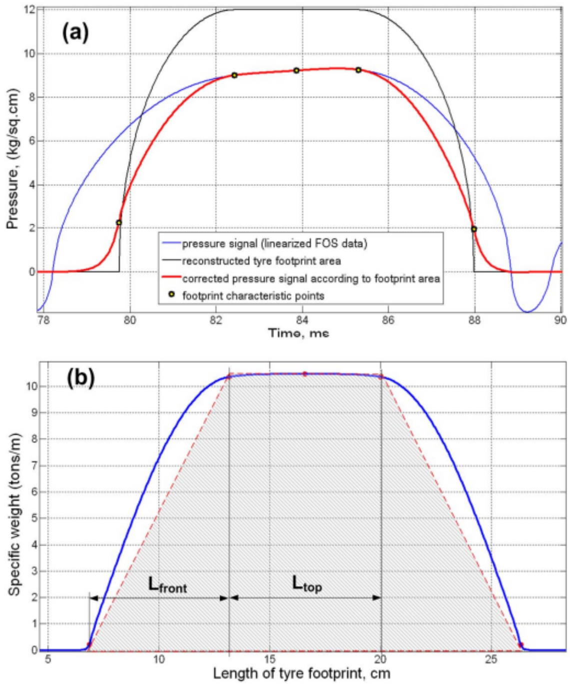


Figure 3.23 – (a) Reconstruction of air pressure distribution after linearization of FOS signal and dynamic tire width correction, and (b) estimated weight distribution along the tire footprint length(Grakovski; Pilipovecs, 2017b) .

($l = S \cdot t$, where $S$ is the vehicle speed). It should be noted that tire footprint estimation methods also involve a calibration process using a reference vehicle with known parameters (speed, tire width, etc.) (Grakovski; Pilipovecs, 2017b; Grakovski *et al.*, 2013; Grakovski *et al.*, 2014).

From a computational perspective, the algorithm for estimating the tire footprint is considerably more demanding than the previously mentioned methods due to the need for computationally intensive operations such as multiplication, division, and potentially even square root operations, depending on the implemented least squares algorithm for signal decomposition. This may be a challenge for WIM systems that must deliver weighing measurements in real-time, such as direct enforcement systems.

## 3.3 Gross Weight Estimation

The accurate determination of a Gross Vehicle Weight (GVW) poses a challenge due to various factors, including dynamic loads caused by the suspension system, vehicle speed, and road surface unevenness, as discussed in Section 3.1. It is evident from the load signals shown in Figure 3.8 that the instantaneous axle weight estimation may not represent the true static weight of the axle, depending on the time the load signal is sampled. The methods and algorithms for axle weight estimation presented in the previous section are unable to solve this problem, as the

WIM sensors are not wide enough to capture the vehicle's dynamic oscillation.

This section aims to explore techniques for mitigating the impact of dynamic components in the vehicle load signal by optimizing the number of sensors employed and determining the optimal sensor distance in the WIM system layout. Furthermore, the section explores statistical and AI-based data fusion methods to estimate the static load of a vehicle (GVW) based on the dynamic axle load data obtained through the approaches presented in Section 3.2. These estimation methods are commonly referred to as "estimators" (Gajda *et al.*, 2020).

### 3.3.1 System Layout Optimization

This phase involves determining the number of sensors to be used in the WIM system and their spacing based on vehicle parameters, such as its speed. The influence of these two variables on system accuracy has been discussed in several studies (Cebon; Winkler, 1991; Burnos *et al.*, 2007; Gajda *et al.*, 2015), and their proper definition can significantly enhance the accuracy of GVW estimation by reducing the impact of vehicle oscillations in the system's measurements.

To begin the analysis of WIM sensor layout, consider that the static axle load is computed as the simple average of axle load samples from successive sensors, while the Gross Vehicle Weight is the sum of these axle loads. Theoretically, if the number of sensors tends to be infinite, the average axle load would converge to the true static value, eliminating the impact of dynamic oscillations. However, optimizing the number of sensors used in WIM applications is necessary for economic reasons and real-time processing constraints (especially in direct enforcement systems). Additionally, optimizing the spacing between sensors is crucial as it enables sampling the moving vehicle load signal at different intervals, leading to a more reliable signal representation.

The relationship between the number of sensors and their spacing is impacted by vehicle speed. Vehicle speed influences the amplitude of the oscillations, as discussed in Section 3.1. Understanding this effect is essential to ensure system accuracy across various vehicles (frequencies) and speeds (Cebon; Winkler, 1991).

In the work presented by Cebon and Winkler (1991), simulations were conducted using the quarter-car model to evaluate different sensor spacings. The simulations considered a road profile characterized as a good road surface and vehicle speeds of 60 km/h and 100 km/h. Based on the results and mathematical analysis of the error coefficient of variation (ECOV), the authors proposed the following equation to find the best sensor spacing:

$$\Delta_{\text{D1}} = \frac{2(N-1)V}{fN^2}, \tag{3.8}$$

where $V$ represents the average traffic speed in meters per second, $N$ is the number of sensors, and $f$ is the frequency in Hz of the dominant spectral component. Equation (3.8) focuses on the first frequency range of the load signal spectrum (Figure 3.9), with a mean value typically around 2.5 - 3 Hz.

Moreover, the study conducted additional simulations using Equation (3.8) with different speeds and different numbers of sensors. The findings indicate that increasing the number of sensors allows the system to maintain accuracy over a broader speed range. The system's accuracy likely decreases as the vehicle speed deviates from the average value $V$.

Based on numerical and statistical assumptions, a new equation to calculate sensor spacing in WIM systems was proposed by Jacob (2001). Equation (3.9) considers the frequency of the load signal as two mean values in the spectrum ($f_1$ and $f_2$), consistent with the results obtained from simulations and experimental tests discussed in Section 3.1.

$$\Delta_{\text{D2}} = \frac{V}{2N}\left(\frac{1}{f_1} + \frac{N-1}{f_2}\right), \tag{3.9}$$

where $V$ represents the average vehicle speed, $N$ is the number of sensors, and $f_1$ and $f_2$ are the mean frequencies of the dynamic components of the load signal. The author Jacob (2001) highlights the significance of the ratio $f_2/f_1$. A system designed with a low $f_2/f_1$ ratio will require fewer sensors, making it more cost-effective compared to systems designed for higher $f_2/f_1$ ratios. However, the specific value of this ratio depends on the characteristics of the vehicles using the road, including their suspension and tire types, as well as the weights of their axles and bodies.

In the work presented by Gajda *et al.* (2015), the author employed the sensor spacing distance described by Equation (3.9) during the system design stage. Since different vehicle speeds generate different ideal sensor spacing according to Equation (3.9), one approach to address this variability is to estimate the ideal sensor spacing for maximum and minimum speeds and then interpolate a distance based on these assumptions (Gajda *et al.*, 2015).

Although Equation (3.9) considers both frequency ranges presented in the load signal spectrum (Figure 3.9), further simulations using this equation can be conducted to evaluate its performance, similar to Equation (3.8). Exploring different sensor distances in MS-WIM systems poses a challenge regarding experimental tests. Conducting such tests in real WIM sites is not feasible, as the sensors are generally installed in the pavement and cannot be easily moved.

### 3.3.2 Estimators

The methods discussed in Section 3.2 enable the WIM system to estimate a vehicle's instantaneous (dynamic) axle loads, depending on the number of sensors employed. When a vehicle with $N_a$ axles passes over an MS-WIM system with $N$ sensors, it generates $N_a \cdot N$ instantaneous weight results. These instantaneous axle load values are then used to estimate the corresponding static axle load using data fusion based on statistical or AI-based methods and algorithms. These estimation techniques, also known as Estimators, are employed to determine the total static weight of the vehicle (GVW), reducing random variability in the weighing results (Stergioulas *et al.*, 2000; Gajda *et al.*, 2020).

Estimators in MS-WIM systems can be applied in two distinct ways. Firstly, they can utilize the instantaneous load of individual axles measured by each sensor and combine these values into the static load of that axle. The GVW is then obtained by summing all static axle loads. Alternatively, estimators can use the sum of loads from all axles measured by each sensor and combine these sums results to estimate the GVW (Gajda *et al.*, 2020).

#### 3.3.2.1 Mean Value

The simplest approach to minimize random fluctuations in any data is to calculate the average of its samples (Stergioulas *et al.*, 2000; Gajda *et al.*, 2020). This method has been widely utilized in various WIM applications (Zhang *et al.*, 2007; Giacinto *et al.*, 2021; Cebon; Winkler, 1991; Ryguła *et al.*, 2021). The mean value, obtained by taking a simple average of the samples, is commonly utilized as:

$$N_{\text{mean}} = \frac{1}{N}\sum_{i=1}^{N} y_i. \tag{3.10}$$

In Equation (3.10), $N_{\text{mean}}$ represents the estimated value, which can be the estimated static load of a specific axle or the Gross Vehicle Weight (GVW), $N$ represents the number of load sensors, and $y_i$ represents the result of weighing a selected axle from the $i$-th sensor or the sum of all axle weighings from this sensor, depending on the chosen solution.

One interesting variation of this method is demonstrated by Gajda *et al.* (2020). Due to variations in technical specifications, installation processes, and sensor wear, successive sensors may exhibit discrepancies in their uncertainty levels. This uncertainty is quantified using the standard deviation, calculated from a dataset of measurements for the same axle under consistent conditions. The authors of Gajda *et al.* (2020) found that, after operating an MS-WIM system for two to three years, the standard deviation for the most and least reliable polymer sensors could differ significantly, often by a factor of two or three. The analysis examined the standard deviation of the measurement results using an exemplary MS-WIM system equipped with 16 piezoelectric load sensors. During experiments, three vehicles with known mass and static load on each axle repeatedly passed through the WIM station. The standard deviation for each load sensor was expressed relative to the mean value of the weighing results for each axle. Averaging across all test runs revealed significant divergence in the measurement uncertainty of sensors indicated by numbers 3 and 4 (Figure 3.24(a)).

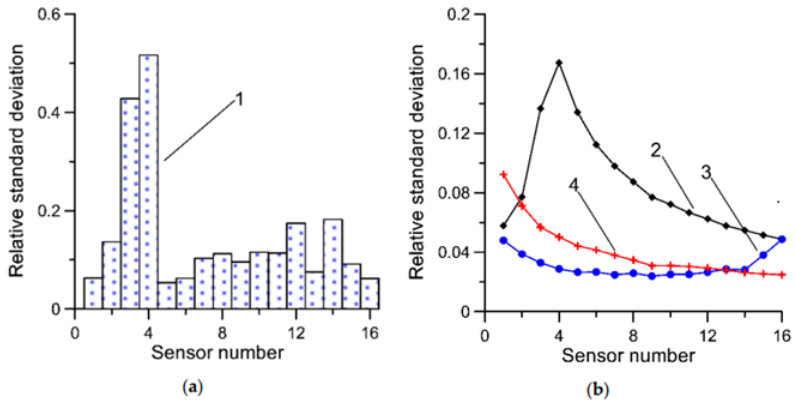


Figure 3.24 – (a) 1 — Standard deviation arbitrarily assumed for successive load sensors, and (b) 2 — averaging in the order in which the sensors are installed in the pavement, 3 — averaging in the order based on the increasing uncertainty of measurement for successive sensors, 4 – measurement uncertainty of all sensors is uniform ($\sigma = 0.1$) (Gajda *et al.*, 2020).

Considering that the measurement uncertainty is not the same for all sensors, one can calculate the result from Equation (3.10) using only the most precise sensors, i.e., sensors with the lowest uncertainty of measurement (curve 3 in Figure 3.24(b)). By considering only nine of the most precise sensors, the authors of Gajda *et al.* (2020) observed a slightly lower standard deviation than when using all 16 sensors (curve 2 in Figure 3.24(b)). Although this indicates a reduction in measurement uncertainty, monitoring individual sensor performance generates additional technical effort (Gajda *et al.*, 2020).

The subsequent section will present a comparative analysis of the Mean Value Estimator and the Maximum Likelihood Estimator (MLE) based on works found in the literature. This analysis is founded on simulations and field tests conducted at WIM sites.

#### 3.3.2.2 Maximum Likelihood Estimator

The Maximum Likelihood Estimator (MLE) has been explored in several studies (Gajda *et al.*, 2020; Stergioulas *et al.*, 2000; Burnos *et al.*, 2007; Jacob, 2001). This technique combines measurement data with expert knowledge gained from experience (Gajda *et al.*, 2020). In an MS-WIM system, the MLE algorithm leverages statistical assumptions and prior information, including the standard deviation of individual sensor measurements, to formulate the likelihood function (Burnos *et al.*, 2007; Jacob, 2001; Gajda *et al.*, 2020). Given the sought value, this function quantifies the probability of obtaining measurement results that align with the model. The key concept of a Maximum Likelihood Estimator involves searching for the sought value at which the likelihood function reaches its maximum value (Gajda *et al.*, 2020).

Assuming the statistical independence of measurement results from multiple sensors, the following equation can be formulated:

$$y_i = N_c + \varepsilon_i, \tag{3.11}$$

where $y_i$ represents the result of weighing a selected axle from the $i$-th sensor or the sum of all axle weighings from this sensor, $N_c$ represents the sought value, which depends on the solution adopted for $y_i$, and $\varepsilon_i$ represents the random additive component, $i = 1, 2, \ldots N$ (the number of load sensors).

Practical application of the maximum likelihood algorithm requires knowledge of the probability distribution of $\varepsilon_i$. Considering a normal distribution of this random component, the following likelihood function is obtained (Gajda *et al.*, 2020):

$$p(y_1, y_2, ...y_N/N_c) = \prod_{i=1}^{N} \left( \frac{1}{\sqrt{2\pi\sigma_i}} e^{-\frac{(y_i - N_c)^2}{2\sigma_i^2}} \right) = \left( \frac{1}{\sqrt{2\pi\sigma_i}} \right)^N e^{-\sum_{i=1}^{N} \frac{(y_i - N_c)^2}{2\sigma_i^2}}. \tag{3.12}$$

The likelihood function is maximized when the sought value is given by Equation (3.13):

$$N_{\text{MLE}} = \frac{\sum_{i=1}^{N} \frac{y_i}{\sigma_i^2}}{\sum_{i=1}^{N} \frac{1}{\sigma_i^2}}, \tag{3.13}$$

where $\sigma_i$ indicates the standard deviation of $\varepsilon_i$. When the measurement uncertainty is uniform for all load sensors, Equation (3.13) simplifies to the mean value of the results obtained from individual sensors. However, when the uncertainty varies among load sensors, the measurement results from each sensor are given different weights based on their respective uncertainties (Gajda *et al.*, 2020). It should be noted that the likelihood function described by Equation (3.12) can vary depending on the statistical assumptions and prior information used.

Numerical experiments conducted by Stergioulas *et al.* (2000) and Jacob (2001) compared the Maximum Likelihood Estimator with the Mean Value Estimator using different vehicle models. Simulations were performed with a 1DOF spring-damper model, a quarter-car model (2DOF), and a walking-beam vehicle model (3DOF), varying the number and spacing of sensors. The results showed that the MLE method is not significantly affected by the resonant frequency of the vehicle model or speed variations over a wide range of sensor spacings in both noiseless and noisy cases. However, the relative benefits of MLE are diminished in the presence of higher noise levels, as the performance of both the mean and MLE methods becomes similar. Another study evaluated the performance of the MLE using an MS-WIM system equipped with piezoelectric strip sensors (Burnos *et al.*, 2007). A pre-weighed vehicle with a constant GVW underwent 21 passes at different speeds. The Maximum Likelihood Estimator's results were compared with those of the Mean Value Estimator to assess the WIM accuracy. The two methods yielded similar results, with the MLE demonstrating slightly better performance (Figure 3.25).

In addition, another comparative analysis was conducted by Gajda *et al.* (2020) using the Mean Value Estimator and the MLE while considering different numbers of sensors. Three pre-weighed vehicles completed a total of 147 runs at the WIM site. The authors concluded that the MLE marginally outperforms the Mean Value Estimator when the number of sensors exceeds 10.

While the MLE method effectively reduces random variability and improves accuracy, it is important to acknowledge its limitations. As WIM systems typically employ a limited number of sensors, achieving the asymptotic properties of the MLE estimator may be challenging (Burnos *et al.*, 2007; Gajda *et al.*, 2020). However, evidence suggests that the MLE method remains justified and accurate even when applied to systems equipped with a moderate number

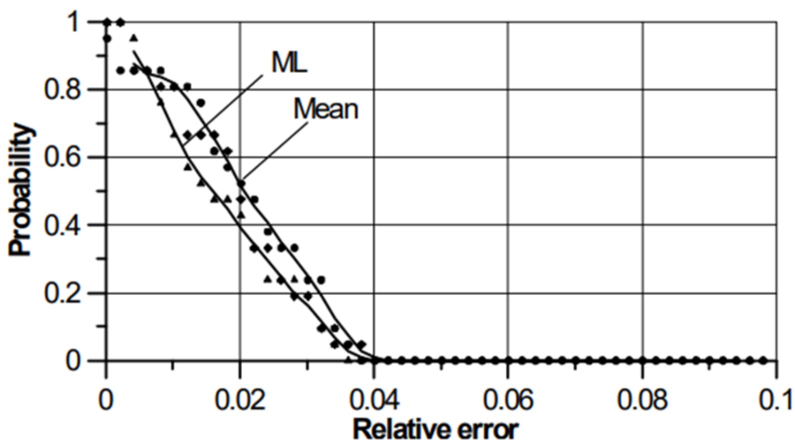


Figure 3.25 – Reliability characteristic of the WIM system. These characteristics correspond to different algorithms of gross weigh estimation: mean value of the measurement results of separate sensors and Maximum Likelihood Estimator (Burnos *et al.*, 2007).

of sensors, such as 8-10 load sensors (Gajda *et al.*, 2020; Jacob, 2001).

Moreover, the MLE method's dependence on the knowledge of each sensor's uncertainty (standard deviation) poses another practical limitation. This information can be acquired by gathering data from individual sensors through multiple passes of a pre-weighed vehicle. Data from previous periodic calibrations can further improve the calculation of the uncertainty of individual sensors (Gajda *et al.*, 2020).

#### 3.3.2.3 Signal Reconstruction

Signal reconstruction techniques typically involve reconstructing a signal from discrete samples obtained from the original signal. They have been widely explored in applications such as image reconstruction, signal processing, and AI algorithms (Oyamada *et al.*, 2018; Haupt; Nowak, 2006; Jonscher *et al.*, 2014; Nagahara, 2015). These methods have also been applied to various types of measurement systems that depend on sensor readings (Jonscher *et al.*, 2014; Yang *et al.*, 2023b; Yang *et al.*, 2023a).

In the context of Weigh-In-Motion systems, signal reconstruction involves reconstructing the original load signal from individual weight samples obtained from load sensors (Oubrich *et al.*, 2018). The reconstructed signal can then be used to estimate the static load of the vehicle, e.g. by calculating the average of its samples.

Common techniques used for signal reconstruction, particularly when dealing with signals of limited bandwidth, include the Inverse Fourier Transform (IFT), the Adaptive weights

Conjugate gradient Toeplitz (ACT), and Lagrange Polynomial Interpolation (Oubrich *et al.*, 2018). The IFT method requires the sampling stage to adhere to the Nyquist-Shannon theorem, which can be difficult to achieve across a broad speed range with a single system layout. The ACT algorithm, although accurate, demands the estimation of the signal bandwidth. Overestimating this parameter may lead to high-frequency noise in the reconstructed signal. In this context, the study by Oubrich *et al.* (2018) proposed using interpolating methods, which often do not require prior information about the signal and can be applied to irregularly sampled time series. Specifically, they employed Lagrange Polynomial Interpolation, adding the Tchebyshev conditions, a modification expected to mitigate extreme errors in signal reconstruction.

This study conducted simulation tests using the half longitudinal vehicle model and 10 load sensors. The evaluation criterion for signal reconstruction quality was the relative error between the original and reconstructed signals. The Lagrange Polynomial Interpolation technique exhibited a relative error of 2% at low speeds (20 km/h) and 0.54% at high speeds (100 km/h), demonstrating robustness across a broad range of vehicle speeds.

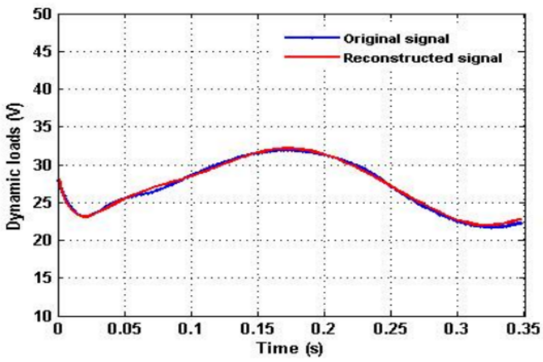


(a) Vehicle speed = 20 km/h.

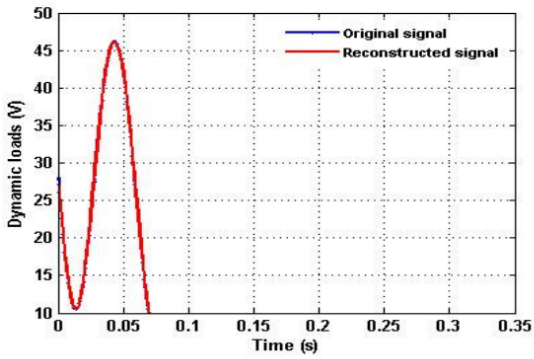


(b) Vehicle speed = 100 km/h.

Figure 3.26 – Axle load reconstructed signals at different speeds (Oubrich *et al.*, 2018).

The authors Oubrich *et al.* (2018) also point out that the Lagrange Polynomial Interpolation may not be an appropriate algorithm to apply when the polynomial approximation degree is higher than three, as the Runge's phenomenon occurs, resulting in oscillations at the edges of the interpolation interval.

Signal reconstruction and interpolation techniques have yet to be extensively explored in WIM systems, particularly for estimating vehicle weight. Further research is necessary to evaluate the advantages and limitations of various signal reconstruction methods in WIM systems, focusing on their accuracy and reliability across different scenarios.

#### 3.3.2.4 Neural Networks

Methods based on neural networks (NN) have emerged as a powerful approach for data fusion in non-linear systems, including MS-WIM systems, demonstrating significant advancements in accuracy and performance. Several studies have investigated the application of neural networks in this context (Mangeas *et al.*, 2002; Jia *et al.*, 2019; Lin *et al.*, 2017; Lin *et al.*, 2014; Lin *et al.*, 2017). Neural networks use interconnected layers of nodes, known as neurons, to process input data and generate predictions for individual axle weights or the GVW. By training on large datasets and optimizing their internal weights, neural networks can capture complex patterns and relationships between sensor measurements and true values, resulting in more accurate estimations (Dornfeld; DeVries, 1990; Maxwell *et al.*, 2021).

The fusion of multiple WIM sensors using neural networks, as explored by Mangeas *et al.* (2002) and Jia *et al.* (2019), improves the estimation of axle weights, particularly in non-linear modeling scenarios. The method presented in Mangeas *et al.* (2002) consists of learning how to estimate efficiently static weight, axle by axle, using a Feedforward Neural Network (FNN) with simulated data from a simple suspension model (1DOF). This approach is shown to be more accurate than traditional linear regression methods (Ono, 2003; Izadmehr; Lee, 1987) commonly used for sensor fusion. In the study Jia *et al.* (2019), the authors designed a Backpropagation Neural Network (BPNN) for signal classification and prediction, improving accuracy by identifying ideal samples acquired by load sensors closest to the tire-pavement contact area. These selected samples were then used to estimate the GVW using another BPNN. Experimental results using real road traffic data show that 96.9% of the analyzed samples had a relative error of less than 5% (Jia *et al.*, 2019).

Furthermore, the studies of Lin *et al.* (2014) and Lin *et al.* (2017) have explored Neural Networks in the GVW estimation. The research by Lin *et al.* (2014) utilizes Prior Knowledge and Neural Network Ensembles (PKNNEs) in neural network-based truck weight estimation. Simulation experiments showed that incorporating prior knowledge into neural networks improved their ability to generalize and compensate for weighing errors using different training sets. When comparing PKNNEs with SPKNNs (Supervised Prior Knowledge Neural Networks), PKNNEs outperformed SPKNNs in this particular case. In the research by Lin *et al.* (2017), a neural network was optimized based on input-vector correlation and prior knowledge of the truck scale. This approach improves the neural network's generalization performance, mainly when training samples are limited.

While neural network-based methods offer promising results for Weigh-In-Motion estimation, they come with certain limitations. As mentioned by Jia *et al.* (2019), these methods' accuracy relies heavily on training data. This implies that the training dataset's quality and the number of samples are critical factors in achieving accurate estimations. The study of Lin *et al.* (2017) proposed a method to improve the NN's generalization ability in the case of a lack of samples. Moreover, it is crucial to maintain optimal performance to regularly retrain these network models with new data to adapt to changes in the system and environment.

Another challenge lies in the regulatory approval of systems employing neural network methods in different countries. Regulatory agencies require thorough validation and testing procedures to ensure system reliability and consistency. Given the variations in results based on different training datasets, obtaining regulatory approval for these methods can be complex and, in some instances, unachievable due to jurisdictional constraints.

## 3.4 Considerations

In this chapter, we provided an in-depth review of key aspects related to weight estimation methods in Weigh-In-Motion systems, including dynamic loads, instantaneous axle load estimation, and Gross Vehicle Weight estimation.

The exploration of dynamic loads involved an examination of theoretical load signals, vehicle model simulations, and experimental data. This analysis provides valuable insights into the complexities involved in dynamic estimating Gross Vehicle Weight. The precision of WIM systems is directly impacted by dynamic loads, potentially resulting in inaccurate weight estimations. Factors such as vehicle mechanical characteristics, road surface conditions, and vehicle speed are the primary sources of impact in dynamic loads.

Moreover, this chapter presented various methods and algorithms for axle weight estimation found in the literature. The examined methods and algorithms each possess their own set of advantages and disadvantages, depending on factors such as vehicle speed compensation, tire footprint estimation, the necessity of employing calibration procedures, and required computational processing power. Some techniques, such as the Peak Voltage Method and the Area Under The Signal Method, offer practical implementation due to their relative mathematical simplicity. However, the Peak Voltage Method is susceptible to variations in air pressure within the vehicle tire, which may be challenging to measure in practical situations. On the other hand, the Area Under The Signal Method is influenced by vehicle speed, a parameter easy to measure in MS-WIM systems. Techniques employing Tire Footprint Reconstruction demonstrate potential for improving axle load estimation. While they may involve additional computational steps, these operations are generally manageable for modern computing systems, given their high processing capabilities.

Instantaneous axle weight measurements provide a means to estimate the Gross Vehicle Weight (GVW). This work explored some estimation methods, also known as estimators. The simplest and most used method is the mean value calculation. Another approach to estimate the GVW is based on the Maximum Likelihood Estimator. This approach has shown minor improvements over the Mean Value Estimator when the number of sensors employed in the system is above 10. In addition to statistical approaches, neural networks and signal reconstruction techniques have been mentioned, although they are not yet widely implemented in WIM systems. Adjusting parameters such as the number of sensors and sensor spacing for a given vehicle speed range aims to mitigate the influence of dynamic loads, as sensor measurements may struggle to estimate the static vehicle weight when the oscillating load is at its maximum and minimum values.

There is a research gap in comparing various instantaneous axle weight estimation methods under similar conditions. Some of these methods remain untested with real-world data, highlighting the need for validation to ensure their efficacy in practical applications. Several studies are conducted exclusively through simulations due to the complexity and costs associated with experimental tests. Conducting simulations under diverse conditions, including varying vehicle speeds and sensor configurations, can enhance the understanding of the relationship between the number of sensors, their spacing, and the system's accuracy. Exploring different GVW estimators using simulated data offers an opportunity to evaluate their performance and robustness across different scenarios, which may be otherwise impracticable in experimental sites. However, simulations do not eliminate the need for experimental tests and validation to ensure the reliability of these systems in direct enforcement applications.

# 4 METHODOLOGY

This work centers on vehicle Weight-in-Motion estimation techniques, organizing them into two stages: firstly, the estimation of instantaneous axle weights using algorithms applied to signals obtained by force sensors; and secondly, the estimation of the Gross Vehicle Weight (GVW) through techniques commonly known as estimators, which calculate the static load based on previously obtained measurements of instantaneous axle loads. This chapter presents the methodological procedures for investigating these techniques using both simulated and experimental data.

The simulations were used to analyze system layout (number of sensors and sensor spacing) while varying vehicle parameters, such as vehicle speed and axle spacing. Subsequently, simulations were developed to evaluate the estimators detailed in Section 3.3.2, using the most appropriate system layouts previously analyzed, while also varying vehicle parameters. Then, the experimental study conducted at a real WIM site is described, detailing system layout, vehicle characteristics, number of runs, and other relevant factors. This study used field data to assess instantaneous axle load estimation techniques detailed in Section 3.2.

## 4.1 Simulation

Simulations were conducted in MATLAB to evaluate system performance, specifically the accuracy and precision of static axle or vehicle weight (GVW) estimation. Figure 4.1 shows a diagram describing the simulation design. This simulation allowed us to analyze the influence of various vehicle and system parameters:

1. Vehicle parameters: frequency and amplitude of vertical oscillations, speed, number of axles, and axle spacing;

2. System parameters: number of sensors and sensor spacing.

This work employed Equation (3.1) with $M = 2$ to generate the dynamic load signal for vehicle simulation. Figures 3.8, 3.10, and 3.11 present the dynamic load of a real vehicle, resembling a sum of sine waves with two main low-frequency oscillations, as expected given the frequency spectra shown in Figures 3.7 and 3.9. This indicates that Equation (3.1) with $M = 2$ is a reasonable approximation of the dynamic load signal (Ono, 2003; Burnos *et*

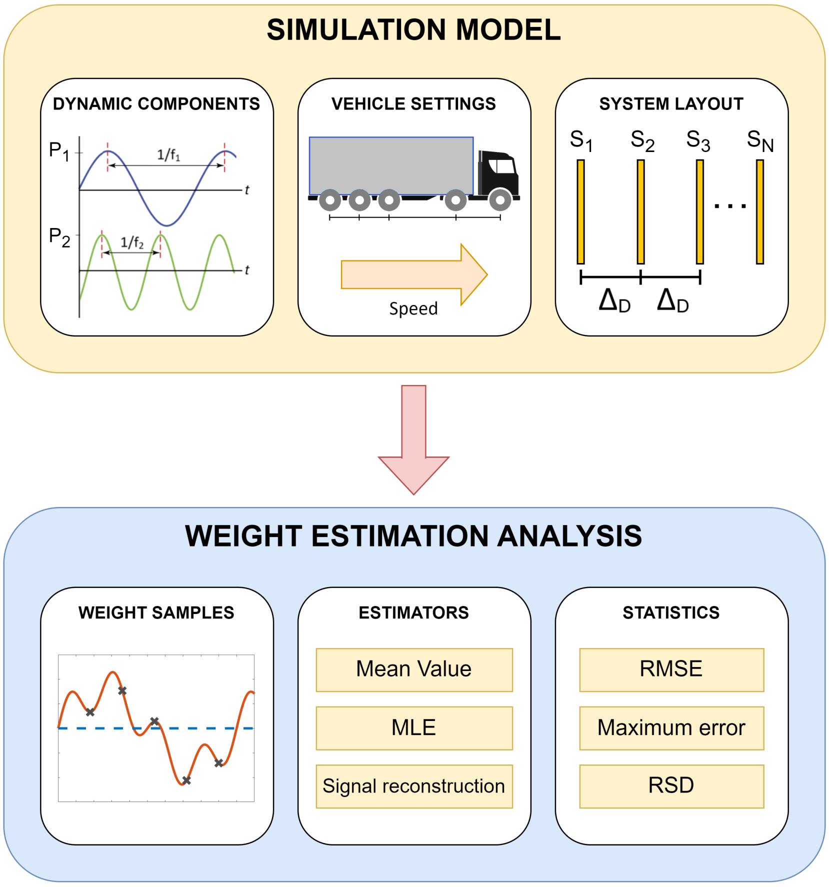


Figure 4.1 – Simulation process using proposed methodologies.

al., 2007; Gajda *et al.*, 2015). While vehicle models from Section 3.1.1 offer a more complete method for generating dynamic load signals, their application can be impractical due to the difficulty in obtaining vehicle parameters, especially when analyzing a variety of vehicles.

The load signal with $M = 2$ is a sinusoidal wave with two frequency components, $f_1$ and $f_2$. Frequency analysis conducted through simulations with vehicle models and real-world data highlights the concentration of spectral density in two primary ranges: 1-5 Hz and 8-15 Hz (Cebon; Winkler, 1991; Huhtala *et al.*, 2000; Oubrich *et al.*, 2017). The values of $f_1$ and $f_2$ were treated as uniformly distributed variables within the ranges of 1-5 Hz and 8-15 Hz, respectively. Additionally, the load signal had a random phase between 0° and 359° to simulate different weighing scenarios, with load signals from axles of the same vehicle sharing the same phase.

It is important to note that a limitation of using Equation (3.1) lies in the amplitude of the two sinusoidal components, which may vary depending on the vehicle speed and road surface (Huhtala *et al.*, 2000; Gajda *et al.*, 2015; Oubrich *et al.*, 2017). Simulating this phenomenon accurately poses a challenge. To address this, we considered the amplitudes of the sinusoidal components ($P_1$ and $P_2$) as being linearly related to vehicle speed. The authors of Huhtala *et al.* (2000) conducted tests with a three-axle vehicle equipped with strain gauges and accelerometers to estimate the dynamic load of the vehicle at various speeds. Using this data, it is possible to estimate the impact of the dynamic component relative to the static axle loads for each vehicle speed. Considering data from the three vehicle axles, an approximation of the dynamic load amplitude compared to the static axle loads was obtained, as shown in Table 4.1.

Table 4.1 – Relative dynamic load amplitude according to vehicle speed (obtained from (Huhtala *et al.*, 2000)).

| **Vehicle Speed [km/h]** | **Relative Dynamic Load** |
|---|---|
| 50 | 0.15 |
| 60 | 0.18 |
| 70 | 0.21 |
| 80 | 0.25 |

The relative dynamic load amplitudes in Table 4.1 focus on the vehicle's sprung mass, i.e., the first dynamic load component ($f_1$). Using this data, the impact of speed on the amplitude of the first dynamic component was estimated using the linear regression method. The linear regression is defined by Equation 4.1:

$$y = 0.0033x - 0.017. \tag{4.1}$$

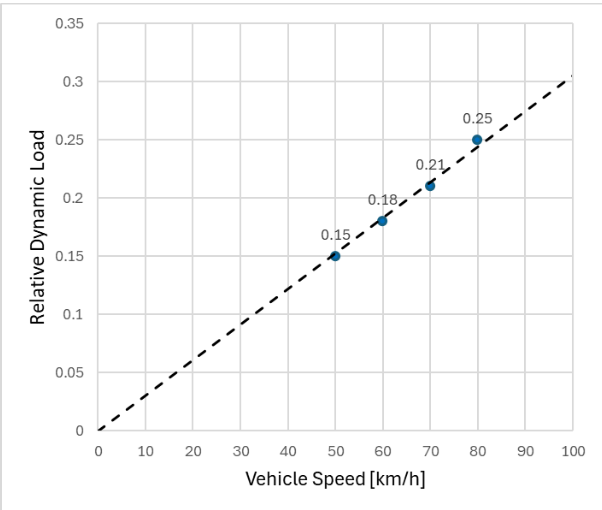


Figure 4.2 – Linear regression of the relative dynamic load (Y-axis) and vehicle speed (X-axis).

The amplitude of the second dynamic component ($f_2$), corresponding to the vehicle's unsprung mass, is considerably smaller than the first. As it would be challenging to measure its precise impact in the load signals obtained by Huhtala *et al.* (2000), the amplitude of this component was considered to be one-fifth of the first dynamic component's amplitude, a reasonable approximation given the signals from Figures 3.10 and 3.11.

It is worth noting that our simulation exclusively addressed the impact of longitudinal oscillations in vehicle load, given that transverse oscillations are typically smaller and mitigated by measuring the whole axle load (Grakovski *et al.*, 2013; Grakovski; Pilipovecs, 2017a). Therefore, our simulation treated the load sensor as an ideal zero-width sensor and a singular element for both vehicle wheels, measuring the overall axle weight. This implies that the entire axle load was represented by a single point of the load signal at the corresponding sensor position. Consequently, the techniques to estimate the instantaneous axle load from the sensor signal, described in Section 3.2, were not evaluated through this simulation.

The most recent legislation from INMETRO, the National Institute of Metrology, Standardization, and Industrial Quality in Brazil, defines the methodology to test WIM systems (Instituto Nacional de Metrologia, Qualidade e Tecnologia (INMETRO), 2022). These tests involve employing four vehicle types, with each vehicle being tested 15 times within the minimum, maximum, and average speeds of the system's operational speed range. This work utilized these definitions as a basis to conduct the simulation tests. However, instead of using only the minimum, maximum, and average speed values, we chose to use a more gradual range of speed variations to further understand their impact on static load estimation.

The four vehicle categories employed in simulations were 3C, 2S3, 3I3, and 34D, as illustrated in Figure 4.3. Tables 4.2, 4.3, 4.4, and 4.5 show the axle load and the distance between the axles for the vehicles 3C, 2S3, 3I3, and 34D, respectively. Each axle distance is calculated relative to the first axle.

Table 4.2 – Axle load and distances of the 3C vehicle.

| **Vehicle Axle** | **Axle Load [kg]** | **Axle Position [m]** |
|---|---|---|
| 1 | 6000 | 0 |
| 2 | 6750 | 3 |
| 3 | 6750 | 4.5 |

A vehicle with $N_A$ axles passing over a system with $N$ sensors generates $N_A \cdot N$ weight samples. These samples are then used to estimate the static load of individual axles and the Gross Vehicle Weight (GVW). The estimated load values are compared to the known static values (Tables 4.2 to 4.5), and statistical data are calculated to assess the system precision and accuracy, including root mean square error (RMSE), maximum relative error, and relative standard deviation (RSD).

Table 4.3 – Axle load and distances of the 2S3 vehicle.

| Vehicle Axle | Axle Load [kg] | Axle Position [m] |
|---|---|---|
| 1 | 6000 | 0 |
| 2 | 10000 | 3 |
| 3 | 8500 | 7 |
| 4 | 8500 | 8.5 |
| 5 | 8500 | 10 |

Table 4.4 – Axle load and distances of the 3I3 vehicle.

| Vehicle Axle | Axle Load [kg] | Axle Position [m] |
|---|---|---|
| 1 | 6000 | 0 |
| 2 | 6750 | 3 |
| 3 | 6750 | 4.5 |
| 4 | 9000 | 7.5 |
| 5 | 9000 | 10.5 |
| 6 | 9000 | 13.5 |

Table 4.5 – Axle load and distances of the 34D vehicle.

| Vehicle Axle | Axle Load [kg] | Axle Position [m] |
|---|---|---|
| 1 | 6000 | 0 |
| 2 | 6750 | 3 |
| 3 | 6750 | 4.5 |
| 4 | 8500 | 7.5 |
| 5 | 8500 | 9 |
| 6 | 8500 | 12 |
| 7 | 8500 | 13.5 |

Using the definitions mentioned earlier in this chapter, the following methodology was proposed to study the two main goals of the simulations: exploring system layouts and evaluating methods to estimate vehicle static loads, known as estimators.

### 4.1.1 System Layout Evaluation

The two main parameters of WIM system layout are the number and distance of sensors. System layout design is a critical aspect of WIM system planning, given that this configuration is not easily altered after the system is installed. In this context, simulation is a valuable tool to evaluate various layouts.

This evaluation involved varying simulation parameters to gain a deeper understanding of the dynamic load and the impact of layout on WIM measurements. Another objective was to assess the accuracy of Equations (3.8) and (3.9) for calculating sensor distance. The simulation parameters analyzed are presented in Table 4.6. The estimator chosen for this analysis

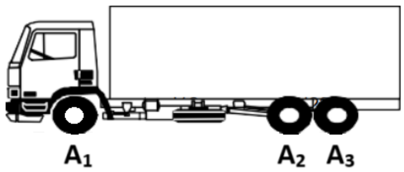


(a) Vehicle category 3C.

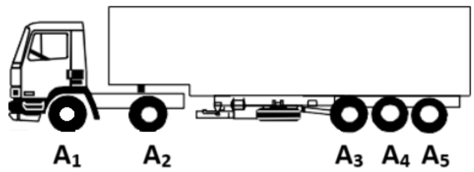


(b) Vehicle category 2S3.

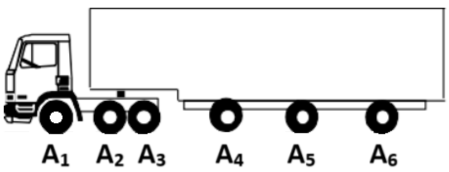


(c) Vehicle category 3I3.

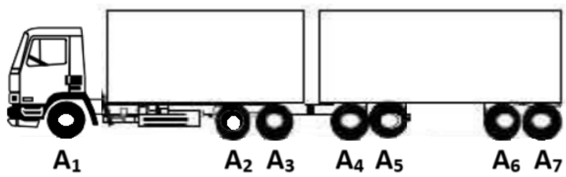


(d) Vehicle category 34D.

Figure 4.3 – Vehicle categories employed in simulations, adapted from (Departamento Nacional de Infraestrutura de Transportes (DNIT), 2012).

was the simple mean value calculation, as other estimators were subsequently evaluated using the methodology detailed in Section 4.1.2. Additionally, sensors were uniformly distributed, meaning the sensor spacing was the same for all sensors.

Table 4.6 – Simulation parameters for system layout evaluation.

| Parameter | Type | Value |
|---|---|---|
| Estimator | Fixed | Mean Value |
| Number of sensors | Variable | 2, 4, 6, 8, 10, 12, 14, 16 |
| Sensor spacing [m] | Variable | 0.5, 1, 2, 3, 4, 5, $\Delta_{D1}$, $\Delta_{D2}$ |
| Vehicle speed [km/h] | Variable | 20, 40, 60, 80, 100 |

Each system layout (set of number of sensors and sensor spacing) was assessed using different vehicle speeds, generating the results presented in Section 5.1. The values $\Delta_{D1}$ and $\Delta_{D2}$ were obtained from Equations (3.8) and (3.9), respectively, and were calculated for each vehicle run as they depend on parameters such as vehicle speed and number of sensors.

### 4.1.2 Estimators Evaluation

After identifying the most suitable sensor distance in the system layout analysis, the estimators detailed in Section 3.3.2, excluding Neural Network techniques, were evaluated. This work employed estimators to combine the instantaneous load of individual axles into the static load of that axle. The Gross Vehicle Weight (GVW) is obtained by summing all these static axle loads. The estimators evaluated in this study are:

- Mean Value Estimator;
- Maximum Likelihood Estimator (MLE);
- Signal Reconstruction Techniques.

The Mean Value estimator does not require prior information about the system being tested, as it involves the straightforward calculation of sample averages. In contrast, the Maximum Likelihood Estimator requires information regarding sensor uncertainty in its computation, as demonstrated in Equation (3.13). In a study conducted by Gajda *et al.* (2020), the standard deviation of measurement results from a WIM system equipped with sixteen load sensors was measured. The relative standard deviations (RSD) measured from the sixteen sensors in this study are used to emulate sensor uncertainty in our experiment, except for the RSD measured from sensors 3 and 4, which clearly deviated from other measurements. To address these outliers, the RSD of these two sensors was considered as the average value of the other fourteen sensors, which is 10%. Figure 4.4 exhibits the RSD values for each load sensor.

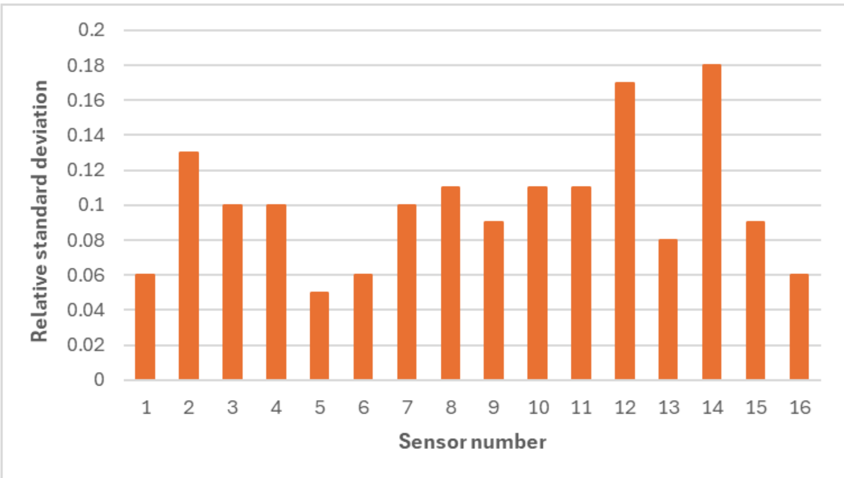


Figure 4.4 – Relative standard deviation of load sensors employed in the simulation.

Additionally, signal reconstruction and interpolation techniques were also evaluated in this work. These methods involved reconstructing axle load signals from the samples measured by load sensors. Each axle's static load was determined by calculating the signal average. The evaluation employed methods available in MATLAB software, including Shape-preserving

Piecewise Cubic interpolation, Modified Akima Cubic Hermite interpolation, and Spline interpolation.

The simulation parameters employed in the estimators analysis are presented in Table 4.7. For this step, we used the sensor distance that demonstrated greater robustness across vehicle speeds in the system layout evaluation.

Table 4.7 – Simulation parameters for the estimators evaluation.

| Parameter | Type | Value |
|---|---|---|
| Estimator | Variable | Mean Value, MLE, Signal Reconstruction |
| Number of sensors | Variable | 2, 4, 6, 8, 10, 12, 14, 16 |
| Sensor spacing | Fixed | Defined by previous analysis |
| Vehicle speed [km/h] | Variable | 20, 40, 60, 80, 100 |

Analyzing Weigh-In-Motion systems in real-world scenarios poses challenges due to the expense and complexity of experimental setups. Simulation offers a preliminary understanding of these systems. While simulations cannot substitute for experimental analysis, they serve as a crucial initial phase in designing Weigh-In-Motion systems.

## 4.2 Experimental Data

To assess instantaneous axle weight estimation, an experimental study was conducted using a real Weigh-In-Motion system. Data were collected from a moving truck, pre-weighed on a static scale. The experimental setup flowchart is presented in Figure 4.5.


Figure 4.5 – Flowchart illustrating the experimental setup, data collection process, and analyses.

The layout of the WIM site used for data collection is presented in Figure 4.6. This site has six in-pavement load cells employing strain-gauge sensors to measure vehicle load.

Additionally, there is one inductive loop utilized to trigger the system measurements. Each load cell has a width of 7 cm, and the distances between the cells are indicated in Figure 4.7.

Figure 4.6 – Experimental WIM system equipped with 6 in-pavement strain-gauge load cells.

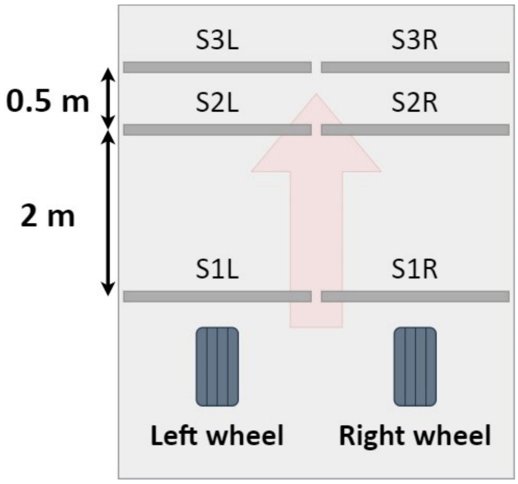


Figure 4.7 – Diagram of the experimental WIM system layout showing sensor distances.

The experimental site is located on a highway detour with a slight incline, making it difficult to conduct experiments with loaded heavy trucks at high speeds. To explore various vehicle speeds, data were collected using a heavy truck both loaded and empty. Figure 4.8 shows the six-axle heavy truck (category 3S3) used in this test. Vehicle static loads for both cases are presented in Table 4.8, along with the distances between vehicle axles. Each axle distance is calculated relative to the first axle.

The tests were conducted at vehicle speeds ranging from 5 to 35 km/h when loaded and 10 to 60 km/h when empty, representing the maximum speeds achievable on the test road

Table 4.8 – Axle loads and distances of the test vehicle.

| Vehicle Axle | Axle Load (Loaded) [kg] | Axle Load (Empty) [kg] | Axle Position [m] |
|---|---|---|---|
| 1 | 5960 | 5630 | 0 |
| 2 | 9090 | 3770 | 3.7 |
| 3 | 6180 | 2370 | 4.95 |
| 4 | 6960 | 1830 | 7.9 |
| 5 | 9160 | 2860 | 9.15 |
| 6 | 7530 | 2240 | 10.4 |

Figure 4.8 – Test vehicle used for experimental data collection.

for both cases.

One of the main challenges of the experimental tests was developing a system capable of reading all six sensors using a sampling frequency high enough to capture axle signals with sufficient resolution. This was accomplished using a custom hardware board containing a microcontroller and six analog-to-digital converters (ADCs) continuously capturing sensor data at 25 kSPS. The ADC features an internal anti-aliasing filter. Moreover, the signal was digitally filtered by the microcontroller using a FIR filter of order 45 with a cutoff frequency of 170 Hz. Filtered data were sent to a PC located near the experimental site through an Ethernet cable. While the development of this embedded system was carried out by an experienced team of technicians and engineers and is not the primary focus of this study, the author made a significant contribution to the firmware development of the system.

The algorithms for estimating instantaneous axle weight, detailed in Section 3.2, were then applied to the collected signals. This study evaluated several methods for estimating instantaneous axle load, such as the Area Under the Signal, Peak Voltage, Re-sampling of Area, and Tire Footprint Reconstruction. In this study, the Tire Footprint Reconstruction method considered footprint length proportional to the load sensor's pulse width multiplied by vehicle speed, while its width was set to 300 mm for single-wheel axles and 600 mm for dual-wheel axles.

The Estimator utilized in the experimental analysis was the Mean Value estimator. The Maximum Likelihood Estimator (MLE) requires information about the standard deviation of measurements from each sensor. However, due to the unavailability of this data in these initial tests, it was not evaluated. Meanwhile, Signal Reconstruction techniques are heavily dependent on the number of samples available. In our setup, each vehicle wheel is weighed by three sensors on each side of the road, resulting in three load samples, which is not sufficient to ensure reliable signal reconstruction (Haupt; Nowak, 2006; Oubrich *et al.*, 2018).

It is crucial to note that the resulting instantaneous axle load values cannot be independently evaluated due to the lack of ground truth information. The ground truth of static axle loads is available, but the ground truth of instantaneous axle loads of the moving vehicle, subject to vertical dynamic oscillations, is not. To properly assess the effectiveness of each axle weight estimation technique, the vehicle ideally should be equipped with load cells and/or accelerometers, providing data of the dynamic weight as the vehicle passes over the WIM sensors. Unfortunately, implementing this instrumentation was not feasible for our experimental study.

After applying the instantaneous axle weight algorithms, the raw values for each axle was calculated using signals from multiple runs, and the algorithms' outputs were combined using the mean value calculation. These results were then used to evaluate the precision and accuracy of each algorithm.

The precision evaluation involved calculating the average of the raw values for a given axle across multiple runs, and then comparing each raw value to this average. This step indicates the consistency of the algorithm in its estimations.

The accuracy of the algorithms was assessed by first calculating the ratios between the raw values of the truck's front axle and all other axles: $A_1/A_2$, $A_1/A_3$, $A_1/A_4$, $A_1/A_5$, and $A_1/A_6$. The ratios produced by each algorithm were then compared to the ratios of the static axle weights shown in Table 4.8. The algorithm with ratios most closely aligned with the static ratios was considered more accurate. The truck's front axle was chosen for all ratios as it is expected to be less affected by dynamic load impacts from the oscillating vehicle body (Huhtala *et al.*, 2000; Grakovski; Pilipovecs, 2018). This step was used to mitigate the lack of ground truth for the dynamic loads and the absence of proper system calibration.

Both analyses were conducted using data from both the empty and loaded truck configuration. Statistics such as the root mean square error and relative deviations were calculated from these analyses.

# 5 RESULTS

This chapter presents the results of this study. Simulations conducted in MATLAB were used to assess the influence of various vehicle and system parameters on weight estimation. Meanwhile, field tests involved collecting data from a six-axle heavy truck as it passed through an experimental site equipped with six in-pavement load cells.

The study categorizes methods into instantaneous axle load estimation and gross vehicle weight (GVW) estimation. Instantaneous axle load algorithms were tested using real-world data, while static axle and vehicle load (GVW) estimators were evaluated using simulation data.

## 5.1 Simulation

Simulations were conducted using Equation (3.1) with $M = 2$ to generate the dynamic load signals. The MATLAB code for the weigh-in-motion (WIM) simulator developed as part of this research is available on (Rocheti, 2024). Figure 5.1 illustrates a single axle load signal at different speeds, using the parameters: $P_0 = 7,500$ kg, $f_1 = 2$ Hz, $f_2 = 8$ Hz, $N = 4$ sensors, and $\Delta_{\text{sensor}} = 2.5\text{m}$.

In various cases, the axle load sampled by the WIM sensors cannot accurately represent the static weight of the axle, even if its instantaneous axle load, calculated by the methods in 3.2, is precisely determined, as considered in this simulation. If the number of sensors increases, the estimated weight tends to approximate the true static load. Additionally, equipping a system with too many sensors is not financially viable due to the high costs involved. This emphasizes the need to identify an adequate number of sensors and their spacing to handle various vehicle types at different speeds.

Figure 5.1 also shows the impact of vehicle speed in determining the instant that the load signal is measured. Higher speeds result in the load signal being sampled over shorter periods compared to lower speeds, a condition also affected by sensor spacing.

The proposed simulations were first used to analyze system layout, including the number of sensors and sensor spacing. Subsequently, simulations evaluated the estimators detailed in Section 3.3.2, using the most appropriate sensor spacing previously identified.

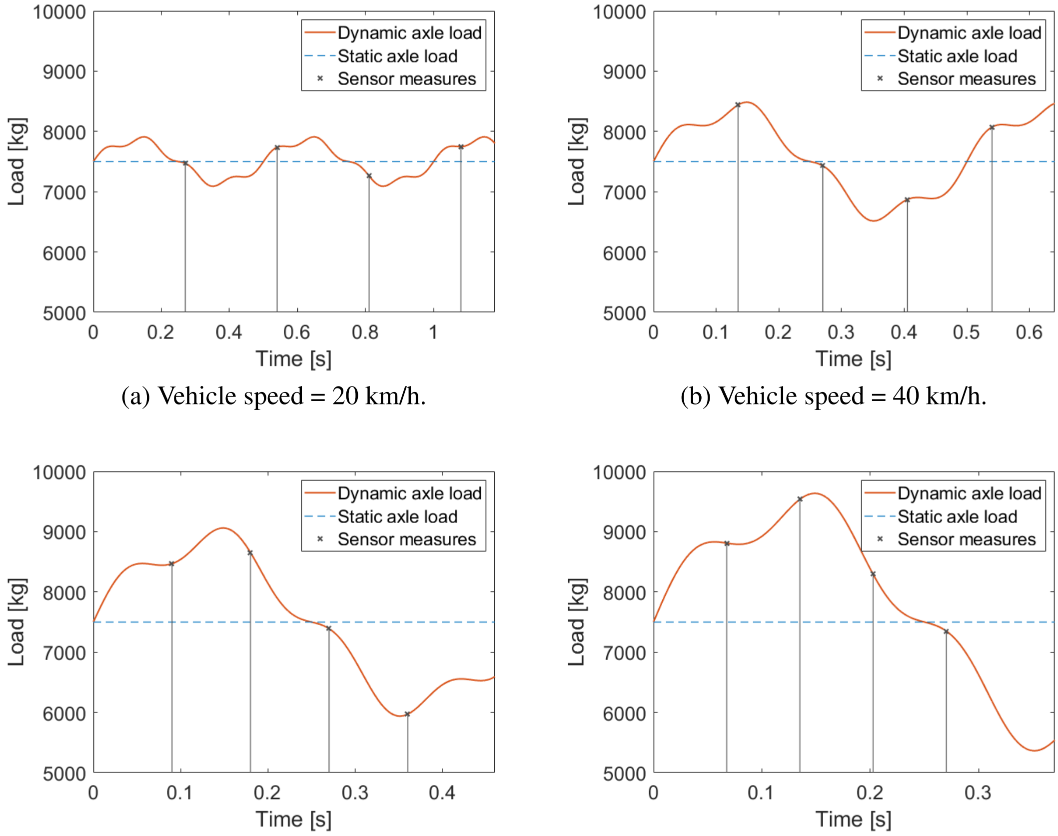


(a) Vehicle speed = 20 km/h. (b) Vehicle speed = 40 km/h.

(c) Vehicle speed = 60 km/h. (d) Vehicle speed = 80 km/h.

Figure 5.1 – Dynamic load of a single vehicle axle for different vehicle speeds.

### 5.1.1 System Layout Evaluation

The evaluation of the system layout involved running the simulation model with the parameters shown in Table 4.6. For each configuration, the simulation was run 15 times, with the signal phase and the $f_1$ and $f_2$ frequencies of the dynamic loads treated as random Gaussian variables within the ranges of 0 to 360°, 1 to 5 Hz, and 8 to 15 Hz, respectively. Various statistical measures, including maximum relative error, root mean square error (RMSE), and relative standard deviation (RSD), were used to compare system performance under different conditions. The results for GVW estimation are presented in Figures 5.2 and 5.3, while the results for axle load estimation are presented in Appendix A, Figures A.1 and A.2. The relative standard deviations (RSD) for vehicle type 3C are presented in Table 5.1. The results for the other vehicle categories (2S3, 3I3, and 34D) are presented in Tables A.1, A.2, and A.3 in Appendix A.

Both the maximum relative error and RMSE of axle weight estimation were consistently higher than those observed for GVW estimation, as expected. This occurs because GVW

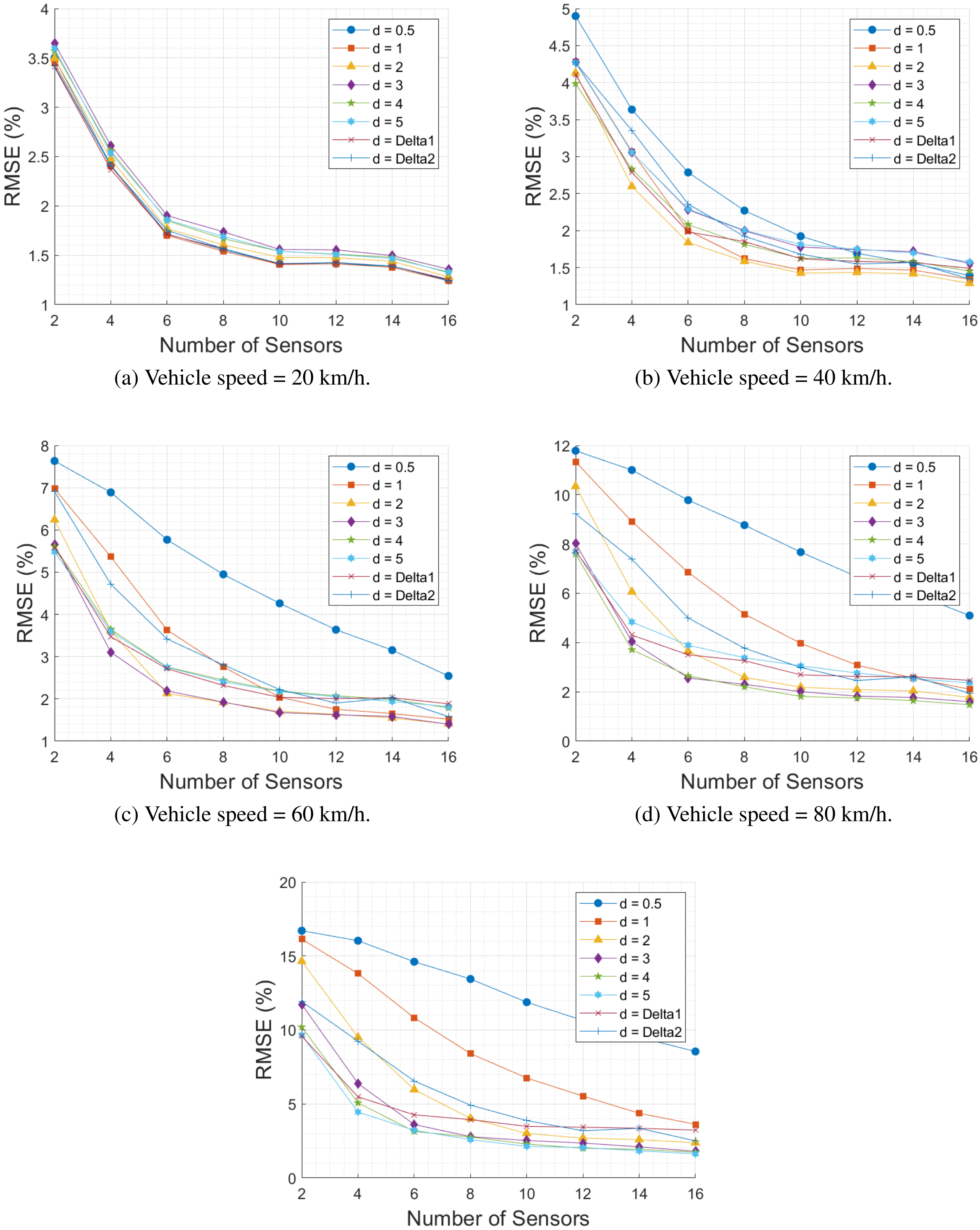


(a) Vehicle speed = 20 km/h.

(b) Vehicle speed = 40 km/h.

(c) Vehicle speed = 60 km/h.

(d) Vehicle speed = 80 km/h.

(e) Vehicle speed = 100 km/h.

Figure 5.2 – GVW root mean square error from the system layout evaluation in the simulation analysis, with each curve representing a different sensor distance.

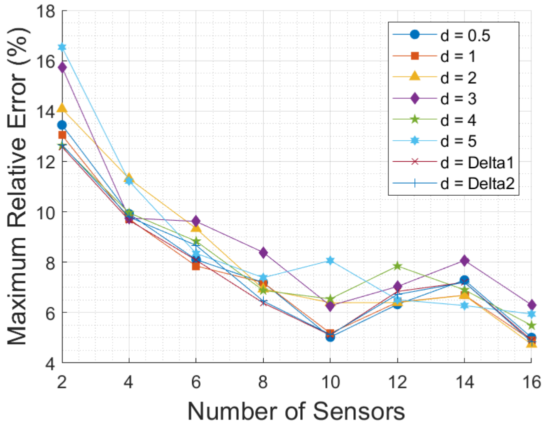


(a) Vehicle speed = 20 km/h.

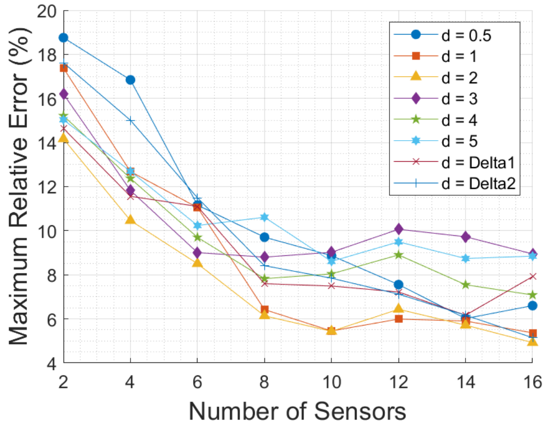


(b) Vehicle speed = 40 km/h.

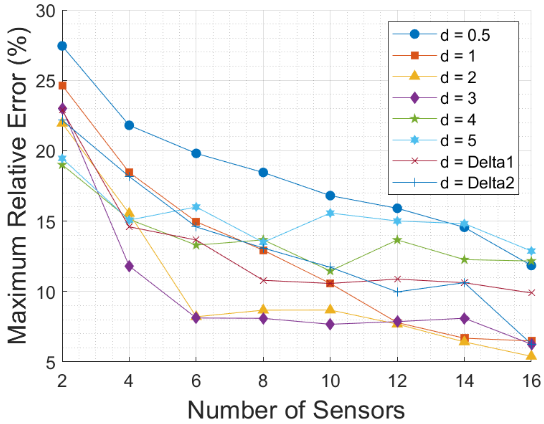


(c) Vehicle speed = 60 km/h.

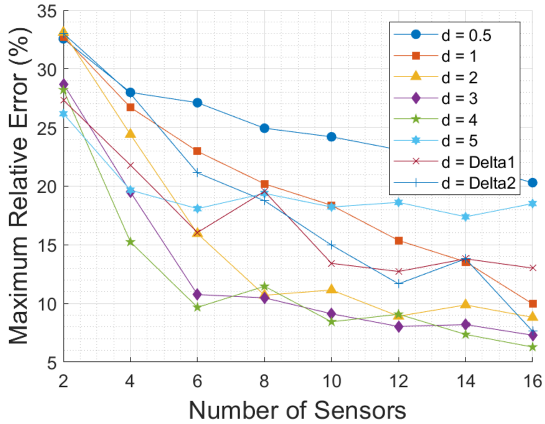


(d) Vehicle speed = 80 km/h.

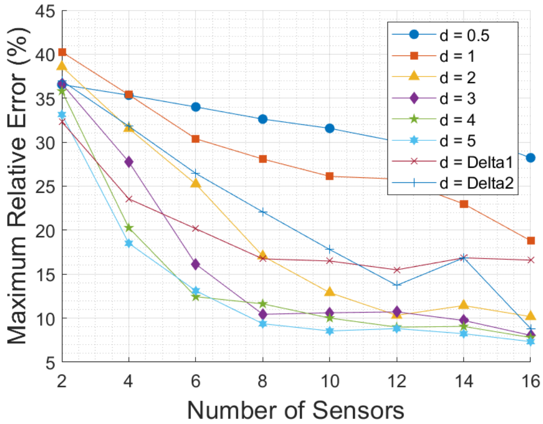


(e) Vehicle speed = 100 km/h.

Figure 5.3 – GVW maximum relative error from the system layout evaluation in the simulation analysis, with each curve representing a different sensor distance.

Table 5.1 – Relative standard deviation of GVW estimation for the system layout evaluation in the simulation analysis, vehicle category 3C.

| Speed | Distance | N = 2 | N = 4 | N = 6 | N = 8 | N = 10 | N = 12 | N = 14 | N = 16 |
|---|---|---|---|---|---|---|---|---|---|
| 20 | 0.5 | 3.76 | 2.98 | 2.01 | 1.61 | 1.58 | 1.54 | 1.66 | 1.45 |
| | 1 | 3.78 | 2.95 | 1.99 | 1.57 | 1.54 | 1.52 | 1.66 | 1.43 |
| | 2 | 3.56 | 3.04 | 1.95 | 1.59 | 1.58 | 1.58 | 1.69 | 1.45 |
| | 3 | 3.97 | 3.04 | 2.21 | 1.89 | 1.77 | 1.53 | 1.70 | 1.46 |
| | 4 | 3.42 | 3.11 | 2.00 | 1.90 | 1.67 | 1.79 | 1.72 | 1.59 |
| | 5 | 3.72 | 3.31 | 2.38 | 1.80 | 1.80 | 1.71 | 1.80 | 1.62 |
| | $\Delta_{D1}$ | 3.66 | 2.89 | 2.00 | 1.60 | 1.56 | 1.52 | 1.70 | 1.44 |
| | $\Delta_{D2}$ | 3.69 | 2.94 | 2.01 | 1.59 | 1.56 | 1.52 | 1.71 | 1.45 |
| 40 | 0.5 | 4.91 | 3.41 | 2.40 | 2.42 | 1.88 | 2.24 | 1.74 | 1.43 |
| | 1 | 4.79 | 3.05 | 2.02 | 1.89 | 1.79 | 1.92 | 1.67 | 1.41 |
| | 2 | 4.49 | 2.73 | 1.87 | 1.90 | 1.75 | 1.85 | 1.62 | 1.39 |
| | 3 | 4.58 | 2.69 | 2.03 | 2.04 | 2.00 | 1.81 | 1.81 | 1.56 |
| | 4 | 4.12 | 2.77 | 2.02 | 2.02 | 1.85 | 1.84 | 1.60 | 1.36 |
| | 5 | 4.46 | 2.67 | 2.02 | 2.04 | 1.91 | 1.84 | 1.61 | 1.43 |
| | $\Delta_{D1}$ | 4.56 | 2.83 | 2.01 | 2.22 | 1.77 | 2.09 | 1.75 | 1.51 |
| | $\Delta_{D2}$ | 4.68 | 3.14 | 2.20 | 2.32 | 1.78 | 2.02 | 1.70 | 1.39 |
| 60 | 0.5 | 6.32 | 6.39 | 4.44 | 4.45 | 5.06 | 2.94 | 2.69 | 2.54 |
| | 1 | 5.95 | 5.62 | 3.38 | 2.82 | 2.32 | 1.86 | 1.97 | 1.79 |
| | 2 | 5.53 | 3.67 | 2.51 | 2.11 | 2.05 | 1.66 | 1.84 | 1.46 |
| | 3 | 5.24 | 3.02 | 2.54 | 2.21 | 1.92 | 1.76 | 1.78 | 1.58 |
| | 4 | 4.28 | 3.21 | 2.41 | 2.17 | 1.92 | 1.66 | 1.95 | 1.59 |
| | 5 | 4.92 | 3.15 | 2.55 | 2.18 | 2.03 | 1.77 | 2.05 | 1.56 |
| | $\Delta_{D1}$ | 5.22 | 3.55 | 3.03 | 2.42 | 2.32 | 2.02 | 2.05 | 2.02 |
| | $\Delta_{D2}$ | 6.11 | 4.80 | 3.25 | 2.85 | 2.57 | 1.99 | 1.98 | 1.82 |
| 80 | 0.5 | 11.16 | 9.70 | 9.55 | 8.96 | 6.44 | 6.64 | 5.02 | 4.09 |
| | 1 | 11.11 | 7.97 | 6.77 | 5.11 | 3.35 | 3.51 | 2.27 | 2.10 |
| | 2 | 9.86 | 5.68 | 3.30 | 2.85 | 2.16 | 2.33 | 1.92 | 1.97 |
| | 3 | 8.47 | 3.91 | 2.92 | 2.66 | 2.33 | 2.11 | 1.75 | 2.09 |
| | 4 | 7.49 | 3.42 | 2.86 | 2.18 | 1.93 | 1.91 | 1.71 | 1.74 |
| | 5 | 7.31 | 4.06 | 3.07 | 2.34 | 2.11 | 2.37 | 1.82 | 1.95 |
| | $\Delta_{D1}$ | 7.92 | 4.23 | 3.10 | 3.51 | 2.60 | 2.95 | 2.30 | 2.45 |
| | $\Delta_{D2}$ | 8.88 | 6.86 | 4.50 | 3.70 | 2.76 | 2.72 | 2.02 | 2.08 |
| 100 | 0.5 | 14.82 | 14.93 | 13.66 | 13.97 | 12.57 | 11.49 | 9.20 | 8.57 |
| | 1 | 14.07 | 13.67 | 8.93 | 10.15 | 6.28 | 5.11 | 4.96 | 4.36 |
| | 2 | 13.03 | 10.39 | 3.76 | 3.95 | 2.76 | 2.79 | 2.90 | 2.59 |
| | 3 | 10.84 | 6.97 | 3.17 | 3.08 | 2.47 | 2.46 | 2.17 | 2.04 |
| | 4 | 9.98 | 5.05 | 3.07 | 3.00 | 2.34 | 2.07 | 2.15 | 2.21 |
| | 5 | 8.77 | 4.39 | 2.75 | 2.72 | 1.91 | 2.24 | 2.09 | 2.00 |
| | $\Delta_{D1}$ | 8.84 | 5.51 | 3.34 | 3.83 | 3.50 | 3.54 | 3.42 | 4.07 |
| | $\Delta_{D2}$ | 10.95 | 10.13 | 4.17 | 5.41 | 3.77 | 3.36 | 2.63 | 2.85 |

is calculated by summing the estimated static axle loads, which helps to average out individual errors and minimize the overall error.

Increasing the number of sensors indeed tends to diminish the weight estimation errors. This is most notable when comparing arrays of two, four, and six sensors, where the errors are sometimes three times lower when using six sensors compared to two sensors. Configurations with more than eight sensors started showing diminishing returns in error reduction, although their robustness to speed variations improved considerably for larger sensor arrays – this was also observed in the study by Cebon (1990). Through simulations involving the quarter-car and walking-beam vehicle models, they noted that system accuracy improves gradually as the number of sensors increases beyond two, with diminishing improvements for larger sensor arrays. The study also denotes that larger arrays generate more insensitivity to vehicle speed variation, as observed in our study.

For both axle weight and GVW estimation, sensor distance for low vehicle speeds (20 km/h) had a minimal impact on the errors, although shorter distances demonstrated slightly lower errors compared to others. However, as vehicle speed increased, the influence of sensor distance became more pronounced. For higher speeds, longer distances showed slightly lower errors. The longest distance experimented, 5 meters, was only viable at the very high speed of 100 km/h. These observations align with the results presented by the authors Cebon and Winkler (1991).

These results highlight the crucial role of vehicle speed in defining sensor distance. The study by Cebon and Winkler (1991) also pointed out that the greater the deviation of vehicle speed from the average speed used in defining the sensor distance, the greater the weight estimation error will be. This is visible in our analysis, as no single sensor distance consistently performed better than all others across the tested vehicle speeds (20, 40, 60, 80, and 100 km/h). Thus, a fixed sensor distance optimized for one speed may not be optimal for others. These results highlight the importance of considering a reasonable average speed at the installation site, so the sensor distance can be adjusted to minimize errors.

This also highlights the influence of vehicle speed in this simulation. As dynamic load amplitude is directly increased by vehicle speed, error statistics are likely to increase correspondingly, with maximum relative errors reaching up to 40% in GVW estimation and 65% in axle weight estimation (Figures A.2 and 5.3). The study by Gajda *et al.* (2015) observed similar variations of up to 40% of the static load when measuring the dynamic load of a real vehicle traveling at 80 km/h. In the present study, the effect of vehicle speed on the amplitude of the dynamic loads was approximated by considering a linear relationship, which may not accurately reflect real-world conditions, especially at high speeds.

The RSD of the GVW values indicates that estimation accuracy improves with an increasing number of sensors, as noted when analyzing the maximum relative error and the RMSE. Comparing different vehicle types, vehicles with fewer axles, such as the 3C vehicle, exhibited higher RSD values, particularly at higher speeds, indicating greater sensitivity to vehicle speed and sensor configuration. In contrast, vehicles with more axles, such as the 2S3, 3I3, and 34D vehicles, showed better stability and lower RSD values across various speeds and sensor configurations. The 34D vehicle, with the most axles, demonstrated the most stable and lowest RSD values. This is because in GVW estimation, having more axles to measure tends to lower the average GVW error.

Based on the simulation results, a sensor distance of 3 meters was selected for subsequent estimator analysis. In general, the 3-meter distance performed better at speeds above 40 km/h, while the 2-meter distance performed better at lower speeds. Although the 2-meter distance showed improved performance at lower speeds, the overall errors at these speeds are generally lower. Considering this, the 3-meter distance offers a balanced solution that provides good performance across a range of speeds.

It is worth noting that $\Delta_{\mathrm{D1}}$ also delivered accurate results across a wide speed range. Equation (3.8) considers only the primary frequency component ($f1$) of the dynamic load signal, which had a more substantial impact than the secondary component ($f2$) in the simulated load signal in this study. However, $\Delta_{\mathrm{D1}}$ is not a fixed distance but is calculated for each vehicle run based on its speed and the number of sensors, making it unsuitable for practical applications where a fixed distance is required. Although both $\Delta_{\mathrm{D1}}$ and $\Delta_{\mathrm{D2}}$ generally demonstrated good performance, they cannot be considered as the optimal distances based on our simulation results.

### 5.1.2 Estimators Evaluation

The evaluation of estimators involved running simulations to assess the performance of different estimation algorithms using the parameters shown in Table 4.7. The sensor distance employed in this analysis was previously evaluated in Section 5.1.1 and defined as 3 meters. The estimators evaluated include Mean Value (MV), Maximum Likelihood Estimator (MLE), and Signal Reconstruction algorithms such as Shape-preserving Piecewise Cubic interpolation (Pchip), Modified Akima Cubic Hermite interpolation (Makima), and Spline interpolation.

Figures 5.4 and 5.5 present the results for the root mean square error (RMSE) and maximum relative error for GVW estimation. Figures A.3 and A.4 present similar results for axle load estimation and are included in Appendix A. Table 5.2 presents the relative standard deviation (RSD) for different vehicle speeds and estimator algorithms for vehicle type 3C. The RSD results for other vehicle types (2S3, 3I3, and 34D) are presented in Tables A.4, A.5, and A.6 in Appendix A. As mentioned in Section 5.1.1, the maximum relative error and RMSE for axle weight estimation were generally higher than those observed for GVW estimation.

The Mean Value estimator, despite its simplicity, showed robust performance across various speeds and sensor configurations. Analyzing the RMSE and the maximum relative error for all simulation scenarios, the mean value calculation was only outperformed by the MLE at very low speed (20 km/h). Furthermore, the mean value calculation maintained lower RSD values compared to other estimators, particularly at higher speeds. This consistency in performance was also observed by Gajda *et al.* (2020).

The MLE demonstrated superior performance at low speeds (20 km/h); however, at speeds greater than 40 km/h, MLE errors increased significantly, surpassing other estimators. For the other estimators, the gains become marginal when more than 10 sensors are employed.

The performance gains of MLE were not as substantial as might be expected from theoretical analysis. The authors Gajda *et al.* (2020) found analogous results when comparing the Mean Value method and the MLE in an experimental study, where both estimators showed similar results. However, the study by Stergioulas *et al.* (2000) conducted a simulation analysis using vehicle models and found that the MLE performed better than the MV for different system layouts, although they grouped results from various vehicle speeds, with the maximum speed being 60 km/h. The referred study also indicated that the mean value calculation performed slightly better than the MLE in high noise levels, which is comparable to high vehicle speeds in our work since dynamic load amplitude is considered linearly dependent on vehicle speed.

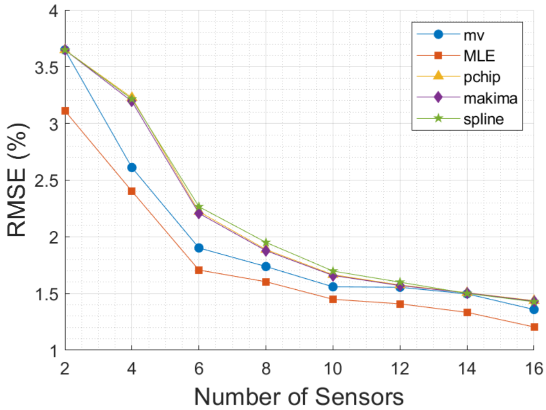


(a) Vehicle speed = 20 km/h.

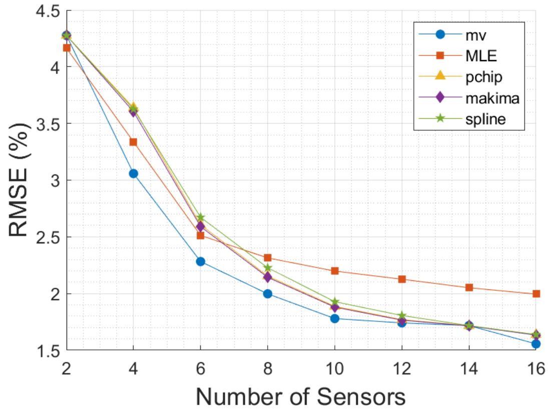


(b) Vehicle speed = 40 km/h.

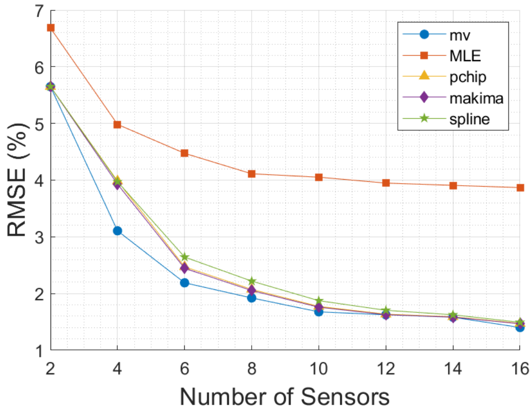


(c) Vehicle speed = 60 km/h.

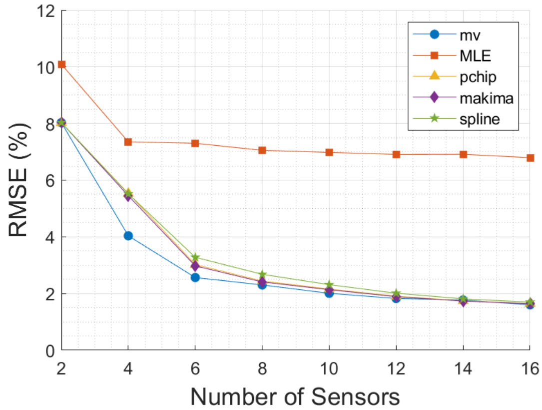


(d) Vehicle speed = 80 km/h.

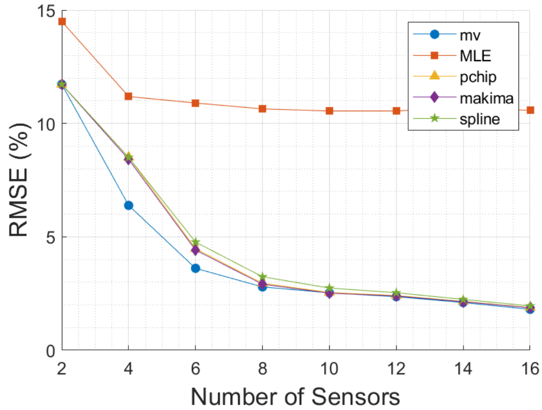


(e) Vehicle speed = 100 km/h.

Figure 5.4 – GVW root mean square error from the estimators evaluation in the simulation analysis, with each curve representing a different estimator.

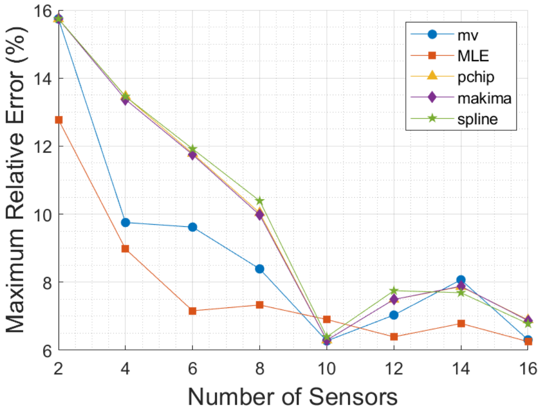


(a) Vehicle speed = 20 km/h.

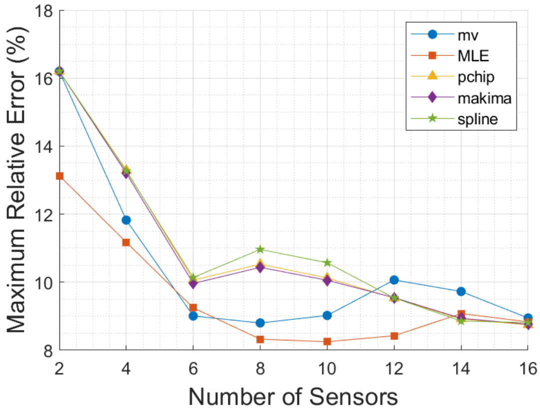


(b) Vehicle speed = 40 km/h.

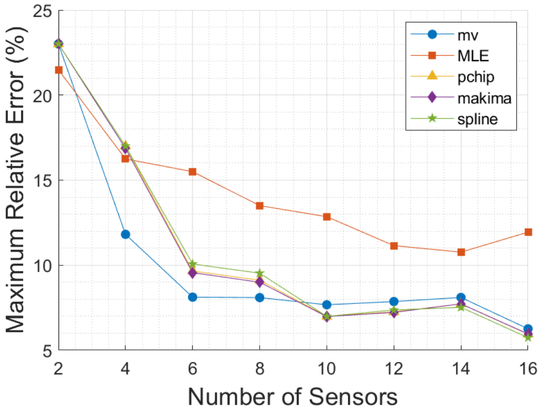


(c) Vehicle speed = 60 km/h.

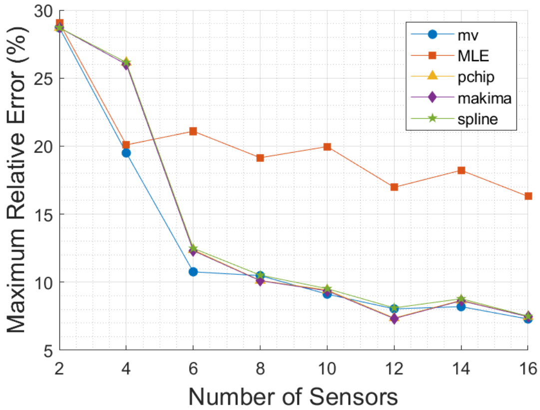


(d) Vehicle speed = 80 km/h.

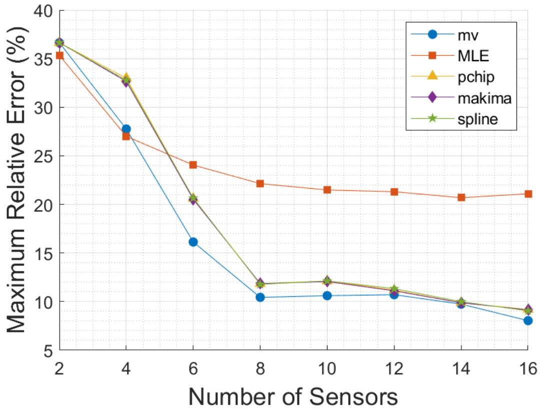


(e) Vehicle speed = 100 km/h.

Figure 5.5 – GVW maximum relative error from the estimators evaluation in the simulation analysis, with each curve representing a different estimator.

Table 5.2 – Relative standard deviation of GVW estimation for the estimators evaluation in the simulation analysis, vehicle category 3C.

| Speed | Estimator | N = 2 | N = 4 | N = 6 | N = 8 | N = 10 | N = 12 | N = 14 | N = 16 |
|---|---|---|---|---|---|---|---|---|---|
| 20 | MV | 3.97 | 3.04 | 2.21 | 1.89 | 1.77 | 1.53 | 1.70 | 1.46 |
| | MLE | 3.45 | 2.86 | 1.93 | 1.82 | 1.74 | 1.33 | 1.41 | 1.22 |
| | Makima | 3.97 | 3.77 | 2.53 | 2.09 | 1.84 | 1.58 | 1.69 | 1.54 |
| | Pchip | 3.97 | 3.81 | 2.55 | 2.10 | 1.84 | 1.59 | 1.69 | 1.55 |
| | Spline | 3.97 | 3.80 | 2.63 | 2.16 | 1.85 | 1.63 | 1.70 | 1.52 |
| 40 | MV | 4.58 | 2.69 | 2.03 | 2.04 | 2.00 | 1.81 | 1.81 | 1.56 |
| | MLE | 4.08 | 2.85 | 1.76 | 1.80 | 1.92 | 1.57 | 1.78 | 1.55 |
| | Makima | 4.58 | 3.56 | 2.42 | 2.09 | 2.14 | 1.81 | 1.78 | 1.60 |
| | Pchip | 4.58 | 3.61 | 2.44 | 2.09 | 2.15 | 1.81 | 1.79 | 1.60 |
| | Spline | 4.58 | 3.59 | 2.50 | 2.17 | 2.21 | 1.87 | 1.80 | 1.58 |
| 60 | MV | 5.24 | 3.02 | 2.54 | 2.21 | 1.92 | 1.76 | 1.78 | 1.58 |
| | MLE | 5.50 | 3.86 | 2.87 | 2.76 | 2.79 | 1.96 | 2.04 | 2.19 |
| | Makima | 5.24 | 4.27 | 2.86 | 2.37 | 2.05 | 1.85 | 1.95 | 1.63 |
| | Pchip | 5.24 | 4.33 | 2.87 | 2.39 | 2.06 | 1.86 | 1.96 | 1.63 |
| | Spline | 5.24 | 4.32 | 2.95 | 2.51 | 2.11 | 1.91 | 2.00 | 1.64 |
| 80 | MV | 8.47 | 3.91 | 2.92 | 2.66 | 2.33 | 2.11 | 1.75 | 2.09 |
| | MLE | 9.99 | 5.07 | 4.73 | 3.92 | 3.43 | 2.88 | 2.90 | 2.85 |
| | Makima | 8.47 | 5.58 | 3.44 | 2.74 | 2.38 | 2.20 | 1.87 | 2.23 |
| | Pchip | 8.47 | 5.66 | 3.48 | 2.77 | 2.40 | 2.22 | 1.88 | 2.24 |
| | Spline | 8.47 | 5.64 | 3.83 | 2.98 | 2.54 | 2.31 | 1.94 | 2.24 |
| 100 | MV | 10.84 | 6.97 | 3.17 | 3.08 | 2.47 | 2.46 | 2.17 | 2.04 |
| | MLE | 12.94 | 8.86 | 6.14 | 4.81 | 4.10 | 4.33 | 3.61 | 3.52 |
| | Makima | 10.84 | 9.46 | 3.63 | 3.40 | 2.45 | 2.50 | 2.26 | 2.26 |
| | Pchip | 10.84 | 9.55 | 3.68 | 3.44 | 2.47 | 2.52 | 2.27 | 2.28 |
| | Spline | 10.84 | 9.55 | 4.05 | 3.67 | 2.64 | 2.68 | 2.31 | 2.29 |

Signal reconstruction techniques, including Pchip, Makima, and Spline interpolations, exhibited similar performance profiles across different vehicle speeds. These techniques showed the exact same performance as the mean value estimator with just two sensors, as the mean of a signal reconstructed with two samples by these methods will be equal to the mean value calculation. Moreover, signal reconstruction techniques exhibited higher errors when compared to the mean value calculation. Notably, tests with four to eight sensors showed higher errors, whereas tests with more than ten sensors showed an approximation to the mean value errors. This result is expected since signal reconstruction performance is heavily dependent on the number of samples available. High-fidelity signal reconstruction can yield valuable data for weight estimation in WIM systems, such as signal spectrum information and dynamic load filtering, as suggested by Oubrich *et al.* (2018).

The observed trends suggest that while the MLE offers advantages under specific conditions, the simple mean value calculation remains a consistently reliable and practical choice for a wide range of WIM applications. It is important to note that the simplest forms of signal reconstruction techniques result in inferior performance compared to the Mean Value method. However, by incorporating knowledge of the typical oscillation spectrum of trucks, more advanced signal reconstruction techniques could be developed to achieve better performance.

## 5.2 Experimental Data

The experimental study was conducted at the Weigh-In-Motion (WIM) site described in Figures 4.6 and 4.7 using the six-axle test truck. Figure 5.6 captures the precise moment when one of the vehicle's tires applies pressure to a strain-gauge load cell. The tire footprint is larger than the sensor width, indicating the need for proper algorithms to calculate the instantaneous axle load, as a single measurement from this sensor is insufficient.

Figure 5.6 – Moment of contact between the vehicle tire and a strain-gauge load cell.

The test vehicle underwent multiple runs at various speeds while being both fully loaded and empty. The empty vehicle was able to reach higher speeds, up to 60 km/h, while the loaded vehicle was tested at a maximum speed of 35 km/h due to the WIM site constraints explained in Section 4.2.

During each vehicle run, load sensor signals were captured by ADCs and digitally filtered by the data collection system. The data, stored on a computer near the WIM site, were then normalized to correct any DC offsets and ensure consistent reference levels across all load sensors. A threshold value was used to detect vehicle axles in the signal. Figure 5.7 shows the readings from the six sensors, three on the left and three on the right, for the loaded vehicle traveling at 30 km/h. The red line present in all plots indicates the threshold value used for vehicle axle detection. The pulses in the signals correspond to the passage of each axle over the sensors.

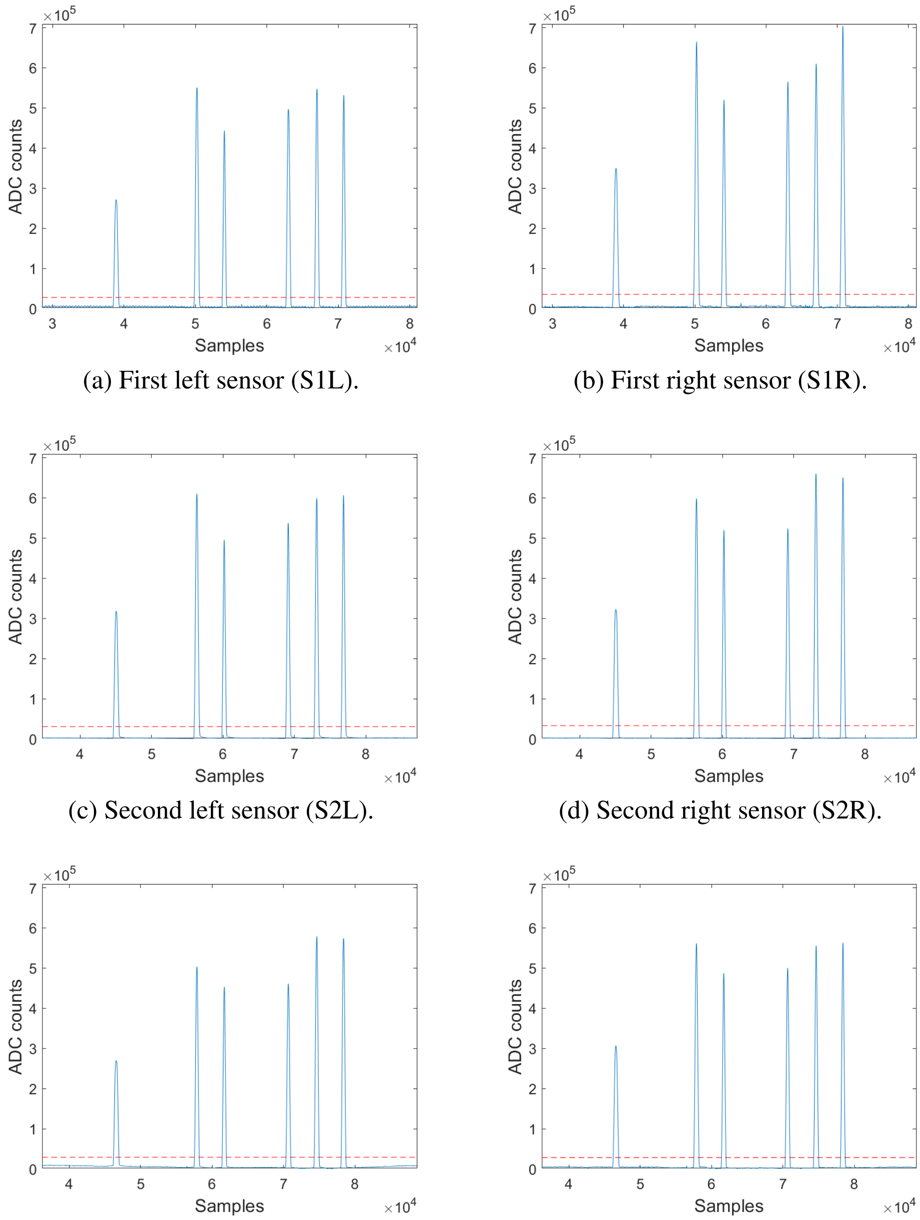


(a) First left sensor (S1L). (b) First right sensor (S1R).

(c) Second left sensor (S2L). (d) Second right sensor (S2R).

(e) Third left sensor (S3L). (f) Third right sensor (S3R).

Figure 5.7 – Readings from the left and right sensors of the loaded vehicle traveling at 30 km/h. The red line indicates the threshold value.

There is a general consistency in the shape of the peaks between the corresponding left and right sensors. However, slight variations in amplitude between the left and right sensors may suggest differences in sensor sensitivity or a variation in the vehicle's transverse load distribution. These discrepancies also highlight the need for calibration adjustments to ensure more accurate measurements, which were not performed in this initial experimental study.

The vehicle axle pulses detected through the threshold value from all vehicle runs were then used by the algorithms described in Section 3.2 to estimate the instantaneous axle weights. The results were separated into precision and accuracy analyses.

### 5.2.1 Precision Evaluation

The precision of the instantaneous axle weight estimation algorithms was evaluated by calculating the mean of the raw results for each vehicle axle. This mean value was then compared to each individual results for that axle, and the relative error of the deviation from the mean was grouped by speed. Figures 5.8 and 5.9 illustrate the relative deviation of each axle's weight estimation method for both loaded and empty configurations, respectively. Additionally, Figure 5.10 presents the same analysis for the gross vehicle weight (GVW) of the vehicle. This approach aimed to assess the consistency of each algorithm across various vehicle runs at different speeds.

The GVW precision exhibited generally lower relative deviations compared to most individual axles, which is expected since GVW is the sum of all axle weights, thereby averaging out the errors from individual axles. This observation aligns with the results from the simulation analysis (Section 5.1). However, the front axle displayed consistently lower deviations compared to other axles, even lower than the GVW. This trend is likely due to the front axle being less affected by dynamic oscillations, which tend to intensify toward the rear of the vehicle due to the cumulative effects of suspension dynamics and load transfer during motion (Hucho; Ahmed, 1998; Jacob, 2001). In the loaded vehicle configuration, the additional mass appears to dampen these dynamic effects, leading to more stable weight measurements across all axles when compared to the empty vehicle configuration.

The experimental study included runs at speeds up to 60 km/h, but the impact of vehicle speed on precision was not entirely clear. Higher speeds reduce the interaction time between the axle and the sensor, making the measurements more susceptible to transient dynamic loads. While higher speeds (above 30 km/h when loaded and 60 km/h when empty) did show increased variability in the results, similar variability was also observed at very low speeds (5 km/h loaded and 10 km/h empty). This suggests that while speed is a factor, the relationship between speed and precision is not straightforward, and other factors, such as vehicle type and sensor configuration, might also influence the results.

Among the algorithms evaluated, the Peak Voltage method demonstrated superior

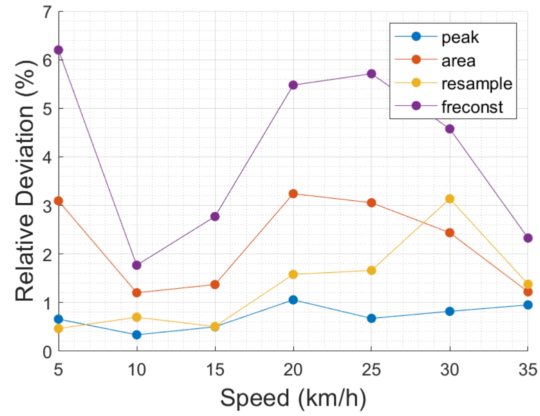


(a) First vehicle axle.

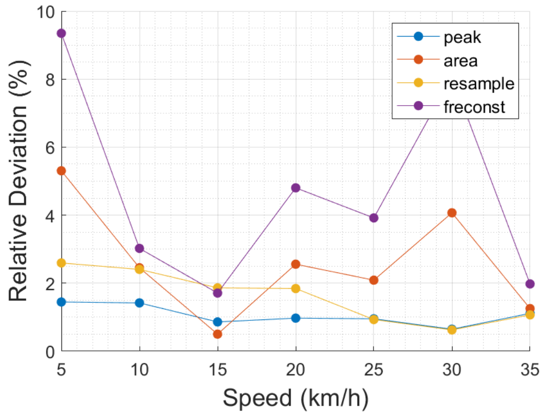


(b) Second vehicle axle.

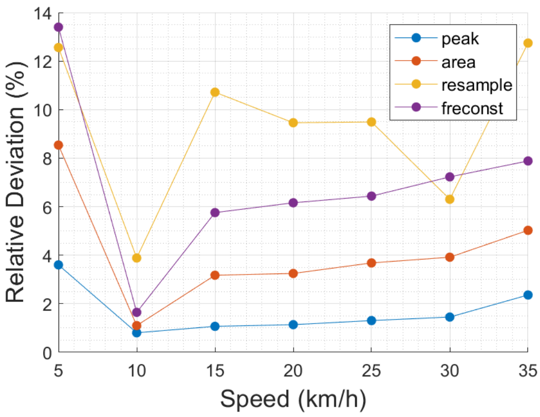


(c) Third vehicle axle.

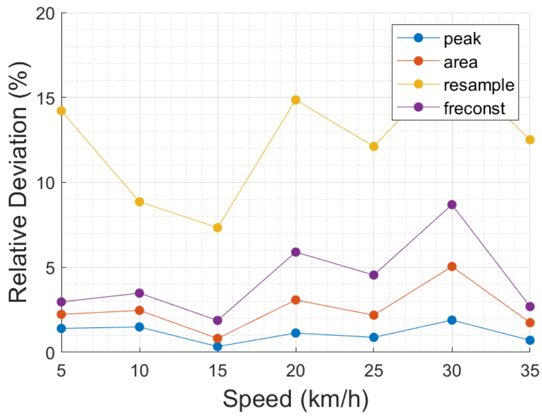


(d) Fourth vehicle axle.

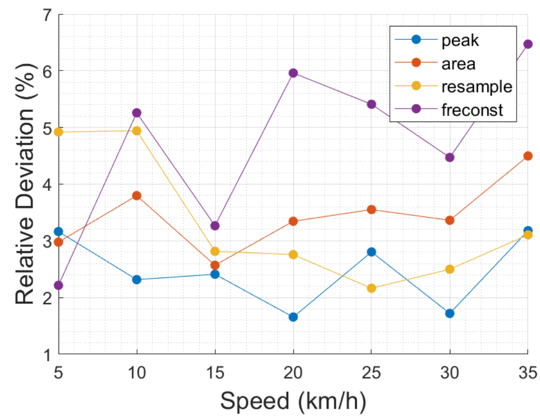


(e) Fifth vehicle axle.

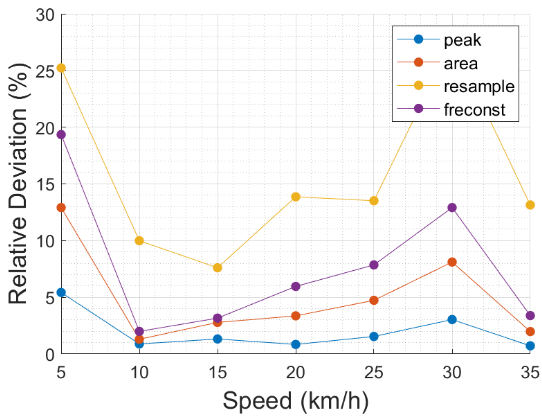


(f) Sixth vehicle axle.

Figure 5.8 – Relative deviation of instantaneous axle weight algorithms for each vehicle axle from the experimental analysis (vehicle loaded).

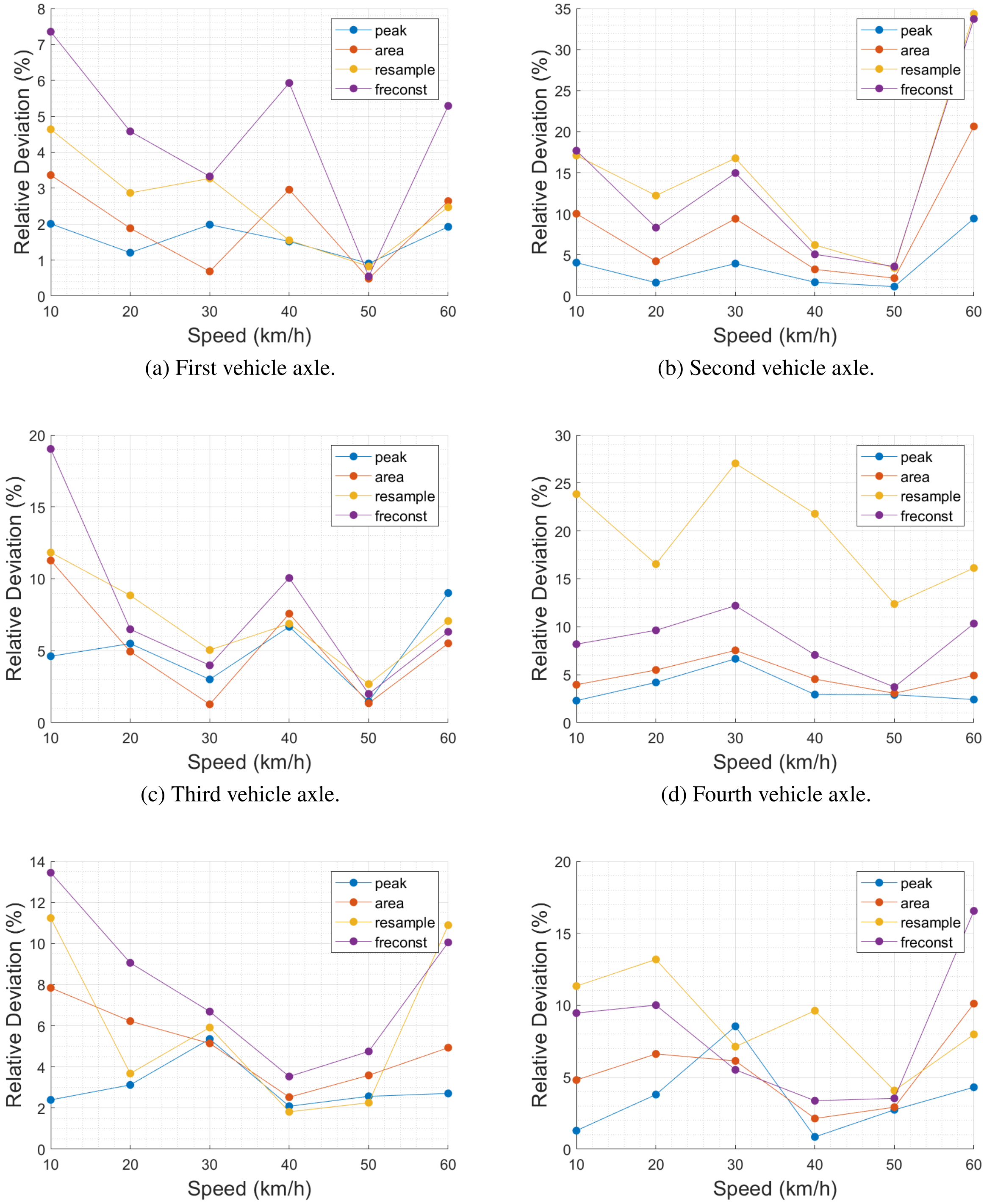


(a) First vehicle axle.

(b) Second vehicle axle.

(c) Third vehicle axle.

(d) Fourth vehicle axle.

(e) Fifth vehicle axle.

(f) Sixth vehicle axle.

Figure 5.9 – Relative deviation of instantaneous axle weight algorithms for each vehicle axle from the experimental analysis (vehicle empty).

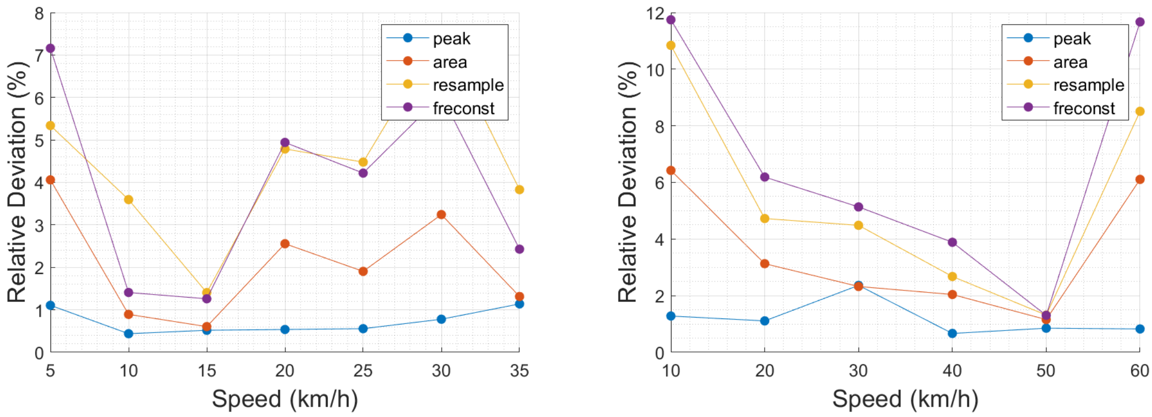


(a) Loaded vehicle. (b) Empty vehicle.

Figure 5.10 – Relative deviation of the gross vehicle weight from the experimental analysis with the test truck, for both loaded and empty conditions.

precision in most scenarios. The Area Under the Signal method also performed well across various vehicle axles, while the Resampling of Area and Tire Footprint Reconstruction algorithms showed higher variability in their results, performing well in a few specific scenarios but generally worse in others. This trend is also evident in Figure 5.10, where the Peak Voltage method consistently shows better GVW precision, followed by the Area Under the Signal method.

Although precision analysis indicates how consistently a measurement can be repeated under a specific scenario, the accuracy of the algorithms remains the most crucial metric of a WIM system, determining whether it is suitable for direct enforcement applications. The results of the precision analysis underscore the need for WIM systems to be carefully calibrated and adjusted based on the typical speed range of vehicles and the various vehicle types, as some axles exhibited higher deviations than others.

### 5.2.2 Accuracy Evaluation

The accuracy analysis involved comparing the ratios of the axle results obtained from the instantaneous axle weight algorithms with the static weight ratios of the test truck presented in Table 4.8. This comparison helps to mitigate the absence of ground truth data for instantaneous axle weight, as the vehicle's dynamic load at the moment of measurement is unknown. Additionally, it allows for the evaluation of algorithms independently of system calibration, which was not performed in these initial experimental tests. The root mean square errors (RMSE) calculated for each algorithm are illustrated in Figures 5.11 and 5.12 for the loaded and empty vehicle configurations, respectively. Data were grouped by vehicle speed and displayed for each axle ratio evaluated.

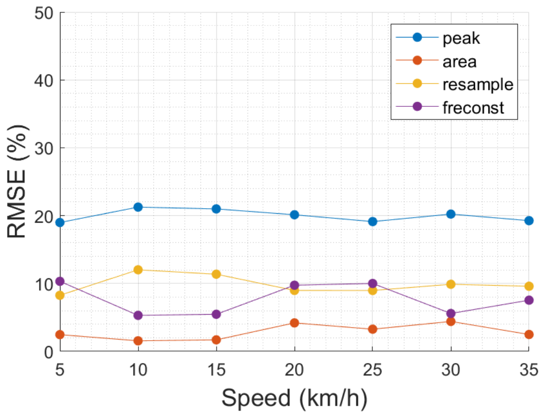


(a) $A_1/A_2$ ratio.

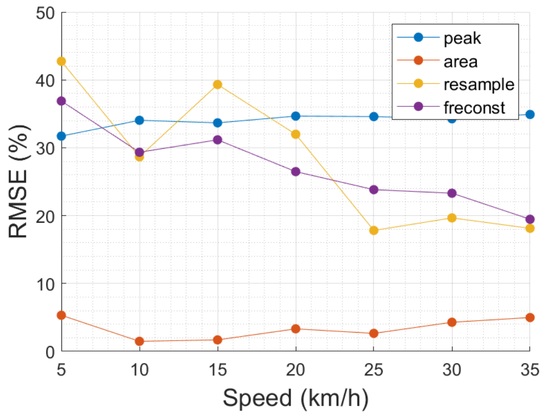


(b) $A_1/A_3$ ratio.

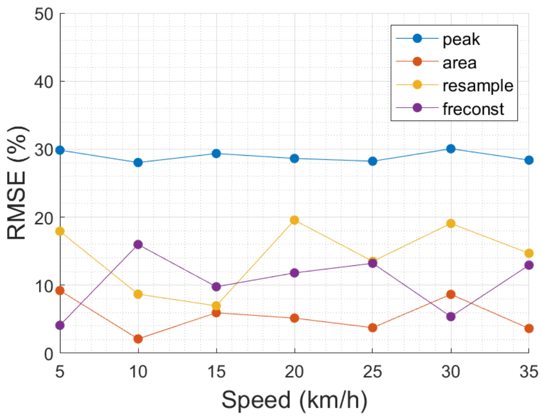


(c) $A_1/A_4$ ratio.

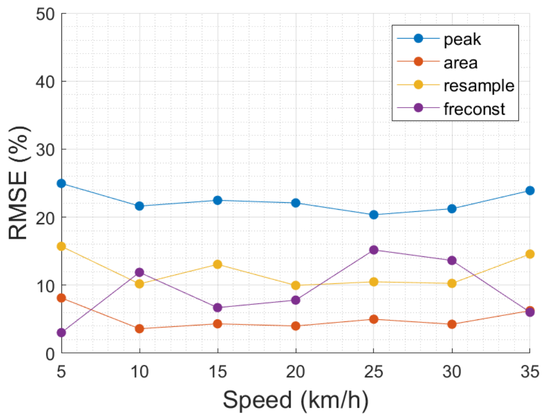


(d) $A_1/A_5$ ratio.

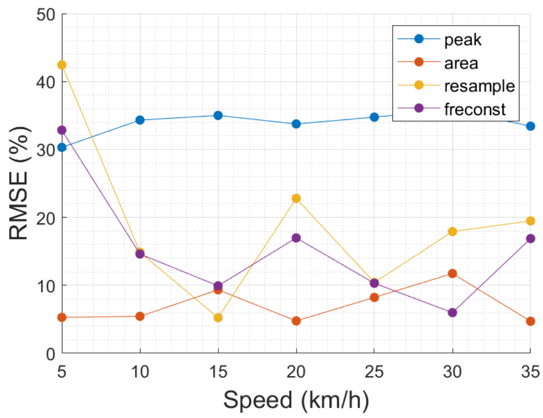


(e) $A_1/A_6$ ratio.

Figure 5.11 – Root mean square error of instantaneous axle weight algorithms for each axle ratio from the experimental analysis with the test truck loaded.

The comparison of results between the loaded and empty vehicle configurations reflects similar trends observed in the precision evaluation (Section 5.2.1), where methods applied to the empty vehicle signals showed substantially higher errors compared to the loaded vehicle.

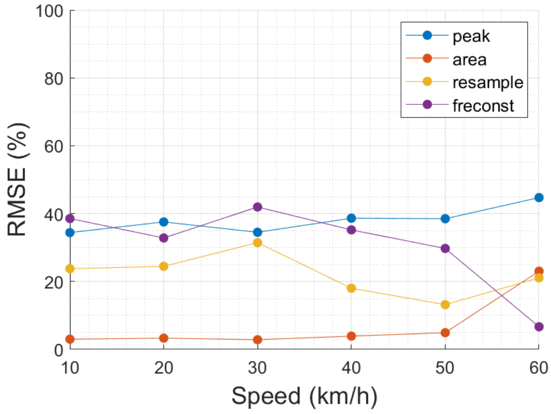


(a) $A_1/A_2$ ratio.

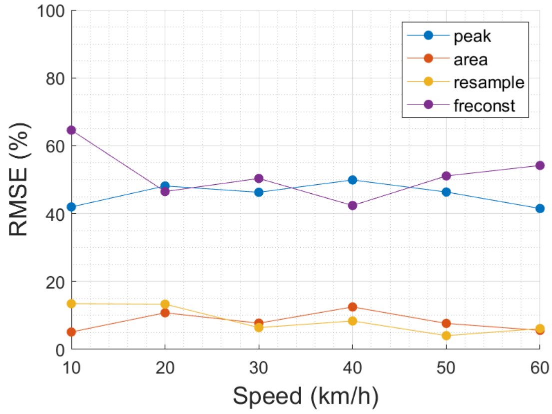


(b) $A_1/A_3$ ratio.

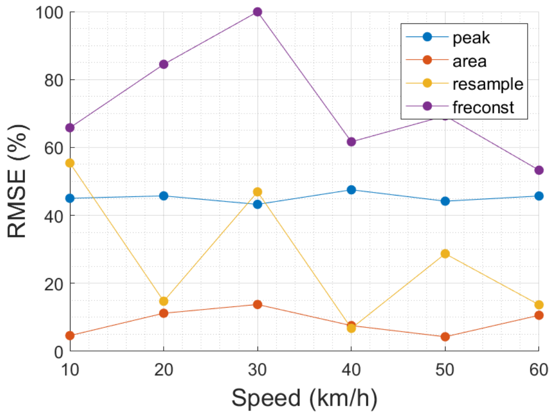


(c) $A_1/A_4$ ratio.

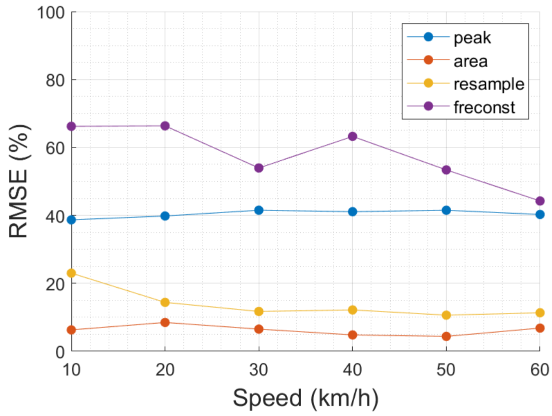


(d) $A_1/A_5$ ratio.

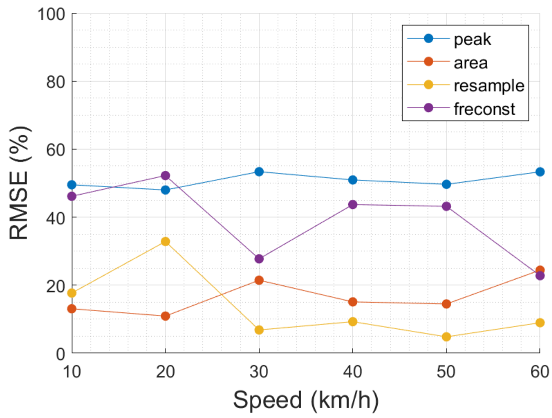


(e) $A_1/A_6$ ratio.

Figure 5.12 – Root mean square error of instantaneous axle weight algorithms for each axle ratio from the experimental analysis with the test truck empty.

This can be attributed to the greater mass of the loaded truck, which dampens the suspension's response to road irregularities, resulting in less oscillation. In contrast, an empty truck, with less mass, allows the suspension to compress more readily, leading to increased oscillations (dynamic load amplitude), which directly contributes to higher errors in weight estimation (Hucho; Ahmed, 1998; Jacob, 2001).

The variability of RMSE across algorithms also aligned with results from the precision analysis, where the Peak Voltage method exhibited the lowest variability among all methods (Figures 5.11 and 5.12). As noted in the precision analysis, the impact of vehicle speed on algorithm accuracy was not as significant as expected, contrasting with the simulation results discussed in Section 5.1.

Despite its consistency, the Peak Voltage method showed higher RMSE when comparing its ratios to the static weight ratios. This method's sensitivity to tire air pressure (Kwon, 2007)–which was not measured in this experimental setup–may explain its inferior performance in this accuracy analysis. On the other hand, the Area Under the Signal method, which compensates for vehicle speed, resulted in the lowest RMSE for most of the tested scenarios. Given that vehicle speed is easily measured by MS-WIM systems (multiple-sensor Weigh-In-Motion), this supports the use of the Area Under the Signal algorithm as one of the most reliable methods for instantaneous axle weight estimation (Cebon; Winkler, 1991; Kistler, 2004; Ryguła *et al.*, 2021).

The Tire Footprint Reconstruction method yielded promising results in the loaded vehicle configuration, showing similar performance to the Resampling of Area method and slightly worse results than the simple area calculation. This technique was implemented using a fixed tire width and tire length proportional to pulse length, the simplest way to reconstruct the tire footprint. However, certain factors such as dynamic tire pressure variations and friction forces (Grakovski; Pilipovecs, 2017b) were not accounted for. More sophisticated approaches, such as elliptical approximation using signal decomposition techniques and diagonally positioned sensors, could further enhance footprint reconstruction (Grakovski; Pilipovecs, 2016; Grakovski; Pilipovecs, 2017b). Unfortunately, this sensor configuration was not available in the experimental setup. In the empty vehicle configuration, this method exhibited one of the highest RMSEs among all methods, which may be related to footprint deformation when the vehicle experiences bouncing (Huang, 1993; Grakovski *et al.*, 2014).

The Resampling of Area algorithm also showed interesting results in some cases. However, it generally performed worse than the simple area calculation, except in very specific scenarios. This method was initially proposed by Kwon (2007) as an improvement of the Area Under the Signal method, but this enhancement did not manifest in this analysis, as the additional computational steps to prevent sampling overlap did not yield significant improvements.

It is important to note that this method had not been extensively tested with experimental data prior to this study, suggesting that further refinements may be needed.

Considering the Area Under the Signal as the most accurate method and the loaded test vehicle as the primary focus of WIM systems, the observed root mean square error (RMSE) values for this scenario were all below 10%, with only a single point exceeding this threshold in the $A_1/A_6$ ratio (Figure 5.11e). In fact, most of these values were around or below the 5% margin. Based on these results, the system would likely be classified as Class B or C according to INMETRO standards (Instituto Nacional de Metrologia, Qualidade e Tecnologia (INMETRO), 2022), which correspond to error thresholds of 6% and 8% for axle weight estimation, respectively. However, it's important to note that this accuracy analysis did not include a system calibration process, which is essential for accurately estimating axle and vehicle weight in kilograms or tons. Additionally, INMETRO's classification relies on the maximum observed error, not the RMSE as used in this study. To achieve the highest INMETRO classifications (Class A for axle load with a 4% error margin and Class 1 for GVW with a 2.5% error margin), the system would require a calibration procedure, ideally using multiple vehicles with varying numbers of axles and configurations. Another significant factor affecting the system's accuracy is the detour from the main road, which requires the vehicle to leave the main lane and navigate a slight incline just before the weighing area. This combination considerably impacts vehicle dynamics and makes it challenging to compensate for through calibration or weighing methods.

# 6 CONCLUSION AND FUTURE WORKS

Weigh-In-Motion (WIM) systems offer a practical solution for measuring vehicle load to ensure road safety and preservation. The dynamic measurement eliminates the need for static scales, reducing traffic congestion and vehicle stoppages. This study provides an analysis of WIM systems through simulation and experimental data, focusing on the two key stages of weight estimation: instantaneous axle load estimation and Gross Vehicle Weight estimation.

The study began with a review of the impact of weather and road conditions on system accuracy. The influence of environmental and structural factors varies depending on the location of the WIM site. Choosing a smooth, straight road without pavement irregularities is crucial to minimize vehicle vibrations and oscillations. The review also highlighted different types of sensors, such as load cells, bending plates, piezoelectric sensors, and fiber optic sensors, discussing their main advantages and disadvantages, including sensitivity to temperature variations and accuracy levels. Some calibration techniques were also reviewed, including static, dynamic, and continuous methods—which have the advantage of being more economical but the drawback of being less accurate.

The simulation analysis revealed that estimation errors were notably high, especially at higher speeds, with maximum relative errors reaching up to 40% in GVW estimation and 65% in axle weight estimation. This is likely due to the dynamic load amplitude being directly proportional to vehicle speed, as well as the introduction of relative standard deviation (RSD) in sensor measurements based on an experimental study using 16 piezoelectric load sensors after operating the WIM system for two to three years, which can lead to sensor degradation and system wear. In contrast to the simulation results, such high errors were not observed in our experimental study.

In the system layout analysis, sensor spacing had a minimal impact on errors at lower speeds but became more significant at higher speeds. No single sensor spacing was ideal across all tested vehicle speeds; however, distances of 2 and 3 meters performed well across multiple scenarios, making them reasonable choices for various conditions. When considering the number of sensors, it was observed that using more than eight sensors resulted in only marginal gains in error reduction. This information is valuable for WIM system design, as the number of sensors directly influences the system's cost. Nevertheless, systems with more sensors exhibited greater robustness to variations in vehicle speed.

Regarding the evaluated estimators, the Mean Value (MV) estimator consistently provided reliable results across all scenarios, making it a practical choice for many WIM applications. The Maximum Likelihood Estimator (MLE) outperformed the Mean Value only at very low speeds, and its overall gains were less substantial than expected. Signal reconstruction techniques demonstrated potential for WIM systems equipped with a larger number of sensors; although these methods showed higher errors with fewer sensors, their performance tended to align with the Mean Value method when more than ten sensors were used. Additionally, advanced signal reconstruction techniques could leverage information about the vehicle's mechanical system, such as the ranges of $f_1$ and $f_2$ values, to better reconstruct the load signal, thereby yielding better weight estimation results. The use of neural networks for more robust signal reconstruction is another potential approach, though it would require network training, which could be supported by simulations. It is also worth noting that the frequency ranges of 1-5 Hz for $f_1$ and 8-15 Hz for $f_2$ used in simulations were the broadest possible. Narrowing these ranges based on specific truck populations could lead to more refined and optimized system designs.

In the experimental analysis, various instantaneous axle weight estimation methods were assessed using data collected from a six-axle truck under both loaded and unloaded conditions. The accuracy and precision of these methods varied significantly depending on the specific algorithm and the vehicle's load condition. Tests with the empty vehicle consistently showed higher errors across all algorithms compared to the loaded vehicle, likely due to increased dynamic oscillations in the unloaded vehicle. However, these errors are less critical for direct enforcement applications, where the focus is on identifying overloaded vehicles. The analysis also indicated that the front axle exhibited consistently lower errors and deviations compared to the rear axles, likely because it is less affected by the dynamic oscillations that intensify toward the rear of the vehicle, where suspension dynamics and load transfer have a more pronounced effect during motion. This finding suggests that front axle measurements could be used as a reference for calibrating or validating other axle measurements for specific truck configurations.

While higher vehicle speeds were expected to introduce greater measurement errors due to reduced interaction time between the axles and sensors, the experimental study did not show a clear, consistent relationship between speed and weight estimation accuracy. This suggests that other factors, such as road surface conditions, tire characteristics, and vehicle dynamics, may play a more significant role in influencing system precision and accuracy at different speeds.

Among the algorithms evaluated, the Peak Voltage method demonstrated good precision but struggled with accuracy. This method's sensitivity to changes in tire footprint area–affected by factors such as tire inflation–may explain its relatively higher errors in accuracy analysis. The Area Under the Signal method exhibited robust performance across both loaded and empty vehicle tests. This method is adjusted based on vehicle speed, and this might have helped it achieve lower root mean square errors (RMSE) compared to the other methods.

The Resampling of Area algorithm, proposed as an improvement over the Area Under the Signal method, demonstrated good results but did not consistently outperform the simpler area calculation method. While it accounted for sensor width and aimed to refine the sampling period to prevent overlap, these additional steps did not yield significant improvements in accuracy in our experimental setup. The higher variability observed in its performance suggests that further refinement and testing with experimental data are needed before this method can be considered a feasible alternative. Finally, the Tire Footprint Reconstruction technique, while theoretically promising, exhibited higher variability and lower accuracy in this study. This can be attributed to the simplified implementation that did not consider the complex interactions between the tire and the road surface, such as tire deformation and load distribution across the contact path.

When comparing the experimental results of the loaded truck with INMETRO legislation (Instituto Nacional de Metrologia, Qualidade e Tecnologia (INMETRO), 2022), the Area Under the Signal method exhibited root mean square error (RMSE) values around the 5% margin in most cases, which would classify the system as Class B or C (with 6% and 8% error thresholds for axle weight estimation, respectively). It is important to note that INMETRO uses the maximum relative error in its classification, rather than the RMSE, and the accuracy analysis conducted in this study did not include calibration procedures using multiple types of vehicles. Therefore, a more comprehensive analysis is required before conducting formal tests in accordance with the current Brazilian legislation.

This study aimed to address the research gap in comparing various instantaneous axle load estimation methods under similar conditions. Although the tests did not account for system calibration or dynamic load amplitude ground truth information, the results indicate that certain algorithms, particularly the Area Under the Signal method, have great potential for application in direct enforcement systems, consistently achieving RMSEs lower than 10% in most loaded vehicle tests.

Furthermore, conducting simulations under diverse conditions, including varying vehicle speeds and sensor configurations, aided in further understanding the system layout stage. Defining an optimal number of sensors for specific conditions is crucial, as this directly impacts the cost of installation and maintenance. While the Mean Value estimator remains a reliable choice, the MLE's gains were not as substantial as anticipated, and signal reconstruction techniques require further development to be effectively applied in WIM applications.

Future research could explore advanced signal reconstruction techniques by leveraging information about the dynamic load signal, such as the frequency ranges characteristic of a specific truck population. Integrating this data into the reconstruction process may help reduce distortions between the original and reconstructed signals, enabling more accurate reconstructions. Such reconstructions can be applied in various ways, including filtering out dynamic components, gaining deeper insights into a vehicle's mechanical system, and even identifying road irregularities that amplify vehicle oscillations. Another promising approach for reconstructing the moving vehicle load signal involves using cameras to capture the vehicle's motion as it passes through the WIM system. By synchronizing these images with the load sensor readings, it becomes possible to calculate vehicle load variations (i.e., vertical acceleration) over time, enabling a highly precise signal reconstruction.

# BIBLIOGRAPHY


Administration, F. H. **Weigh-in-Motion Pocket Guide Part I - WIM Technology Selection, Data Acquisition Requirements, and Procurement Guide**. [S.l.], 2018.

Agape, I.; Dontu, A. I.; Maftei, A.; Gaiginschi, L.; Barsanescu, P. D. Actual types of sensors used for weighing in motion. **IOP Conference Series: Materials Science and Engineering**, v. 572, n. 1, p. 012102, jul 2019.

Al-Qadi, I.; Wang, H.; Ouyang, Y.; Grimmelsman, K.; Purdy, J. E.; Pennoni Associates Incorporated. **LTBP Program's Literature Review on Weigh-in-Motion Systems**. [S.l.], 2016. Disponível em: <https://rosap.ntl.bts.gov/view/dot/35735>.

ASTM International. **Standard Specification for Highway Weigh-In-Motion (WIM) Systems with User Requirements and Test Methods**. 2010.

Balsom, M.; Wilson, F. R.; Hildebrand, E. Impact of wind forces on heavy truck stability. **Transportation Research Record**, v. 1969, n. 1, p. 115–120, 2006.

Batenko, A.; Grakovski, A.; Kabashkin, I.; Petersons, E.; Sikerzhicki, Y. Weight-in-motion (wim) measurements by fiber optic sensor: Problems and solutions. v. 12, 01 2011.

Batenko, A.; Grakovski, A.; Kabashkin, I.; Petersons, E.; Sikerzhicki, Y. Weight-in-motion (wim) measurements by fiber optic sensor: Problems and solutions. **Transport and Telecommunication**, v. 12, n. 4, p. 27–33, 01 2011.

Benekohal, R. F.; El-Zohairy, Y. M.; Wang, S. Truck travel time around weigh stations: Effects of weigh in motion and automatic vehicle identification systems. **Transportation Research Record**, n. 1716, p. 135–143, 2000.

Burnos, P. Auto-calibration and temperature correction of wim systems. In: **International Conference on Weigh-in-Motion of Heavy Vehicles, Paris**. [S.l.: s.n.], 2008. ISBN 9781848210592.

Burnos, P.; Gajda, J. Optimised autocalibration algorithm of weigh-in-motion systems for direct mass enforcement. **Sensors**, v. 20, n. 11, 2020.

Burnos, P.; Gajda, J.; Piwowar, P.; Sroka, R.; Stencel, M.; Zeglen, T. Accurate weighing of moving vehicles. **Metrology and Measurement Systems**, v. 14, p. 507–516, 01 2007.

Carlson, A.; Vieira, T. **The Effect of Water and Snow on the Road Surface on Rolling Resistance**. [S.l.], 2021. 43 p. (VTI rapport, 971A). Disponível em: <http://www.vti.se/>.

Cebon, D. Design of multiple-sensor weigh-in-motion systems. **Proceedings of the Institution of Mechanical Engineers, Part D: Journal of Automobile Engineering**, v. 204, n. 2, p. 133–144, 1990.

Cebon, D.; Winkler, C. B. **A Study of Road Damage Due to Dynamic Wheel Loads Using a Load Measuring Mat**. [S.l.], 1990. Disponível em: <https://api.semanticscholar.org/CorpusID:208779278>.

Cebon, D.; Winkler, C. B. Multiple-sensor weigh-in-motion, theory and experiments. **Transportation Research Record**, n. 1311, p. 70–78, 1991.

Cole, D. J.; Cebon, D. A capacitance strip sensor for measuring dynamic tyre forces. In: Institution of Electrical Engineers. **Proc., 2nd International Conference on Road Traffic Monitoring**. London, 1989.

Cole, D. J.; Cebon, D. Spatial repeatability of dynamic tyre forces generated by heavy vehicles. **Proceedings of the Institution of Mechanical Engineers, Part D: Journal of Automobile Engineering**, v. 206, n. 1, p. 17–27, 1992.

Departamento Nacional de Infraestrutura de Transportes (DNIT). **Quadro de Fabricantes de Veículos**. 2012. Disponível em: <https://www.gov.br/dnit/pt-br/rodovias/operacoes-rodoviarias/pesagem/QFV2012ABRIL.pdf>.

Dornfeld, D. A.; DeVries, M. Neural network sensor fusion for tool condition monitoring. **CIRP Annals**, v. 39, n. 1, p. 101–105, 1990.

Gajda, J.; Burnos, P. Temperature properties of weigh-in-motion systems. In: **7th International Conference on Weigh-in-Motion & PIARC workshop, Foz do Iguacu, Brazil**. [S.l.: s.n.], 2016. p. 46–55.

Gajda, J.; Sroka, R.; Burnos, P. Sensor data fusion in multi-sensor weigh-in-motion systems. **Sensors**, v. 20, n. 12, 2020.

Gajda, J.; Sroka, R.; Burnos, P. Designing the calibration process of weigh-in-motion systems. **Electronics**, v. 10, n. 20, 2021.

Gajda, J.; Sroka, R.; Stencel, M.; Zeglen, T.; Piwowar, P.; Burnos, P.; Marszalek, Z. Design and accuracy assessment of the multi-sensor weigh-in-motion system. In: **2015 IEEE International Instrumentation and Measurement Technology Conference (I2MTC) Proceedings**. [S.l.: s.n.], 2015. p. 1036–1041.

Gajda, J.; Sroka, R.; Zeglen, T.; Burnos, P. The influence of temperature on errors of wim systems employing piezoelectric sensors keywords: Piezoelectric sensors, temperature influence, temperature error of wim systems, error correction. **Metrology and Measurement Systems**, v. 20, p. 171–182, 06 2013.

Di Giacinto, D.; Musone, V.; Laudante, G.; Grassia, L.; Ruocco, E. Weight-in-motion system for traffic overload detection: Development and experimental testing. In: **Civil Structural Health Monitoring**. Cham: Springer International Publishing, 2021. p. 403–413. ISBN 978-3-030-74258-4.

Grakovski, A.; Krasnitski, Y.; Kabashkin, I.; Truhachov, V. Some approaches to the rolling wheels' dynamics modelling in the weight-in-motion problem. **Transport and Telecommunication Journal**, v. 14, n. 1, p. 57–78, 2013.

Grakovski, A.; Pilipovec, A.; Kabashkin, I.; Petersons, E. Weight-in-motion estimation based on reconstruction of tyre footprint's geometry by group of fibre optic sensors. **Transport and Telecommunication Journal**, v. 15, n. 2, p. 97–110, 2014.

Grakovski, A.; Pilipovecs, A. The problem of tyre footprint width estimation by fibre optic wim sensors in condition of geometric complexity. In: Zamojski, W.; Mazurkiewicz, J.; Sugier, J.; Walkowiak, T.; Kacprzyk, J. (Ed.). **Dependability Engineering and Complex Systems**. Cham: Springer International Publishing, 2016. p. 219–227. ISBN 978-3-319-39639-2.

Grakovski, A.; Pilipovecs, A. Dynamics of interaction between the road surface and vehicle's wheel in fibre-optic system for automatic weighing in motion of transport. **Procedia Engineering**, v. 178, p. 5–12, 12 2017.

Grakovski, A.; Pilipovecs, A. Multi-purpose fibre optic system for automated vehicle's weighting-in-motion and classification in applications of intelligent transport systems. In: **2017 5th IEEE International Conference on Models and Technologies for Intelligent Transportation Systems (MT-ITS)**. [S.l.: s.n.], 2017. p. 610–615.

Grakovski, A.; Pilipovecs, A. Multi-purpose fibre optic system for automated vehicle's weighting-in-motion and classification in applications of intelligent transport systems. In: . [S.l.: s.n.], 2017. p. 610–615.

Grakovski, A.; Pilipovecs, A. Weigh-in-motion by fibre-optic sensors: Problem of measurement errors compensation for longitudinal oscillations of a truck. In: Kabashkin, I.; Yatskiv, I.; Prentkovskis, O. (Ed.). **Reliability and Statistics in Transportation and Communication**. Cham: Springer International Publishing, 2018. p. 371–380.

Grakovski, A.; Pilipovecs, A.; Kabashkin, I.; Petersons, E. Tyre footprint geometric form reconstruction by fibre-optic sensor's data in the vehicle weight-in-motion estimation problem. In: Ferrier, J.-L.; Gusikhin, O.; Madani, K.; Sasiadek, J. (Ed.). **Informatics in Control, Automation and Robotics**. [S.l.]: Springer International Publishing, 2015. p. 123–137. ISBN 978-3-319-10891-9.

Hallenbeck, M.; Weinblatt, H. **Equipment for Collecting Traffic Load Data**. Washington, DC, United States, 2004. Disponível em: <http://www.trb.org/main/blurbs/154106.aspx>.

Haupt, J.; Nowak, R. Signal reconstruction from noisy random projections. **IEEE Transactions on Information Theory**, v. 52, n. 9, p. 4036–4048, 2006.

Huang, Y. H. **Pavement Analysis and Design**. 2nd. ed. Englewood Cliffs, New Jersey: Prentice Hall, 1993.

Hucho, W.; Ahmed, S. **Aerodynamics of Road Vehicles: From Fluid Mechanics to Vehicle Engineering**. 4th. ed. Society of Automotive Engineers, 1998. ISBN 9780768000290.

Huhtala, M.; Halonen, P.; Dolcemascolo, V.; O'Brien, E.; Stanczyck, D. **Weigh-in-Motion of Axles and Vehicles for Europe (WAVE). Report Package 3.2**. Paris, 2000.

Instituto Nacional de Metrologia, Qualidade e Tecnologia (INMETRO). **Portaria nº 19, de 12 de janeiro de 2022**. 2022.

International Organization for Standardization. International Standard, **Mechanical Vibration – Road Surface Profiles – Reporting of Measured Data**. 1995.

International Organization of Legal Metrology (OIML). International Recommendation, **Automatic instruments for weighing road vehicles in motion and measuring axle loads - Part 1: Metrological and technical requirements – Tests**. 2006.

Izadmehr, B.; Lee, C. E. Accuracy and tolerances of weigh-in-motion systems. **Transportation Research Record**, v. 1123, p. 127–135, 1987.

Jacob, B. **Weigh-In-Motion of Axles and Vehicles for Europe (WAVE). General Report of 4th Framework Programme Transport**. Paris, 2001.

Jacob, B.; O'Brien, E. J.; Jehaes, S. (Ed.). **Weigh-in-Motion of Road Vehicles: Final Report of the COST 323 Action**. [S.l.], 2002. 538 p. (COST 323, v. 1).

Janota, A.; Nemec, D.; Hruboš, M.; Pirník, R. Knowledge-based approach to selection of weight-in-motion equipment. In: Mikulski, J. (Ed.). **Challenge of Transport Telematics**. Cham: Springer International Publishing, 2016. p. 1–12. ISBN 978-3-319-49646-7.

Jia, Z.; Fu, K.; Lin, M. Tire–pavement contact-aware weight estimation for multi-sensor wim systems. **Sensors**, v. 19, n. 9, 2019.

Jonscher, M.; Seiler, J.; Richter, T.; Kaup, A. Reducing randomness of non-regular sampling masks for image reconstruction. In: **2014 IEEE Visual Communications and Image Processing Conference**. [S.l.: s.n.], 2014. p. 266–269.

Kistler. **Planning of a WIM (Weigh in Motion) Station, Type 9195E**. [S.l.], 2004.

Kwon, T. Signal processing of piezoelectric weight-in-motion systems. In: **Proceedings of the Fifth IASTED International Conference on Circuits, Signals and Systems**. [S.l.: s.n.], 2007. p. 233–238.

Lee, C. E.; Ferguson, P. M. Concepts of weigh-in-motion systems. In: **National Weigh in Motion Conference Proceedings**. Stapleton Plaza Hotel, Denver, Colorado: [s.n.], 1983.

Lee, Y.-T.; Seo, H.-D.; Kawamura, A.; Yamada, T.; Matsumoto, Y.; Ishida, M.; Nakamura, T. Compensation method of offset and its temperature drift in silicon piezoresistive pressure sensor using double wheatstone-bridge configuration. In: **Proceedings of the International Solid-State Sensors and Actuators Conference - TRANSDUCERS '95**. [S.l.: s.n.], 1995. v. 2, p. 570–573.

Li, R.; Tan, Y.; Chen, Y.; Hong, L.; Zhou, Z. Investigation of sensitivity enhancing and temperature compensation for fiber bragg grating (fbg)-based strain sensor. **Optical Fiber Technology**, v. 48, p. 199–206, 2019.

Li, W.; Cheng, C.; Lo, Y. Investigation of strain transmission of surface-bonded fbgs used as strain sensors. **Sensors and Actuators A: Physical**, v. 149, n. 2, p. 201–207, 2009.

Lin, H.; Li, S.; Wang, L.; Yang, J. Weighing method for a truck scale based on optional neural network with penalty function. **Transactions of the Institute of Measurement and Control**, v. 39, n. 7, p. 1088–1096, 2017.

Lin, H.; Lin, Y.; Yu, J.; Teng, Z.; Wang, L. Weighing fusion method for truck scales based on prior knowledge and neural network ensembles. **IEEE Transactions on Instrumentation and Measurement**, v. 63, n. 2, p. 250–259, 2014.

Lin, H.; Wang, L.; Teng, Z.; Dai, H.; Li, S. Optimization for a neural network based on input-vectors correlation and its application to a truck scale. **IEEE Transactions on Industrial Electronics**, v. 64, n. 6, p. 4917–4927, 2017.

Lu, P.; Tolliver, D. **Sensitivity and Accuracy Assessment of Vehicle Weigh-in-Motion System Measurement Errors Using In-Pavement Strain-Based Sensors**. 1320 Albrecht Boulevard, Fargo, ND, United States, 581052, 2023.

Mangeas, M.; Glaser, S.; Dolcemascolo, V. Neural networks estimation of truck static weights by fusing weight-in-motion data. In: **Proceedings of the Fifth International Conference on Information Fusion. FUSION 2002. (IEEE Cat.No.02EX5997)**. [S.l.: s.n.], 2002. v. 1, p. 456–462 vol.1.

Maxwell, A. E.; Warner, T. A.; Guillén, L. A. Accuracy assessment in convolutional neural network-based deep learning remote sensing studies—part 1: Literature review. **Remote Sensing**, v. 13, n. 13, 2021.

Mimbela, L.-E. Y.; Pate, J.; Copeland, S.; Kent, P. M.; Hamrick, J. **Applications of Fiber Optics Sensors in Weigh-in-Motion (WIM) Systems for Monitoring Truck Weights on Pavements and Structures**. [S.l.], 2003. Disponível em: <https://rosap.ntl.bts.gov/view/dot/17836>.

Nagahara, M. Discrete signal reconstruction by sum of absolute values. **IEEE Signal Processing Letters**, v. 22, n. 10, p. 1575–1579, 2015.

Ono, T. On dynamic weighing of highway vehicles in motion. In: **SICE 2003 Annual Conference (IEEE Cat. No.03TH8734)**. [S.l.: s.n.], 2003. v. 2, p. 2108–2115 Vol.2.

Oubrich, L.; Ouassaid, M.; Maaroufi, M. Dynamic loads, source of errors of high speed weigh in motion systems. In: **2017 14th International Multi-Conference on Systems, Signals & Devices (SSD)**. [S.l.: s.n.], 2017. p. 354–359.

Oubrich, L.; Ouassaid, M.; Maaroufi, M. Reconstruction of axle load signal, measurement basis of static load of vehicle axles through the high speed weigh in motion system. In: **2018 4th International Conference on Optimization and Applications (ICOA)**. [S.l.: s.n.], 2018. p. 1–6.

Oyamada, K.; Kameoka, H.; Kaneko, T.; Tanaka, K.; Hojo, N.; Ando, H. Generative adversarial network-based approach to signal reconstruction from magnitude spectrogram. In: **2018 26th European Signal Processing Conference (EUSIPCO)**. [S.l.: s.n.], 2018. p. 2514–2518.

Pais, J. C.; Amorim, S. I. R.; Minhoto, M. J. C. Impact of traffic overload on road pavement performance. **Journal of Transportation Engineering**, v. 139, n. 9, p. 873–879, 2013.

Pratt, D.; Choi, Y.; Plemel, M.; Papagiannakis, A. T. Continuous calibration weigh-in-motion system using static weight data. **Transportation Research Record**, v. 2676, n. 12, p. 740–749, 2022.

Oliveira Rocheti, E. **Weigh-In-Motion Simulator**. 2024. Accessed: 2024-10-16. Disponível em: <https://github.com/enricorocheti/wim-sim>.

Oliveira Rocheti, E.; Moreira Bacurau, R. Weigh-in-motion systems review: Methods for axle and gross vehicle weight estimation. **IEEE Access**, v. 12, p. 134822–134836, 2024.

Ryguła, A.; Maczyński, A.; Brzozowski, K.; Grygierek, M.; Konior, A. Influence of trajectory and dynamics of vehicle motion on signal patterns in the wim system. **Sensors**, v. 21, n. 23, 2021.

Saburdo, G. A.; Topolev, V. P. Investigation of dynamic errors in weighing loads in motion. **Measurement Techniques**, v. 7, n. 11, p. 954–957, 1964.

Stergioulas, L. K.; Cebon, D.; Macleod, M. D. Static weight estimation and system design for multiple-sensor weigh-in-motion. **Proceedings of the Institution of Mechanical Engineers, Part C: Journal of Mechanical Engineering Science**, v. 214, n. 8, p. 1019–1035, 2000.

Sujon, M.; Dai, F. Application of weigh-in-motion technologies for pavement and bridge response monitoring: State-of-the-art review. **Automation in Construction**, v. 130, p. 103844, 2021.

Tutak, P. Application of strain gauges in measurements of strain distribution in complex objects. **Journal of Applied Computer Science Methods**, v. 6, 12 2014.

Wang, Z.; Wang, Q.; Hou, J. The research of weigh-in-motion sensor layout based on data fusion. In: **2009 Sixth International Conference on Fuzzy Systems and Knowledge Discovery**. [S.l.: s.n.], 2009. v. 2, p. 127–131.

Xiong, L.; Jiang, G.; Guo, Y.; Kuang, Y.; Liu, H. Investigation of the temperature compensation of fbgs encapsulated with different methods and subjected to different temperature change rates. **Journal of Lightwave Technology**, v. 37, n. 3, p. 917–926, 2019.

Yang, J.; Yan, T.; Sun, W. Polynomial fitting and interpolation method in tdoa estimation of sensors network. **IEEE Sensors Journal**, v. 23, n. 4, p. 3837–3847, 2023.

Yang, X.; Zhao, Q.; Wang, Y.; Cheng, K. Fault signal reconstruction for multi-sensors in gas turbine control systems based on prior knowledge from time series representation. **Energy**, v. 262, p. 124996, 2023.

Zhang, L.; Haas, C.; Tighe, S. Evaluating weigh-in-motion sensing technology for traffic data collection. In: **Annual Conference of the Transportation Association of Canada Saskatoon, Saskatchewan**. [S.l.: s.n.], 2007.

Zhang, Z.; Huang, Y.; Bridgelall, R.; Palek, L.; Strommen, R. Sampling optimization for high-speed weigh-in-motion measurements using in-pavement strain-based sensors. **Measurement Science and Technology**, v. 26, n. 6, p. 065003, may 2015.

# Appendix

# APPENDIX A – SIMULATION FIGURES AND TABLES

This appendix contains additional figures that complement the main analysis presented in Chapter 5. These figures include detailed results for axle load estimation, as well as the relative standard deviation (RSD) for different vehicle categories (2S3, 3I3, and 34D), covering both the system layout and estimators evaluation.

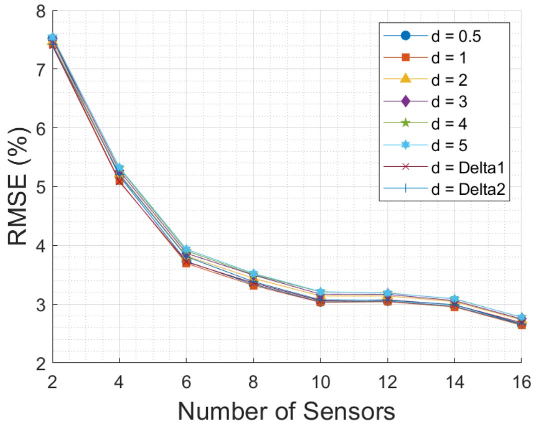


(a) Vehicle speed = 20 km/h.

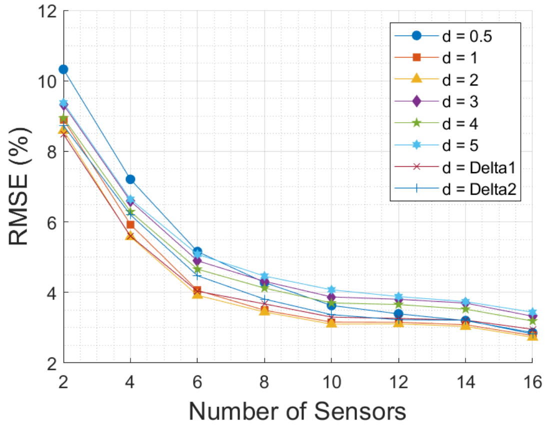


(b) Vehicle speed = 40 km/h.

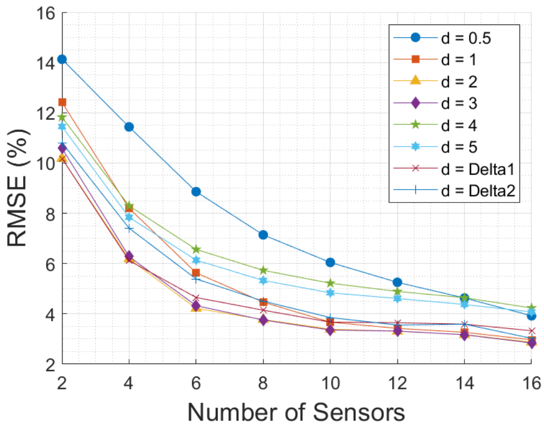


(c) Vehicle speed = 60 km/h.

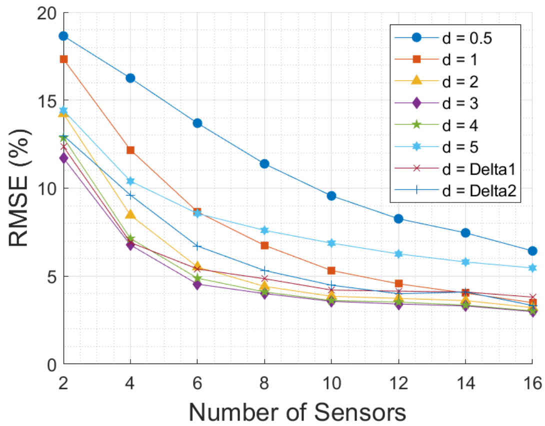


(d) Vehicle speed = 80 km/h.

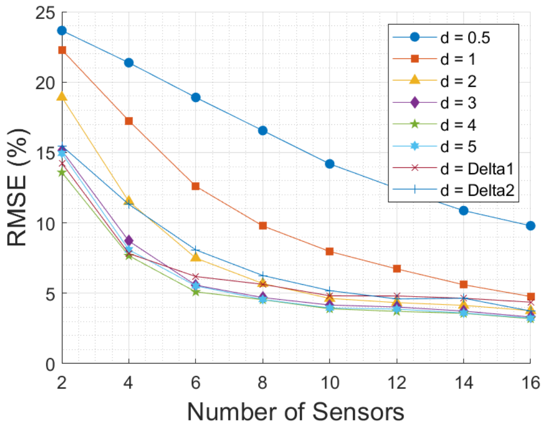


(e) Vehicle speed = 100 km/h.

Figure A.1 – Axle root mean square error from the system layout evaluation in the simulation analysis, with each curve representing a different sensor distance.

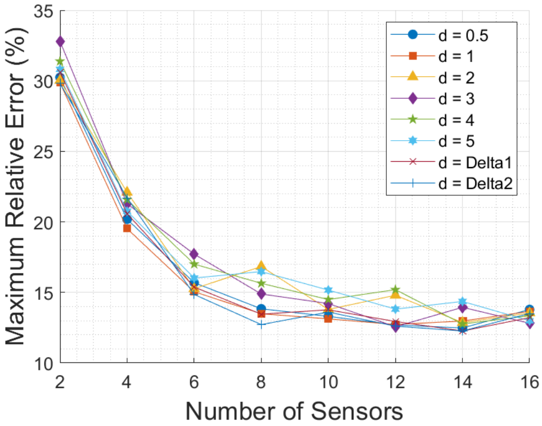


(a) Vehicle speed = 20 km/h.

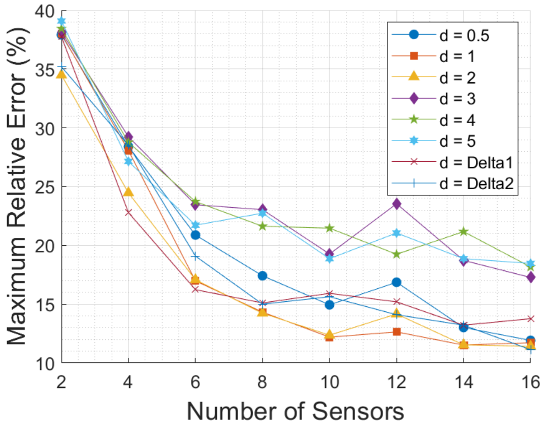


(b) Vehicle speed = 40 km/h.

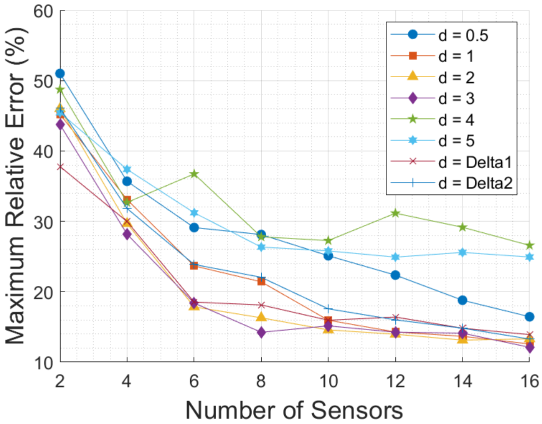


(c) Vehicle speed = 60 km/h.

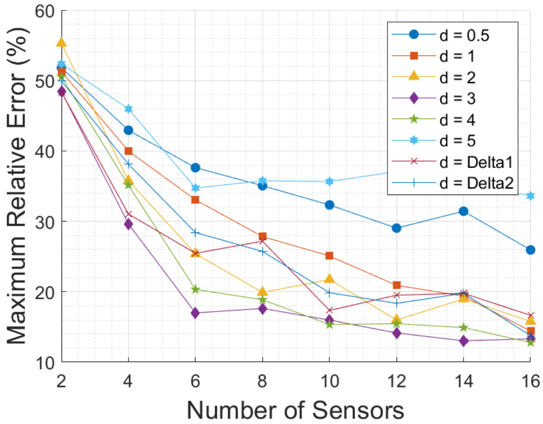


(d) Vehicle speed = 80 km/h.

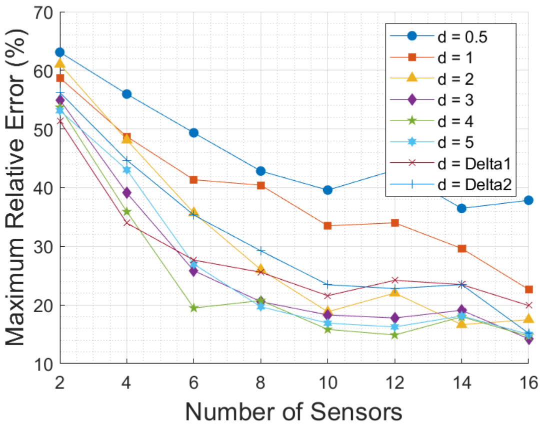


(e) Vehicle speed = 100 km/h.

Figure A.2 – Axle maximum relative error from the system layout evaluation in the simulation analysis, with each curve representing a different sensor distance.

Table A.1 – Relative standard deviation of GVW estimation for the system layout evaluation in the simulation analysis, vehicle category 2S3.

| Speed | Distance | N = 2 | N = 4 | N = 6 | N = 8 | N = 10 | N = 12 | N = 14 | N = 16 |
|---|---|---|---|---|---|---|---|---|---|
| 20 | 0.5 | 3.26 | 2.46 | 1.46 | 1.48 | 1.43 | 1.45 | 1.29 | 1.28 |
| | 1 | 3.13 | 2.42 | 1.51 | 1.48 | 1.42 | 1.45 | 1.31 | 1.25 |
| | 2 | 3.24 | 2.44 | 1.59 | 1.50 | 1.48 | 1.48 | 1.33 | 1.21 |
| | 3 | 3.45 | 2.50 | 1.67 | 1.54 | 1.46 | 1.52 | 1.35 | 1.30 |
| | 4 | 3.31 | 2.45 | 1.60 | 1.49 | 1.45 | 1.46 | 1.40 | 1.25 |
| | 5 | 3.22 | 2.50 | 1.55 | 1.55 | 1.50 | 1.55 | 1.39 | 1.32 |
| | $\Delta_{D1}$ | 3.17 | 2.38 | 1.47 | 1.47 | 1.40 | 1.48 | 1.30 | 1.25 |
| | $\Delta_{D2}$ | 3.25 | 2.42 | 1.54 | 1.45 | 1.41 | 1.49 | 1.31 | 1.26 |
| 40 | 0.5 | 5.58 | 3.12 | 2.04 | 2.05 | 1.65 | 1.53 | 1.51 | 1.29 |
| | 1 | 4.53 | 2.96 | 1.91 | 1.76 | 1.41 | 1.27 | 1.46 | 1.31 |
| | 2 | 4.09 | 2.18 | 1.67 | 1.64 | 1.35 | 1.26 | 1.38 | 1.18 |
| | 3 | 4.62 | 3.20 | 2.25 | 2.44 | 2.21 | 2.02 | 2.04 | 1.56 |
| | 4 | 3.91 | 2.45 | 1.94 | 1.84 | 1.48 | 1.36 | 1.40 | 1.29 |
| | 5 | 4.02 | 3.17 | 2.18 | 1.67 | 1.91 | 1.27 | 1.62 | 1.37 |
| | $\Delta_{D1}$ | 4.19 | 2.68 | 1.90 | 1.75 | 1.43 | 1.44 | 1.53 | 1.45 |
| | $\Delta_{D2}$ | 4.27 | 3.02 | 1.88 | 1.90 | 1.48 | 1.43 | 1.39 | 1.30 |
| 60 | 0.5 | 6.33 | 5.82 | 5.56 | 4.31 | 3.99 | 3.37 | 2.85 | 2.64 |
| | 1 | 5.94 | 4.22 | 4.20 | 2.88 | 1.98 | 1.71 | 1.47 | 1.38 |
| | 2 | 4.97 | 2.61 | 2.01 | 1.71 | 1.49 | 1.54 | 1.33 | 1.35 |
| | 3 | 5.12 | 2.56 | 2.10 | 1.69 | 1.39 | 1.53 | 1.37 | 1.42 |
| | 4 | 3.94 | 3.14 | 2.61 | 1.95 | 1.94 | 1.88 | 1.56 | 1.47 |
| | 5 | 4.16 | 2.42 | 1.76 | 1.63 | 1.51 | 1.45 | 1.38 | 1.40 |
| | $\Delta_{D1}$ | 5.06 | 2.56 | 2.62 | 2.21 | 1.98 | 1.84 | 1.77 | 1.88 |
| | $\Delta_{D2}$ | 5.30 | 3.89 | 4.00 | 2.93 | 2.17 | 1.76 | 1.56 | 1.47 |
| 80 | 0.5 | 9.61 | 9.62 | 10.21 | 6.83 | 8.52 | 6.57 | 5.12 | 5.12 |
| | 1 | 8.80 | 8.40 | 7.67 | 3.84 | 4.69 | 2.97 | 2.65 | 2.44 |
| | 2 | 8.53 | 5.79 | 3.35 | 1.85 | 1.95 | 1.89 | 1.60 | 1.80 |
| | 3 | 8.82 | 3.73 | 2.34 | 2.04 | 2.22 | 1.80 | 1.69 | 1.67 |
| | 4 | 7.08 | 3.21 | 2.13 | 1.70 | 1.75 | 1.70 | 1.66 | 1.59 |
| | 5 | 6.01 | 2.91 | 2.33 | 1.83 | 1.89 | 1.81 | 1.76 | 1.54 |
| | $\Delta_{D1}$ | 7.52 | 4.21 | 3.18 | 2.18 | 3.24 | 2.62 | 2.69 | 2.79 |
| | $\Delta_{D2}$ | 8.59 | 7.03 | 5.15 | 2.95 | 3.60 | 2.45 | 2.26 | 2.14 |
| 100 | 0.5 | 14.96 | 15.36 | 13.31 | 12.59 | 12.31 | 9.03 | 9.40 | 8.67 |
| | 1 | 13.62 | 13.88 | 9.92 | 9.04 | 6.06 | 4.56 | 4.90 | 2.98 |
| | 2 | 11.26 | 8.52 | 5.77 | 3.23 | 2.98 | 2.36 | 2.14 | 2.01 |
| | 3 | 10.62 | 5.61 | 3.24 | 3.18 | 2.35 | 2.45 | 2.08 | 1.70 |
| | 4 | 8.90 | 5.22 | 2.64 | 2.48 | 2.57 | 1.91 | 1.84 | 1.51 |
| | 5 | 8.12 | 4.14 | 2.76 | 2.62 | 2.20 | 2.00 | 1.96 | 1.45 |
| | $\Delta_{D1}$ | 8.07 | 5.40 | 4.15 | 3.17 | 3.84 | 3.07 | 3.90 | 2.64 |
| | $\Delta_{D2}$ | 10.76 | 8.23 | 6.34 | 4.28 | 4.13 | 2.86 | 3.00 | 2.27 |

Table A.2 – Relative standard deviation of GVW estimation for the system layout evaluation in the simulation analysis, vehicle category 3I3.

| Speed | Distance | N = 2 | N = 4 | N = 6 | N = 8 | N = 10 | N = 12 | N = 14 | N = 16 |
|---|---|---|---|---|---|---|---|---|---|
| 20 | 0.5 | 3.26 | 2.13 | 1.64 | 1.53 | 1.17 | 1.24 | 1.07 | 1.02 |
| | 1 | 3.31 | 2.08 | 1.63 | 1.47 | 1.13 | 1.21 | 1.07 | 1.01 |
| | 2 | 3.41 | 2.22 | 1.80 | 1.54 | 1.21 | 1.24 | 1.11 | 1.03 |
| | 3 | 3.43 | 2.22 | 1.90 | 1.78 | 1.45 | 1.41 | 1.33 | 1.19 |
| | 4 | 3.42 | 2.45 | 1.86 | 1.70 | 1.48 | 1.40 | 1.20 | 1.14 |
| | 5 | 3.08 | 2.38 | 1.83 | 1.72 | 1.33 | 1.37 | 1.11 | 1.03 |
| | $\Delta_{D1}$ | 3.21 | 2.12 | 1.63 | 1.53 | 1.18 | 1.20 | 1.05 | 1.00 |
| | $\Delta_{D2}$ | 3.10 | 2.24 | 1.59 | 1.50 | 1.20 | 1.19 | 1.03 | 0.97 |
| 40 | 0.5 | 3.95 | 3.26 | 2.61 | 2.34 | 1.78 | 1.54 | 1.47 | 1.08 |
| | 1 | 4.11 | 2.39 | 1.72 | 1.46 | 1.17 | 1.24 | 1.25 | 1.02 |
| | 2 | 3.90 | 1.96 | 1.62 | 1.34 | 1.11 | 1.28 | 1.19 | 1.05 |
| | 3 | 3.45 | 1.99 | 1.82 | 1.44 | 1.43 | 1.52 | 1.28 | 1.34 |
| | 4 | 3.28 | 2.23 | 1.79 | 1.48 | 1.38 | 1.58 | 1.35 | 1.15 |
| | 5 | 4.03 | 2.59 | 2.04 | 1.89 | 1.41 | 1.41 | 1.40 | 1.32 |
| | $\Delta_{D1}$ | 3.78 | 2.08 | 1.69 | 1.70 | 1.25 | 1.46 | 1.48 | 1.10 |
| | $\Delta_{D2}$ | 4.00 | 2.95 | 2.13 | 1.79 | 1.33 | 1.44 | 1.36 | 1.03 |
| 60 | 0.5 | 7.33 | 6.20 | 5.20 | 5.24 | 4.00 | 3.40 | 2.31 | 1.66 |
| | 1 | 6.71 | 4.86 | 3.35 | 3.10 | 1.81 | 2.03 | 1.31 | 1.39 |
| | 2 | 5.94 | 3.32 | 1.81 | 1.84 | 1.66 | 1.86 | 1.27 | 1.24 |
| | 3 | 5.08 | 2.65 | 2.02 | 1.99 | 1.60 | 1.69 | 1.39 | 1.18 |
| | 4 | 4.82 | 3.29 | 2.27 | 2.23 | 2.03 | 1.87 | 1.79 | 1.18 |
| | 5 | 4.61 | 3.01 | 2.61 | 2.65 | 2.33 | 1.95 | 1.54 | 1.57 |
| | $\Delta_{D1}$ | 4.91 | 3.16 | 2.27 | 2.67 | 1.81 | 2.26 | 1.53 | 1.60 |
| | $\Delta_{D2}$ | 6.59 | 4.21 | 3.16 | 3.13 | 1.97 | 2.16 | 1.45 | 1.28 |
| 80 | 0.5 | 11.99 | 11.46 | 10.17 | 8.70 | 8.40 | 7.21 | 4.75 | 5.49 |
| | 1 | 12.42 | 8.11 | 7.58 | 4.86 | 4.53 | 3.14 | 2.09 | 1.91 |
| | 2 | 10.63 | 5.44 | 3.53 | 2.50 | 2.15 | 2.08 | 1.69 | 1.47 |
| | 3 | 7.24 | 3.29 | 2.62 | 2.28 | 2.01 | 1.72 | 1.66 | 1.58 |
| | 4 | 7.33 | 3.67 | 2.59 | 2.04 | 1.77 | 1.88 | 1.57 | 1.32 |
| | 5 | 8.36 | 4.54 | 3.86 | 3.21 | 2.17 | 2.79 | 2.39 | 2.15 |
| | $\Delta_{D1}$ | 7.21 | 3.60 | 3.38 | 3.05 | 2.73 | 2.73 | 2.13 | 2.45 |
| | $\Delta_{D2}$ | 9.08 | 5.85 | 5.56 | 3.73 | 3.20 | 2.54 | 1.90 | 1.68 |
| 100 | 0.5 | 16.99 | 17.00 | 15.81 | 14.87 | 11.96 | 11.67 | 8.74 | 9.36 |
| | 1 | 16.25 | 14.84 | 10.58 | 10.11 | 5.63 | 6.17 | 3.92 | 3.90 |
| | 2 | 14.64 | 10.12 | 5.68 | 4.39 | 2.96 | 2.91 | 2.85 | 2.52 |
| | 3 | 12.72 | 7.04 | 3.24 | 3.13 | 2.55 | 2.60 | 2.16 | 1.59 |
| | 4 | 10.96 | 5.72 | 2.61 | 2.79 | 2.01 | 2.11 | 2.07 | 1.75 |
| | 5 | 10.58 | 4.56 | 3.06 | 2.49 | 1.88 | 2.02 | 1.72 | 1.53 |
| | $\Delta_{D1}$ | 10.27 | 6.26 | 4.16 | 4.25 | 3.33 | 4.07 | 3.66 | 3.46 |
| | $\Delta_{D2}$ | 12.85 | 9.82 | 6.18 | 5.18 | 3.33 | 3.72 | 2.94 | 2.49 |

Table A.3 – Relative standard deviation of GVW estimation for the system layout evaluation in the simulation analysis, vehicle category 34D.

| Speed | Distance | N = 2 | N = 4 | N = 6 | N = 8 | N = 10 | N = 12 | N = 14 | N = 16 |
|---|---|---|---|---|---|---|---|---|---|
| 20 | 0.5 | 3.11 | 2.02 | 1.42 | 1.12 | 1.17 | 1.11 | 1.19 | 1.06 |
| | 1 | 2.83 | 1.99 | 1.49 | 1.08 | 1.17 | 1.08 | 1.13 | 1.02 |
| | 2 | 3.30 | 2.20 | 1.61 | 1.34 | 1.41 | 1.24 | 1.35 | 1.21 |
| | 3 | 3.26 | 2.17 | 1.64 | 1.43 | 1.25 | 1.16 | 1.28 | 1.10 |
| | 4 | 3.56 | 2.34 | 1.72 | 1.53 | 1.55 | 1.34 | 1.51 | 1.43 |
| | 5 | 3.09 | 2.40 | 1.77 | 1.39 | 1.36 | 1.24 | 1.25 | 1.13 |
| | $\Delta_{D1}$ | 2.81 | 2.01 | 1.39 | 1.21 | 1.15 | 1.09 | 1.20 | 1.05 |
| | $\Delta_{D2}$ | 2.90 | 2.03 | 1.58 | 1.10 | 1.17 | 1.07 | 1.17 | 1.06 |
| 40 | 0.5 | 5.93 | 3.86 | 3.00 | 2.56 | 2.31 | 1.30 | 1.47 | 1.21 |
| | 1 | 4.29 | 2.69 | 1.58 | 1.61 | 1.31 | 1.30 | 1.28 | 1.16 |
| | 2 | 4.21 | 1.92 | 1.57 | 1.57 | 1.18 | 1.28 | 1.16 | 1.07 |
| | 3 | 4.37 | 3.27 | 2.18 | 2.12 | 1.85 | 1.82 | 1.91 | 1.53 |
| | 4 | 3.95 | 2.71 | 2.25 | 1.85 | 1.55 | 1.61 | 1.53 | 1.57 |
| | 5 | 4.57 | 3.14 | 2.58 | 2.64 | 1.96 | 2.17 | 2.08 | 1.38 |
| | $\Delta_{D1}$ | 4.20 | 2.25 | 1.52 | 2.01 | 1.50 | 1.30 | 1.48 | 1.38 |
| | $\Delta_{D2}$ | 4.58 | 3.56 | 2.22 | 2.08 | 1.67 | 1.31 | 1.38 | 1.22 |
| 60 | 0.5 | 8.91 | 8.94 | 6.79 | 5.26 | 4.73 | 4.74 | 3.35 | 3.02 |
| | 1 | 8.21 | 6.72 | 3.56 | 3.06 | 2.17 | 1.78 | 1.53 | 1.41 |
| | 2 | 7.38 | 4.03 | 2.29 | 2.10 | 1.60 | 1.66 | 1.41 | 1.19 |
| | 3 | 6.49 | 3.37 | 2.00 | 2.05 | 1.35 | 1.56 | 1.38 | 1.18 |
| | 4 | 7.39 | 4.10 | 3.81 | 3.92 | 3.02 | 2.25 | 2.50 | 2.53 |
| | 5 | 5.72 | 4.67 | 4.42 | 3.07 | 2.73 | 2.63 | 2.43 | 1.63 |
| | $\Delta_{D1}$ | 5.91 | 3.83 | 2.84 | 2.60 | 2.17 | 2.29 | 2.10 | 1.94 |
| | $\Delta_{D2}$ | 8.67 | 5.71 | 3.36 | 3.10 | 2.32 | 2.15 | 1.82 | 1.31 |
| 80 | 0.5 | 13.38 | 13.24 | 10.72 | 10.64 | 8.78 | 7.15 | 6.33 | 5.93 |
| | 1 | 12.68 | 10.70 | 6.51 | 5.79 | 3.38 | 3.70 | 2.45 | 2.49 |
| | 2 | 12.82 | 6.65 | 3.91 | 3.02 | 2.79 | 1.98 | 2.22 | 1.94 |
| | 3 | 8.43 | 3.89 | 2.41 | 2.25 | 1.73 | 1.74 | 1.90 | 1.83 |
| | 4 | 9.78 | 4.12 | 2.71 | 2.24 | 2.10 | 1.69 | 1.70 | 1.80 |
| | 5 | 10.61 | 6.18 | 4.42 | 4.60 | 4.19 | 4.14 | 3.86 | 3.04 |
| | $\Delta_{D1}$ | 9.96 | 4.20 | 3.67 | 3.53 | 2.48 | 3.03 | 2.57 | 2.51 |
| | $\Delta_{D2}$ | 10.96 | 7.72 | 4.37 | 4.21 | 2.64 | 2.83 | 2.19 | 2.30 |
| 100 | 0.5 | 19.42 | 18.57 | 17.43 | 14.05 | 12.71 | 10.55 | 8.78 | 8.15 |
| | 1 | 19.01 | 15.16 | 11.95 | 7.99 | 7.83 | 5.23 | 3.58 | 3.75 |
| | 2 | 18.60 | 10.85 | 6.99 | 4.21 | 3.58 | 3.28 | 2.54 | 2.83 |
| | 3 | 12.92 | 6.38 | 3.43 | 2.65 | 2.79 | 2.31 | 1.78 | 1.61 |
| | 4 | 10.95 | 5.86 | 4.05 | 2.82 | 2.63 | 2.52 | 1.92 | 2.10 |
| | 5 | 10.72 | 5.53 | 3.32 | 2.94 | 2.60 | 2.04 | 1.75 | 1.51 |
| | $\Delta_{D1}$ | 10.55 | 5.42 | 3.99 | 4.02 | 3.50 | 3.49 | 2.72 | 3.31 |
| | $\Delta_{D2}$ | 13.21 | 10.50 | 7.32 | 4.83 | 3.78 | 3.38 | 2.81 | 2.40 |

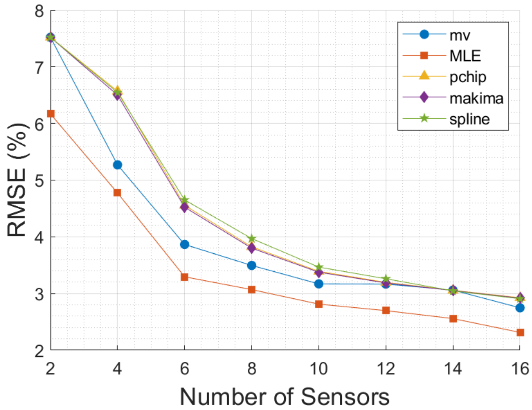


(a) Vehicle speed = 20 km/h.

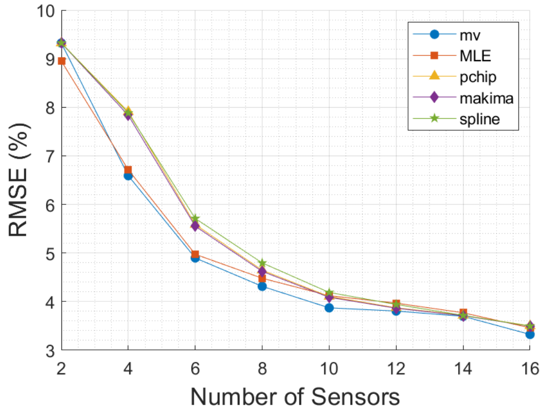


(b) Vehicle speed = 40 km/h.

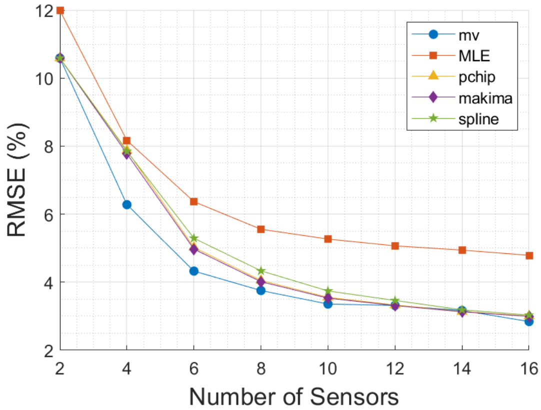


(c) Vehicle speed = 60 km/h.

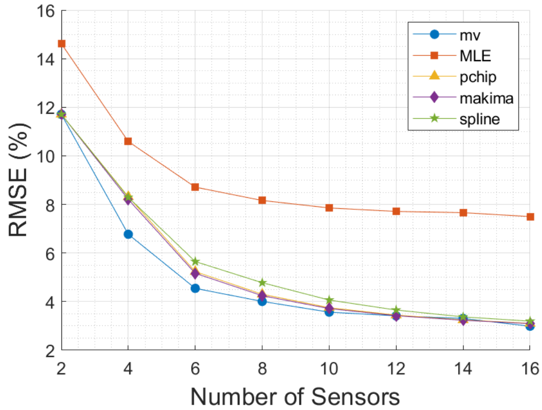


(d) Vehicle speed = 80 km/h.

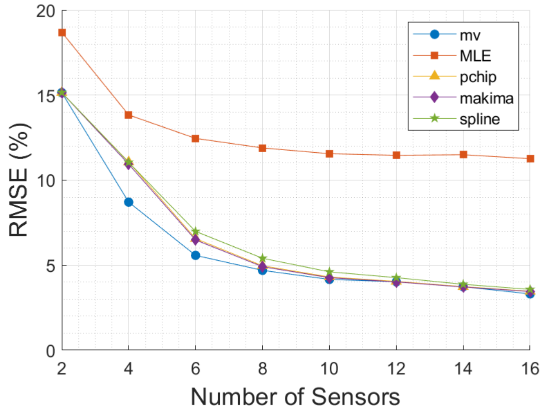


(e) Vehicle speed = 100 km/h.

Figure A.3 – Axle root mean square error from the estimators evaluation in the simulation analysis, with each curve representing a different estimator.

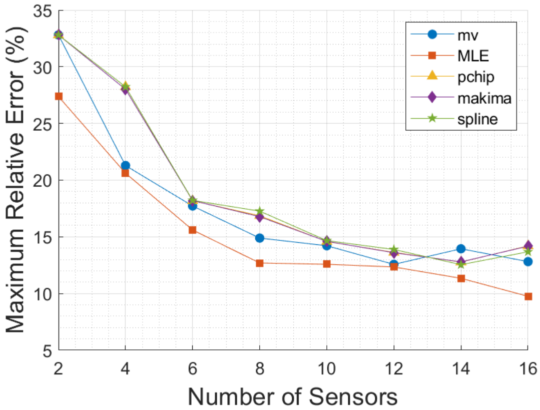


(a) Vehicle speed = 20 km/h.

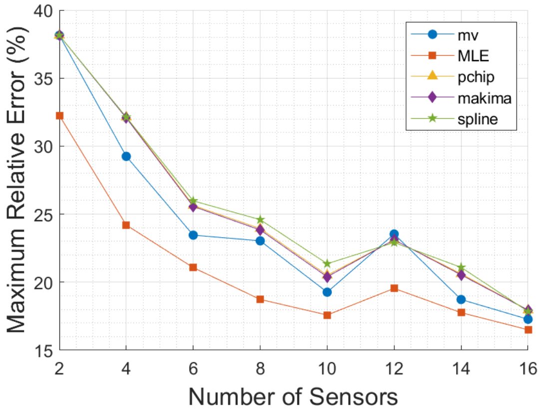


(b) Vehicle speed = 40 km/h.

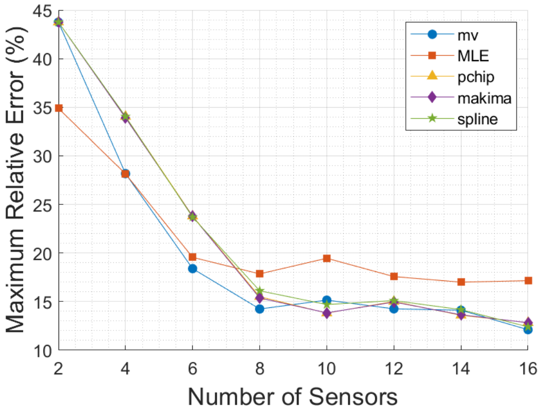


(c) Vehicle speed = 60 km/h.

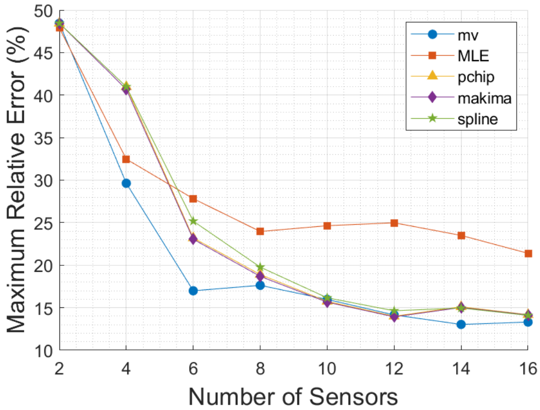


(d) Vehicle speed = 80 km/h.

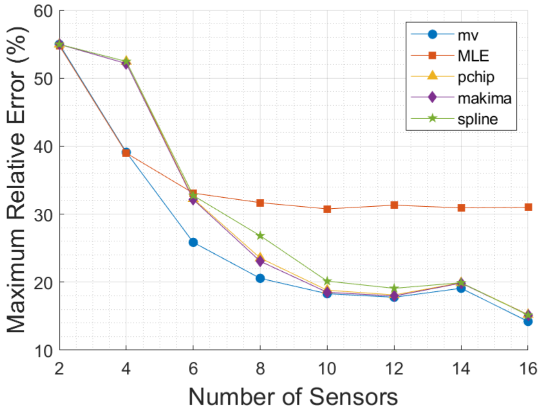


(e) Vehicle speed = 100 km/h.

Figure A.4 – Axle maximum relative error from the estimators evaluation in the simulation analysis, with each curve representing a different estimator.

Table A.4 – Relative standard deviation of GVW estimation for the estimators evaluation in the simulation analysis, vehicle category 2S3.

| Speed | Estimator | N = 2 | N = 4 | N = 6 | N = 8 | N = 10 | N = 12 | N = 14 | N = 16 |
|---|---|---|---|---|---|---|---|---|---|
| 20 | MV | 3.45 | 2.50 | 1.67 | 1.54 | 1.46 | 1.52 | 1.35 | 1.30 |
| | MLE | 2.94 | 2.03 | 1.42 | 1.30 | 1.29 | 1.34 | 1.07 | 1.08 |
| | Makima | 3.45 | 3.26 | 2.05 | 1.70 | 1.56 | 1.50 | 1.31 | 1.37 |
| | Pchip | 3.45 | 3.30 | 2.07 | 1.71 | 1.56 | 1.50 | 1.31 | 1.37 |
| | Spline | 3.45 | 3.29 | 2.11 | 1.77 | 1.58 | 1.52 | 1.31 | 1.34 |
| 40 | MV | 4.62 | 3.20 | 2.25 | 2.44 | 2.21 | 2.02 | 2.04 | 1.56 |
| | MLE | 4.07 | 3.29 | 2.20 | 2.30 | 2.34 | 2.14 | 2.13 | 1.39 |
| | Makima | 4.62 | 3.72 | 2.59 | 2.50 | 2.32 | 2.06 | 2.14 | 1.63 |
| | Pchip | 4.62 | 3.75 | 2.61 | 2.51 | 2.32 | 2.06 | 2.15 | 1.63 |
| | Spline | 4.62 | 3.74 | 2.67 | 2.57 | 2.33 | 2.08 | 2.15 | 1.61 |
| 60 | MV | 5.12 | 2.56 | 2.10 | 1.69 | 1.39 | 1.53 | 1.37 | 1.42 |
| | MLE | 5.79 | 2.94 | 3.30 | 2.27 | 2.19 | 1.93 | 2.01 | 1.75 |
| | Makima | 5.12 | 3.53 | 2.19 | 1.95 | 1.43 | 1.47 | 1.39 | 1.44 |
| | Pchip | 5.12 | 3.57 | 2.20 | 1.97 | 1.44 | 1.48 | 1.40 | 1.45 |
| | Spline | 5.12 | 3.57 | 2.36 | 2.09 | 1.45 | 1.52 | 1.42 | 1.45 |
| 80 | MV | 8.82 | 3.73 | 2.34 | 2.04 | 2.22 | 1.80 | 1.69 | 1.67 |
| | MLE | 10.59 | 5.58 | 5.04 | 3.25 | 3.18 | 3.02 | 2.47 | 2.78 |
| | Makima | 8.82 | 5.02 | 2.62 | 2.22 | 2.27 | 1.92 | 1.67 | 1.64 |
| | Pchip | 8.82 | 5.08 | 2.65 | 2.25 | 2.29 | 1.93 | 1.68 | 1.64 |
| | Spline | 8.82 | 5.08 | 2.79 | 2.35 | 2.39 | 1.98 | 1.74 | 1.66 |
| 100 | MV | 10.62 | 5.61 | 3.24 | 3.18 | 2.35 | 2.45 | 2.08 | 1.70 |
| | MLE | 13.74 | 8.64 | 5.85 | 5.03 | 4.65 | 4.17 | 4.08 | 3.36 |
| | Makima | 10.62 | 7.39 | 4.17 | 3.37 | 2.56 | 2.49 | 2.24 | 1.73 |
| | Pchip | 10.62 | 7.48 | 4.22 | 3.41 | 2.60 | 2.51 | 2.26 | 1.74 |
| | Spline | 10.62 | 7.47 | 4.39 | 3.62 | 2.77 | 2.63 | 2.33 | 1.79 |

Table A.5 – Relative standard deviation of GVW estimation for the estimators evaluation in the simulation analysis, vehicle category 3I3.

| Speed | Estimator | N = 2 | N = 4 | N = 6 | N = 8 | N = 10 | N = 12 | N = 14 | N = 16 |
|---|---|---|---|---|---|---|---|---|---|
| 20 | MV | 3.43 | 2.22 | 1.90 | 1.78 | 1.45 | 1.41 | 1.33 | 1.19 |
| | MLE | 2.89 | 2.19 | 1.73 | 1.69 | 1.54 | 1.32 | 1.38 | 1.01 |
| | Makima | 3.43 | 2.62 | 2.11 | 1.86 | 1.47 | 1.47 | 1.37 | 1.27 |
| | Pchip | 3.43 | 2.65 | 2.12 | 1.86 | 1.47 | 1.47 | 1.37 | 1.27 |
| | Spline | 3.43 | 2.64 | 2.13 | 1.88 | 1.46 | 1.50 | 1.37 | 1.26 |
| 40 | MV | 3.45 | 1.99 | 1.82 | 1.44 | 1.43 | 1.52 | 1.28 | 1.34 |
| | MLE | 3.76 | 2.37 | 1.82 | 1.65 | 1.53 | 1.57 | 1.25 | 1.44 |
| | Makima | 3.45 | 2.59 | 2.03 | 1.67 | 1.41 | 1.52 | 1.28 | 1.44 |
| | Pchip | 3.45 | 2.62 | 2.04 | 1.69 | 1.41 | 1.52 | 1.28 | 1.44 |
| | Spline | 3.45 | 2.62 | 2.07 | 1.76 | 1.45 | 1.58 | 1.29 | 1.46 |
| 60 | MV | 5.08 | 2.65 | 2.02 | 1.99 | 1.60 | 1.69 | 1.39 | 1.18 |
| | MLE | 6.34 | 4.00 | 2.98 | 2.74 | 1.94 | 2.29 | 1.94 | 1.87 |
| | Makima | 5.08 | 3.09 | 2.55 | 2.13 | 1.61 | 1.73 | 1.42 | 1.25 |
| | Pchip | 5.08 | 3.14 | 2.59 | 2.16 | 1.62 | 1.74 | 1.42 | 1.25 |
| | Spline | 5.08 | 3.12 | 2.79 | 2.26 | 1.70 | 1.82 | 1.44 | 1.28 |
| 80 | MV | 7.24 | 3.29 | 2.62 | 2.28 | 2.01 | 1.72 | 1.66 | 1.58 |
| | MLE | 10.31 | 4.76 | 4.75 | 3.79 | 3.80 | 2.92 | 2.84 | 2.82 |
| | Makima | 7.24 | 4.87 | 2.60 | 2.40 | 2.05 | 1.85 | 1.64 | 1.49 |
| | Pchip | 7.24 | 4.95 | 2.65 | 2.43 | 2.07 | 1.87 | 1.65 | 1.50 |
| | Spline | 7.24 | 4.93 | 2.84 | 2.62 | 2.16 | 2.03 | 1.74 | 1.51 |
| 100 | MV | 12.72 | 7.04 | 3.24 | 3.13 | 2.55 | 2.60 | 2.16 | 1.59 |
| | MLE | 15.43 | 8.80 | 5.86 | 5.35 | 5.18 | 4.22 | 4.30 | 4.29 |
| | Makima | 12.72 | 8.98 | 4.57 | 3.03 | 2.42 | 2.53 | 2.11 | 1.68 |
| | Pchip | 12.72 | 9.05 | 4.64 | 3.07 | 2.45 | 2.55 | 2.13 | 1.69 |
| | Spline | 12.72 | 9.06 | 4.95 | 3.37 | 2.69 | 2.65 | 2.15 | 1.78 |

Table A.6 – Relative standard deviation of GVW estimation for the estimators evaluation in the simulation analysis, vehicle category 34D.

| Speed | Estimator | N = 2 | N = 4 | N = 6 | N = 8 | N = 10 | N = 12 | N = 14 | N = 16 |
|---|---|---|---|---|---|---|---|---|---|
| 20 | MV | 3.26 | 2.17 | 1.64 | 1.43 | 1.25 | 1.16 | 1.28 | 1.10 |
| | MLE | 3.16 | 2.29 | 1.73 | 1.35 | 1.09 | 1.10 | 1.27 | 0.99 |
| | Makima | 3.26 | 2.73 | 1.83 | 1.59 | 1.37 | 1.20 | 1.29 | 1.14 |
| | Pchip | 3.26 | 2.76 | 1.84 | 1.60 | 1.38 | 1.21 | 1.29 | 1.15 |
| | Spline | 3.26 | 2.75 | 1.89 | 1.64 | 1.42 | 1.24 | 1.28 | 1.13 |
| 40 | MV | 4.37 | 3.27 | 2.18 | 2.12 | 1.85 | 1.82 | 1.91 | 1.53 |
| | MLE | 4.79 | 3.68 | 2.35 | 2.50 | 2.05 | 1.89 | 2.04 | 1.74 |
| | Makima | 4.37 | 3.81 | 2.49 | 2.15 | 1.87 | 1.80 | 1.85 | 1.60 |
| | Pchip | 4.37 | 3.85 | 2.51 | 2.16 | 1.88 | 1.80 | 1.85 | 1.60 |
| | Spline | 4.37 | 3.84 | 2.59 | 2.21 | 1.93 | 1.80 | 1.85 | 1.62 |
| 60 | MV | 6.49 | 3.37 | 2.00 | 2.05 | 1.35 | 1.56 | 1.38 | 1.18 |
| | MLE | 8.19 | 5.44 | 3.17 | 3.20 | 2.85 | 2.99 | 2.58 | 2.37 |
| | Makima | 6.49 | 4.35 | 2.51 | 2.09 | 1.39 | 1.39 | 1.48 | 1.26 |
| | Pchip | 6.49 | 4.43 | 2.56 | 2.12 | 1.41 | 1.40 | 1.49 | 1.27 |
| | Spline | 6.49 | 4.41 | 2.79 | 2.30 | 1.56 | 1.44 | 1.55 | 1.35 |
| 80 | MV | 8.43 | 3.89 | 2.41 | 2.25 | 1.73 | 1.74 | 1.90 | 1.83 |
| | MLE | 10.77 | 6.06 | 5.35 | 4.56 | 4.08 | 3.41 | 3.34 | 3.67 |
| | Makima | 8.43 | 5.97 | 2.46 | 2.41 | 1.80 | 2.00 | 2.10 | 1.78 |
| | Pchip | 8.43 | 6.09 | 2.54 | 2.46 | 1.83 | 2.03 | 2.12 | 1.79 |
| | Spline | 8.43 | 6.07 | 3.02 | 2.83 | 2.09 | 2.26 | 2.35 | 1.88 |
| 100 | MV | 12.92 | 6.38 | 3.43 | 2.65 | 2.79 | 2.31 | 1.78 | 1.61 |
| | MLE | 15.77 | 8.31 | 7.67 | 5.09 | 4.15 | 4.94 | 4.68 | 4.37 |
| | Makima | 12.92 | 8.29 | 4.05 | 2.58 | 2.97 | 2.31 | 1.91 | 1.52 |
| | Pchip | 12.92 | 8.39 | 4.11 | 2.63 | 3.02 | 2.34 | 1.94 | 1.53 |
| | Spline | 12.92 | 8.38 | 4.42 | 3.08 | 3.42 | 2.54 | 2.13 | 1.67 |